

**The functional characterization of a root knot nematode
effector Mi131**

and

**An investigation of the role of jasmonic acid during the
Arabidopsis-root knot nematode interaction**

Dissertation

For the award of the degree

Doctor of Philosophy (Ph. D)

of the George-August-Universität, Göttingen

Within the doctoral program: Promotionsprogramm Biologie
of the George-August University School of Science (GAUSS)

Submitted by

Natthanon Leelarasamee

From Bangkok

Göttingen, 2015

Thesis Committee

Jun. Prof. Dr. Cynthia Gleason

(Department of Molecular Plant Sciences, Georg-August-Universität, Göttingen)

Prof. Dr. Christiane Gatz

(Department of Plant Molecular Biology and Physiology, Georg-August-Universität, Göttingen)

PD Dr. Thomas Teichmann

(Department of Plant Cell Biology, Georg-August-Universität, Göttingen)

Members of the Examination Board

1st Referee: **Jun. Prof. Dr. Cynthia Gleason**

(Department of Molecular Plant Sciences, Georg-August-Universität, Göttingen)

2nd Referee: **Prof. Dr. Christiane Gatz**

(Department of Plant Molecular Biology and Physiology, Georg-August-Universität, Göttingen)

Further members of the Examination Board

PD Dr. Thomas Teichmann

(Department of Plant Cell Biology, Georg-August-Universität, Göttingen)

Prof. Dr. Volker Lipka

(Department of Plant Cell Biology, Georg-August-Universität, Göttingen)

Prof. Dr. Ivo Feußner

(Department of Plant Biochemistry, Georg-August-Universität, Göttingen)

Prof. Dr. Andrea Polle

(Department of Forest Botany and Tree Physiology, Georg-August-Universität, Göttingen)

Date of oral examination: 10.12.2015

Declaration

Hereby, I declare that this dissertation was undertaken independently and without any unauthorized aid.

I declare that this Ph.D. dissertation has not been presented to any other examining body either in its present or similar form.

Furthermore, I also affirm that I have not applied for a Ph.D. or Dr.rer.nat. at any other higher school of education.

Göttingen, _____

Natthanon Leelarasamee

Table of contents

| | |
|--|----|
| List of abbreviation | i |
| Abstract | vi |
| 1. Introduction..... | 1 |
| 1.1 Root knot nematode | 1 |
| 1.2 Root knot nematode life cycle..... | 2 |
| 1.3 The discovery of Mi131 effector..... | 5 |
| 1.4 Mi131 encodes a profilin | 8 |
| 1.5 The significant role of profilin in the cell | 9 |
| 1.6 The jasmonic acid biosynthesis pathway | 12 |
| 1.7 Jasmonic acid signaling pathway | 14 |
| 1.8 JA-triggered Immunity..... | 16 |
| 1.9 The manipulation of JA pathway by pathogen effectors | 16 |
| 1.10 Jasmonic acid in plant defense against RKN | 17 |
| 1.11 The aim of my thesis | 19 |
| 2. Materials and Methods..... | 20 |
| 2.1 Materials..... | 20 |
| 2.1.1 Devices | 20 |
| 2.1.2 Consumables..... | 22 |
| 2.1.3 Chemicals | 23 |
| 2.1.4 Media | 26 |
| 2.1.5 Buffers..... | 32 |
| 2.1.6 Primers | 40 |
| 2.1.7 Organisms | 43 |
| 2.1.8 Plasmids | 44 |
| 2.1.9 Kits..... | 45 |
| 2.2 Methods..... | 46 |
| 2.2.1 General molecular methods | 46 |

| | |
|--|-----|
| 2.2.2 Plant growth conditions..... | 51 |
| 2.2.3 Pathogen assays..... | 52 |
| 2.2.4 RNA extraction and gene expression analysis | 53 |
| 2.2.5 Subcellular localization of fluorescence tagged proteins | 55 |
| 2.2.6 Protein analysis using Western blot | 56 |
| 2.2.7 Protein interaction assays using yeast..... | 57 |
| 2.2.8 <i>In vitro</i> actin sedimentation assay (Cytoskeleton #BK013 protocol)..... | 60 |
| 2.2.9 Plant phytohormone measurement by HPLC/MS | 61 |
| 3. Results..... | 62 |
| 3.1 Functional characterization of <i>M. incognita</i> effector Mi131 | 62 |
| 3.1.1 Searching for an Mi131 interaction partner in plants by performing a Y2H screen..... | 62 |
| 3.1.2 Further investigation of Mi131 interacting with Arabidopsis actins. | 64 |
| 3.1.3 Endogenous AtACT7 coimmunoprecipitates with GFP-Mi131 | 69 |
| 3.1.4 Mi131 sequesters G actin <i>in vitro</i> | 71 |
| 3.1.5 Mi131 can suppress the AtACT1 overexpression phenotype | 75 |
| 3.1.6 Mi131 can disrupt actin filaments <i>in vivo</i> | 78 |
| 3.2 Role of Jasmonic acid in plant protection against RKN | 80 |
| 3.2.1 The regulation of JA related gene expression in gall-enriched tissue | 80 |
| 3.2.2 Nematode susceptibility is COI1 independent..... | 82 |
| 3.3.3 Exogenous application of MeJA can reduce galling in Arabidopsis | 84 |
| 3.3.4 MeJA does not interfere with nematode penetration | 86 |
| 3.3.5 MeJA treatment increases OPDA and JA production in Arabidopsis..... | 87 |
| 3.3.6 MeJA treated <i>aos</i> seedlings are susceptible to RKN..... | 89 |
| 4. Discussion..... | 91 |
| 4.1 The role of Mi131 as RKN effector | 91 |
| 4.1.1 Mi131 interacts with Arabidopsis actins..... | 91 |
| 4.1.2 Mi131 can rescue 35S::ACT1 dwarf phenotype..... | 93 |
| 4.1.3 Mi131 sequesters non-muscle actin <i>in vitro</i> | 94 |
| 4.1.4 Why would RKNs secrete profilin into plant cells? | 97 |
| 4.2 OPDA mediates RKN defense | 99 |
| 4.2.1 COI1 is not involved in defense against RKN | 99 |
| 4.2.2 MeJA application induces accumulation of JA and OPDA in the root | 102 |

| | |
|---|-----|
| 4.2.3 Suppression of JA biosynthesis genes in gall-enriched tissue..... | 103 |
| 5. References..... | 106 |
| 6. Supplementary figures | 118 |
| Acknowledgement | 125 |
| Curriculum vitae | 126 |

List of abbreviation

| | |
|------------------|-----------------------------------|
| % | Percent |
| µm | Micrometer |
| ACX | Acyl-CoA oxidase |
| Amp | Ampicilin |
| AOC | Allene oxide cyclase |
| AOS | Allene oxide synthase |
| APS | Ammonium persulfate |
| AtACT | Arabidopsis actin |
| BLAST | Basic Local Alignment Search Tool |
| BSA | Bovine serum albumin |
| CaMV | Cauliflower mosaic virus |
| CDS | Coding sequence |
| <i>C.elegans</i> | <i>Caenorhabditis elegans</i> |
| co-IP | Co-immunoprecipitation |
| COI1 | Coronatine insensitive 1 |
| COR | Coronatine |
| DNA | Desoxyribonucleic acid |
| dNTP | Nucleosidtriphosphate |
| dpi | Days post inoculation/infection |
| ET | Ethylene |

| | |
|------------------|---|
| ETI | Effector triggered immunity |
| ETS | Effector triggered susceptibility |
| EDTA | Ethylenediaminetetraacetic acid |
| FAD | Fatty acid desaturase |
| flg22 | Flagellin 22 |
| FLS2 | Flagelin sensitive 2 |
| <i>FRK1</i> | Flagelin induced receptor-like kinase |
| F actin | Filamentous actin |
| g (weight) | Gram |
| g (centrifuge) | Gravity force |
| GFP | Green fluorescent protein |
| GST 6 | Glutathionine S-transferase 6 |
| G actin | Globular actin or actin monomer |
| H | Histidine |
| H ₂ O | Water |
| HCl | Hydrochloric acid |
| HPLC-MS | High performance liquid chromatography conjugated with mass spectrometry |
| HR | Hypersensitive response |
| J2 | Stage 2 Juvenile |
| JA | Jasmonic acid |
| Kan | Kanamycin |

| | |
|----------------------|--|
| kDa | Kilodalton |
| l | Liter |
| L | Leucine |
| LB | Lysogeny broth |
| LOX | Lipoxygenase |
| LRR | Leucin rich repeat |
| MAMPs | Microbial associated molecular patterns |
| ml | Milliliter |
| mM | Milimolar |
| mm | Millimeter |
| M | Molar |
| min | Minute |
| μ M | Micro molar |
| <i>M.incognita</i> | <i>Meloidogyne incognita</i> |
| <i>M.graminicola</i> | <i>Meloidogyne graminicola</i> |
| <i>M.hapla</i> | <i>Meloidogyne hapla</i> |
| <i>M.javanica</i> | <i>Meloidogyne javanica</i> |
| MES | 2-(N-morpholino) ethanesulfonic acid |
| MS | Murashige and Skoog |
| NCBI | National Center for Biotechnology Information |
| nM | Nanomolar |

| | |
|----------------|---|
| OPDA | 12-oxo phytodienoic acid |
| PAMPs | Pathogen associated molecular patterns |
| PEG | Polyethylene glycol |
| PIP2 | Phosphatidylinositol (4,5)-bisphosphate |
| PRR | Pattern recognition receptor |
| qRT-PCR | Quantitative real time polymerase chain reaction |
| <i>Pst-LUX</i> | <i>Pseudomonas syringae</i> pv. <i>tomato</i> DC3000 <i>-LUX</i> |
| RFP | Red fluorescence protein |
| RKN | Root-knot nematode |
| RNA | Ribonucleic acid |
| rpm | Round per minute |
| SA | Salicylic acid |
| SC media | Synthetic complete media |
| SDS | Sodium lauryl sulfate |
| SEM | Standard error of mean |
| Spec | Spectinomycin |
| T2 | Transformant of Arabidopsis generation 2 |
| TAIR | The Arabidopsis Information Resource |
| TEMED | Tetramethylethylenediamine |
| TTSS | Type three secretion system |
| UBQ5 | Ubiquitin 5 |

| | |
|------|---------------------------------------|
| W | Tryptophan |
| YEB | Yeast extract broth |
| YFP | Yellow fluorescent protein |
| YPAD | Yeast extract peptone dextrose medium |
| Y2H | Yeast two hybrid |

Abstract

Root knot nematodes (*Meloidogyne* spp.) are devastating pests to agriculture worldwide. The best control measure for these small, microscopic roundworms is to fumigate the field with nematicides prior to planting. However nematicides are problematic because they have non-target toxicity and are being phased-out of use. Therefore, new control measures are urgently required. My thesis looks at both sides of the plant-nematode interaction in order to understand nematode virulence determinants and the plant responses to nematodes. We hope that with this new knowledge, we can one day engineer novel ways to combat nematodes.

During plant-RKN interactions, the nematode is presumably secreting molecules into the plant that are crucial for successful infection. These proteins are called “effectors,” and they are postulated to be involved in both plant defense suppression and RKN feeding site generation. In Gleason lab, we are trying to characterize the function of several RKN effectors. One of the potential effectors from *Meloidogyne incognita* is called Mi131. Mi131 is a protein with a profilin domain, which is typically involved in actin binding. When Mi131 was expressed in plants, the plants were more susceptible to nematodes. To elucidate Mi131 function, I performed yeast two hybrid screens to find Mi131 interaction partner(s) in *Arabidopsis*. I found that Mi131 can interact with both vegetative and reproductive isoforms of plant actin. *In vitro* actin polymerization assays indicated that Mi131 inhibits actin polymerization. Further investigations using protoplasts with a GFP-labelled actin cytoskeleton showed that when Mi131 was expressed in these cells, the actin cytoskeleton appeared fragmented. Plants which overexpress *AtActin1* have a mutant, dwarf phenotype. Co-expression of Mi131 in these plants could rescue the dwarf phenotype. This indicated that Mi131 can act as an actin-binding profilin in plants and titer out the toxic levels of *AtActin1*. Previous cell biology studies of the root-knot nematode giant cells had shown that actin re-organization is crucial for RKN feeding site development and expansion. The nematode may secrete Mi131 to interfere with the actin dynamics in the cell and thereby promote RKN feeding site establishment.

The Gleason lab is also interested in how the plant responds to RKNs during the compatible interaction, with a focus on the phytohormone jasmonic acid (JA). Some publications had indicated that JA is involved in promoting defence against nematodes. Other publications

suggested that JA is required for nematode susceptibility. Therefore, I investigated the role of JA using the model plant *Arabidopsis thaliana*. From my studies, I found that exogenous methyl jasmonate application on *Arabidopsis* significantly reduced the number of galls caused by RKNs. Interestingly, I found that MeJA induced resistance was independent of COI1, the JA receptor. The work carried out by myself and others in the lab shows that *Arabidopsis* mutants in trienoic fatty acid (*fad3/7/8*) or the octadecanoid pathway (*aos*) were more susceptible to nematodes. Meanwhile, plants inhibited in JA signaling (*coi1-t*) showed normal, wildtype levels of infection. Importantly, mutants in which the conversion of 12-oxophytodienoic acid (OPDA) to JA is inhibited (*opr3* and *acx1/5*) also showed wild-type levels of nematode disease. Overall, the data suggests that the JA precursor, OPDA, has a role in plant defence against nematodes.

1. Introduction

1.1 Root knot nematode

Plant parasitic nematodes are microscopic round worms which can cause significant economic damage to crop plants. Nematodes comprise a diverse phylum, and many nematodes are parasitic on plants or animals. Root-knot nematodes (RKNs) of the *Meloidogyne* species are particularly damaging plant parasites. During infection, RKNs have an intimate relationship with their host plants because they must adopt a sedentary lifestyle in the root and manipulate plant cells into feeding sites (Absmanner et al., 2013; Hewezi and Baum, 2012; Kyndt et al., 2013; Teillet et al., 2013). Root-knot nematodes cause a disruption of the root vascular system and cause root galling, which can interfere with water and nutrient transport (Figure 1.1). As a whole, RKNs are estimated to cause up to 5% of crop losses worldwide (Perry et al., 2009) and this damage, on the global scale, translates into billions of dollars in crop losses.



Figure 1.1. Tomato root infected by *Meloidogyne incognita*. The infected root exhibits extensive root galling (Jones et al., 2013).

In the *Meloidogyne* genus, there are more than 90 species of RKNs (Perry et al., 2009). The top three RKN species that are the most damaging to plants in tropical regions are *Meloidogyne incognita*, *Meloidogyne arenaria* and *Meloidogyne javanica*, and the main problematic nematode in the northern hemisphere is *Meloidogyne hapla* (Bird and Wallace, 1965; Mitkowski and Abawi, 2003).

It has been estimated that a majority of vascular plants are susceptible to RKN infection, and susceptible plants range from trees to grasses, and includes the model plant *Arabidopsis thaliana* (Sijmons et al., 1991; Trudgill and Blok, 2001). The broad host range means that nematode control by crop rotation is limited and requires a lot of forward planning by farmers. Only a few resistance genes against RKN have been identified. Unfortunately, the usefulness of naturally resistant plants is limited, mainly due to the fact that nematodes can evolve and break plant resistance. For example, when avirulent RKNs were placed on resistant tomato, the selection pressure forced the avirulent nematodes to evolve into a virulent strain within just a few generations (Castagnone-Sereno et al., 1994; Janssen et al., 1998; Petrillo and Roberts, 2005). The most successful method to control RKNs is to use nematicides; however, most front-line nematicides have been banned due to their toxicity to the environment (Chitwood, 2003). The lack of new nematicides worries many farmers today, but in the future, even more farmers will have reason to worry. Global warming likely will increase the distribution of RKNs into new, larger geographic areas, bringing the root-knot nematode problem to even more communities (Bebber et al., 2014). The increased range of the pathogen will be compounded by an increased the demand for food production by the world's growing population. Projects that help us understand how the nematode infects plants will give us new knowledge and eventually lead us to find a new methods to control RKNs (Abad et al., 2008; Mbeunkui et al., 2010; Opperman et al., 2008).

1.2 Root knot nematode life cycle

The nematode life cycle begins in the egg. In the suitable conditions, the cells develop, leading to a stage 1 juvenile (J1). J1 will stay in the egg and molt to become the stage 2 juvenile (J2). Therefore, all the hatchlings are in stage J2, which is the only life stage of RKN that is motile. Since they are dependent on their fat reserves to survive, the J2 will rapidly locate the roots of

the host plant to initiate infection. The J2 has chemosensory organs that can sense root exudates/secondary metabolites or phytohormones (Curtis, 2008), although the exact molecules that are required for RKNs to locate the root are still unknown. After RKNs locate the root, they will penetrate specifically behind the root cap. Once in the root, they move intercellularly toward the root tip and turn to enter the opening of the vascular cylinder (Figure 1.2 A). After entering the vascular cylinder, the nematodes will migrate through the root cortex until they select a feeding site. In general, the nematode chooses between 2-12 parenchyma cells to become its feeding sites and can move its head between them to feed (Wyss et al., 1992). The feeding cells are highly metabolically active and undergo several rounds of endoreduplication without cytokinesis. As a result, they become large and multinucleate. For root-knot nematodes, the feeding cells are called giant cells (Figure 1.2 C). The vascular system surrounding the giant cells also divides, forming the root galls, which are the most obvious disease symptom of the root-knot nematode infection (Figure 1.2 B) (Jones and Goto, 2011; Jones and Gunning, 1976). The nematode will molt into stage three and then stage four juveniles. During the stage three juvenile phase, the males and females can be distinguished. Although most RKNs are parthenogenetic, they can still molt into non-feeding males. In non-suitable environments, RKN populations tend to contain more males than females (Snyder et al., 2006). During the fourth stage molt, the males leave the root and the female swells into a large, pear shape. The fully mature female eventually lays eggs up to 1,000 eggs within a gelatinous matrix on the outside of the root. One life cycle of RKNs generally takes approximately 28 days but this can vary due to the environmental conditions (Bird and Wallace, 1965; Chitwood and Perry, 2009).

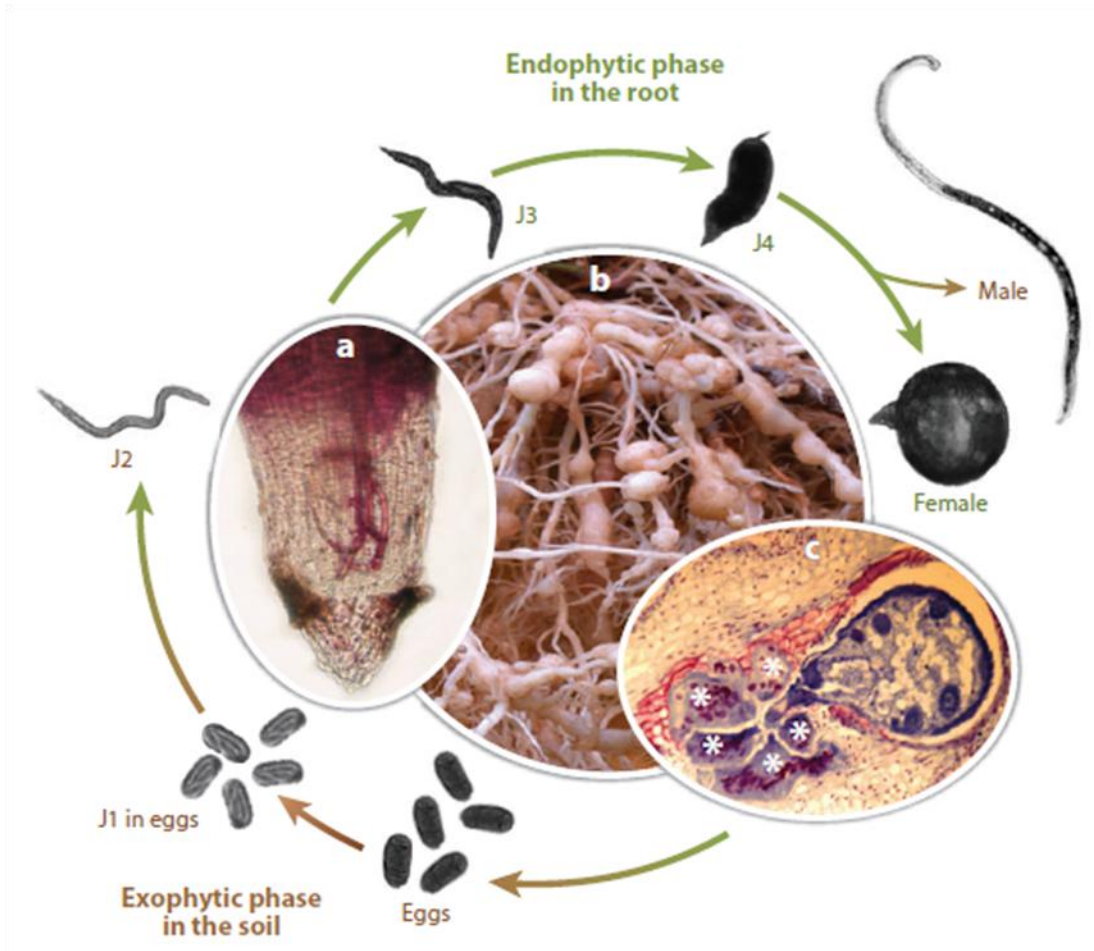


Figure 1.2. Root knot nematode life cycle. A) Stage J2 juveniles infect the root. The J2 migrating through the root can be visualized with acid fuschsin stain. B) Once the J2 becomes sedentary, it starts to feed. The giant cells form, and around the giant cell, the neighboring cells divide to form root galls, a typical symptom of RKN infection. C) A cross section of the gall shows the nematode feeding sites (giant cells(*)) and the adult female (Castagnone-Sereno et al., 2013).

As mentioned earlier, RKNs cause significant economic damage to many crop plants. The key to engineer novel resistance to nematodes is to understand how RKNs are so successful. This knowledge lies in studying both the plant and the pathogen sides of the interaction. On the pathogen side of this pathosystem, the nematode is presumably secreting molecules and proteins that help them suppress plant defence responses and facilitate the creation and maintenance of the giant cells. A small molecule which is introduced to the plant by the pathogen in order to benefit the infection is called an “effector.” Therefore, a main goal of the Gleason lab has been the identification and characterization of the potential effectors which may be involved during the early stages of RKN infection. In addition, the plant side of the pathosystem is also an area of research in the Gleason lab. In particular, the lab is interested in understanding the role of the phytohormone jasmonic acid during infection.

My thesis will explore both sides of the plant-nematode interaction. First, I will characterize a novel nematode effector and then I will elucidate the role of jasmonic acid and its precursors during infection.

1.3 The discovery of Mi131 effector

The study of effectors from RKNs is the key to understanding how RKNs are so successful in infecting various plant species without inducing obvious defence responses from host plant. The goal in the Gleason lab is to find nematode effectors that are vital to nematode success, and then to identify the plant targets of these effectors. With this information, it may be possible to manipulate the plant so that it can no longer support nematode infections. Therefore, the Gleason lab identified several effector candidates from the published secretome from *M. incognita*. This secretome contains 486 unique peptides that were secreted from juveniles exposed to root exudates and identified by mass spectrometry (Bellafiore et al., 2008).

In the secretome of *M. incognita*, there are two peptides with profilin domains (pfam00235), which is a known actin binding domain (Bellafiore et al., 2008). Because the root-knot nematode feeding sites undergo cytoskeleton rearrangements, secreted nematode proteins that could be involved in actin restructuring were of interest (De Almeida Engler et al., 2004). Therefore, a full length coding sequence for one of these profilins (called Mi131) was cloned for further study.

To classify Mi131 as a nematode effector, it should exhibit three characteristics: 1) the gene expression should be up-regulated during parasitic stages (J2) of the nematode, 2) the transcript should be localized to nematode secretory organ(s), and 3) ectopic expression of the nematode gene in *Arabidopsis* should enhance plant susceptibility.

Quantitative reverse transcription polymerase chain reaction (qRT-PCR) showed that this gene is highly upregulated in the stage 2 juvenile compared to the egg (Figure 1.3 A). This result indicated the gene may serve an important function during the pre-parasitic and early stages of the plant-RKN interaction.

Next, *in situ* hybridizations were performed with a digoxigenin-(DIG) labelled antisense Mi131 cDNA probe. The probe hybridized to the esophageal gland region of the whole mount juvenile. No hybridization signal was detected with the sense *Mi131* cDNA probe. The glands are directly connected to the nematode stylet, a needle-like head structure that can pierce plant cell walls and the plant plasma membrane. The specific gland localization of Mi131 suggests that Mi131 is likely to be secreted into plant cells via stylet (Figure 1.3 B).

Lastly, two homozygous Col-0 lines, that ectopically express Mi131, were generated and tested for altered nematode susceptibility. These *Arabidopsis* transgenic lines exhibited enhanced susceptibility to RKN infection (Figure 1.3 C).

Since the preliminary data in the lab suggested that Mi131 could be a nematode effector, the goal of my thesis was to functionally characterize Mi131 in order to understand its role in the RKN-plant interaction.

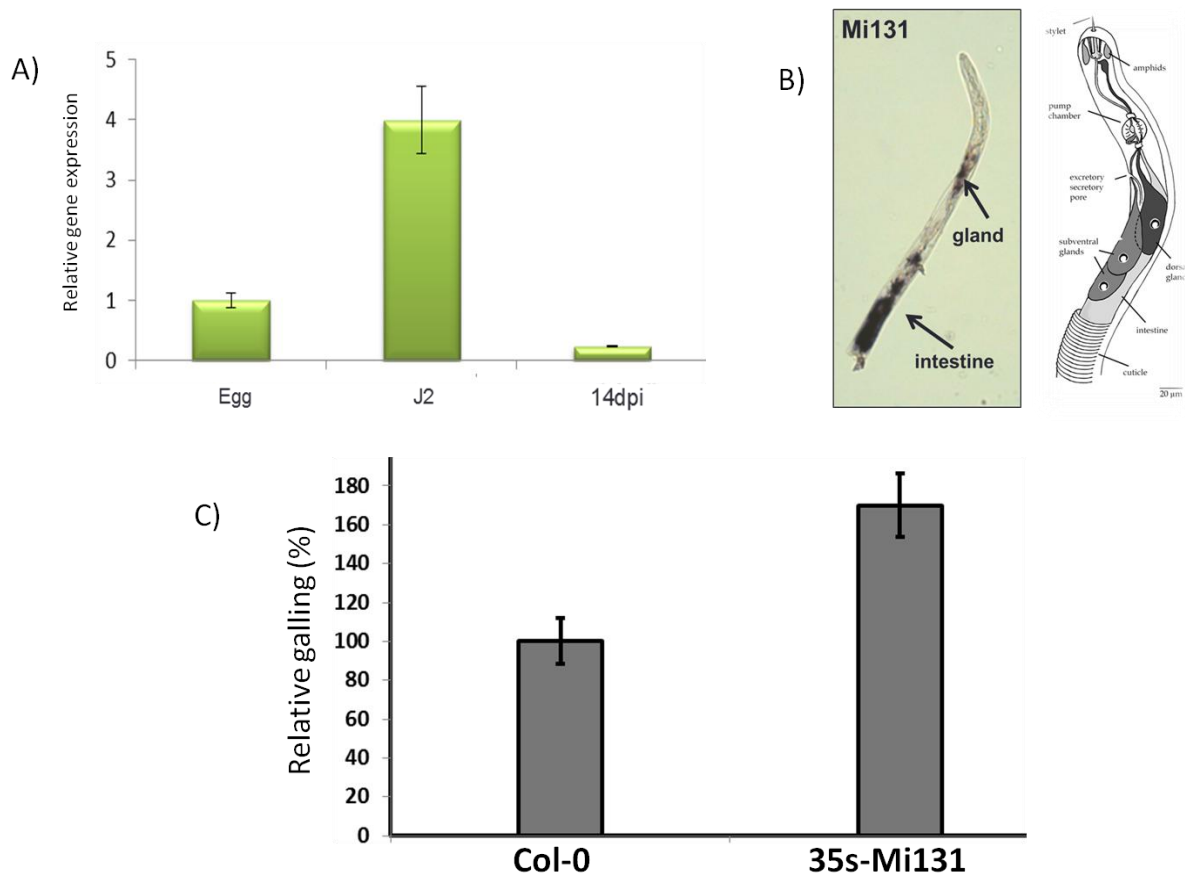


Figure 1.3. Prescreen of Mi131 effector (Cynthia Gleason, personal communication).

A) Quantification of Mi131 expression in different life stages. The quantitative real time PCR was performed on *M. incognita* at 3 different stages, egg, J2 and Col-0 infected tissue at 14 dpi. Bars represent relative gene expression to geometric mean of the housekeeping gene MiGAPDH and Mi18S. The graphs represent results from 2 biological replicates of egg and J2 and 1 biological replicate from Col-0 infected tissue at 14 dpi. The error bars represent stand error of mean.

B) Localization of Mi131 transcript visualized by *in situ* hybridization.. The *in situ* localization of Mi131 was performed by using Mi131 anti-sense cDNA probe. The localization of Mi131 is specific to the glands and intestine of *M. incognita*.

C) Transgenic plants expressing 35S::Mi131 are more susceptible to RKN compared to Col-0. Ten-day-old Col-0, 35s-Mi131 seedlings grown on MS were transferred to petri dishes containing KNOPs media. Each plant was inoculated with 100 *M. incognita* J2 and the number of galls per plant were counted at 14 dpi. Bars represent mean of gall per plant normalized to internal Col-0 control combined from 3 independent experiments. Error bar represents standard error of mean.

1.4 Mi131 encodes a profilin

Mi131 is a small gene of 381 bp which codes for a 126 amino acids. A BLASTn search and contig analysis of the *M. incognita* genome indicates that Mi131 is a single gene in the *M. incognita* genome (N. Elashry, personal communication). Mi131 contains a profilin domain, putative poly-proline binding sites and phosphatidylinositol 4,5-biphosphate (PIP2) interaction sites (Figure 1.4).

Profilins are small proteins that are involved in the actin monomer binding and the organization of actin cytoskeleton in the cell (Jockusch et al., 2007). Profilins are found in all eukaryotic organisms, including nematodes and plants. A BLASTp search of the non-redundant protein database showed that Mi131 is 75% identical to the animal parasitic nematode *Ascaris suum* profilin 3, 63 % to a free living nematode *Caenorhabditis elegans* profilin, and approximately 20-35% similarity to *Arabidopsis thaliana* profilins.

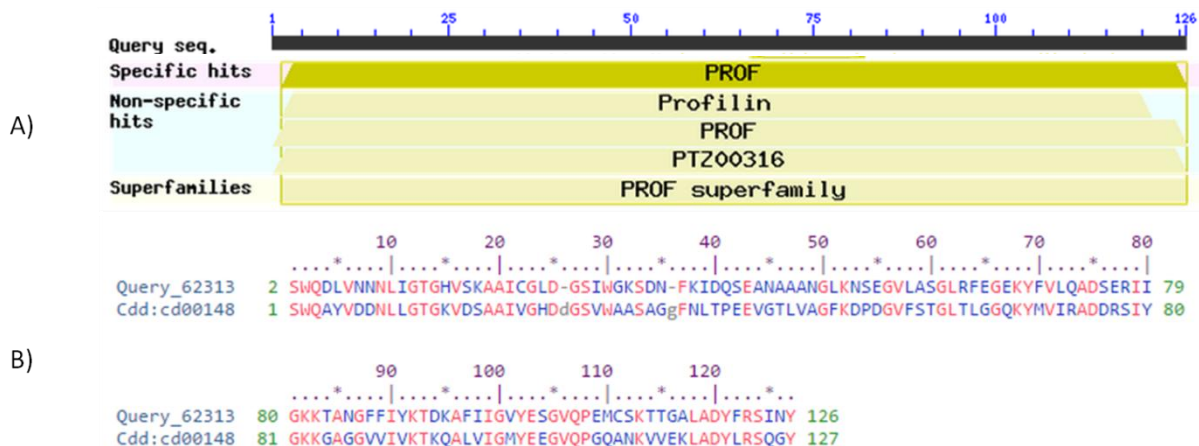


Figure 1.4. Mi131 protein domain information

A) A BLASTp search of the non-redundant protein database using Mi131 protein as the query sequence shows that Mi131 belongs to profilin super family.

B) Alignment of Mi131 protein sequence to a consensus profilin domain (as Query_62313 and Cdd:cd00148 respectively).

1.5 The significant role of profilin in the cell

At the cellular level, the actin cytoskeleton is crucial for cellular trafficking, signaling, cell division, development and motility (Henty-Ridilla et al., 2013; Hussey, 2004; Hussey et al., 2006; Liu et al., 2011; Sheahan et al., 2004a; Witke, 2004). One of the basic building blocks of the actin cytoskeleton is globular (G) actin, a small 42 kDA protein. The G actins are assembled into filamentous (F) actin in a directional manner to form the actin cytoskeleton. The organization and rearrangement of the actin filaments is a dynamic process, and actin remodeling is regulated by various type of actin binding proteins (ABPs), which include formins, cofilins, thymosin, actin depolymerization factors (ADFs) and profilins (Figure 1.5). In particular, ADFs and profilins are involved in the polymerization and depolymerization of the actin filaments.

Profilin are an actin binding proteins and are some of the most abundant and highly conserved actin binding protein present in the cell (Jockusch et al., 2007). Profilins were first reported in 1976, where it was shown that profilins could inhibit actin monomer polymerization (Carlsson et al., 1976). In addition to binding actin monomers, profilin can also bind to poly-L-proline (PLP), and phosphoinositides, which are phospholipids. The binding of profilin to the cellular phospholipids suggests that profilin is playing a role in actin assembly at the plasma membrane. In addition, profilin can promote the exchange of ADP-actin to ATP-actin (Porta and Borgstahl, 2012; Wolven et al., 2000).

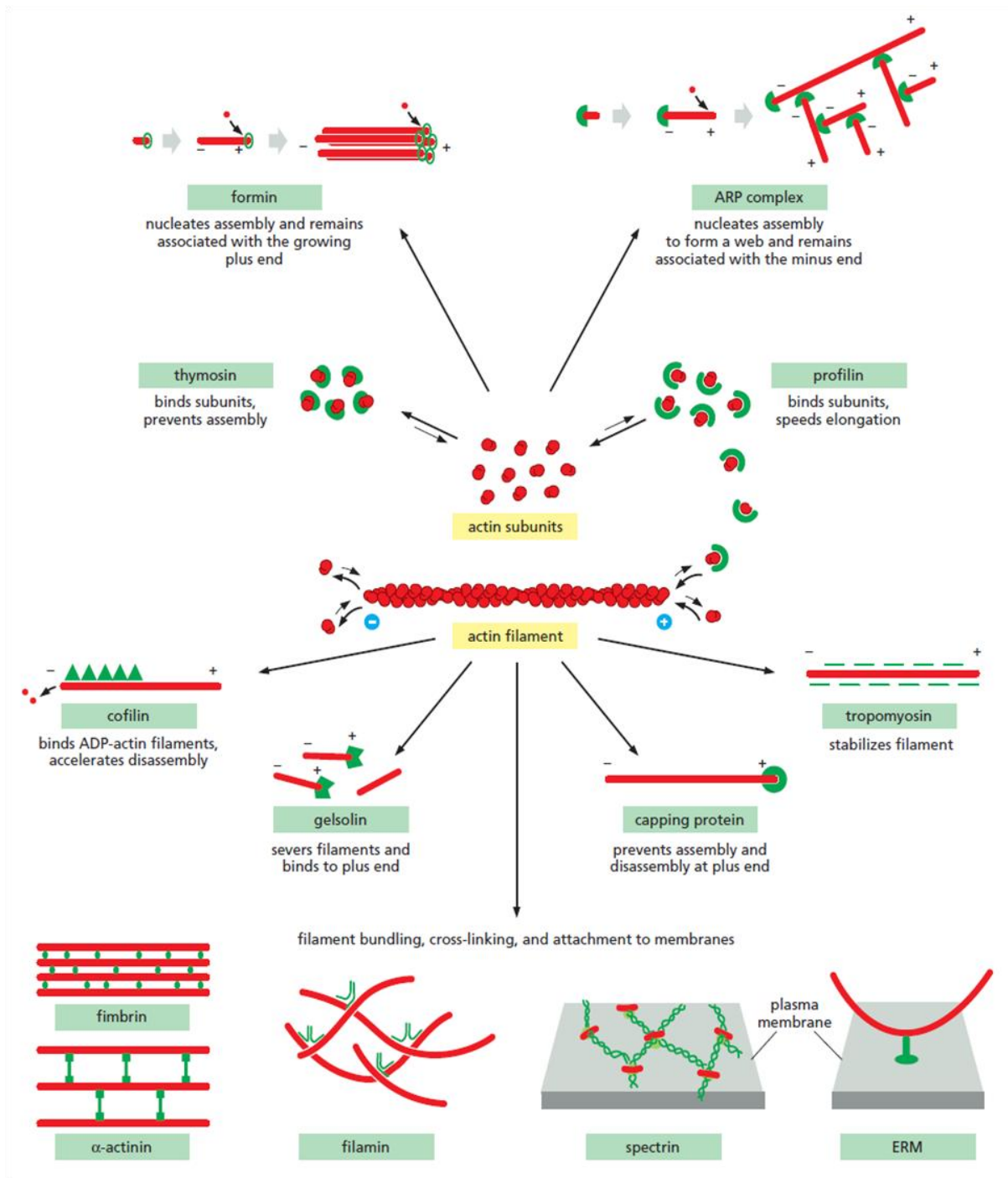


Figure 1.5. An example of major accessory proteins involve in actin cytoskeleton organization (Bruce Alberts et al., 2007).

Current evidence suggests that profilin can promote actin polymerization. By promoting the exchange of ADP for ATP, the ATP-actin monomers are ready to be polymerized into the actin filament. The profilin-actin complex only allows actin to be added on to the plus end of the growing filament and prevents actin monomer to be added at the minus end (Bruce Alberts et al., 2007). Conversely, profilin can also promote the depolymerization of the actin filament. Under high concentrations of profilin, for example, when it is injected into animal cells, profilin can cause actin filament depolymerization through G actin sequestration and through uncapping of actin filaments (Bubb et al., 2003). Thus, the functional role of profilin is complex and seems to be dependent on many factors, including the concentration of profilin in the cell (Yarmola and Bubb, 2006).

A nematode profilin may be acting as a plant profilin when secreted into the plant cell. Profilins exhibit relatively low (25%) amino acid conservation across kingdoms, but they are highly conserved across plant species (Sun et al., 2013). In Arabidopsis, there are 5 profilin isoforms (AtPRF1-AtPRF5). Three of the isoforms (AtPRF1-AtPRF3) are expressed in vegetative tissue. The other 2 isoforms (AtPRF 4 and AtPRF5) are specifically expressed in reproductive organs (Kandasamy et al., 2007). The vegetative profilins AtPFN1 and AtPFN2 share very high homology, with only 10 of the 131 amino acid residues differing. However, a recent study revealed that these two isoforms have different binding affinities for poly-L-proline and G actin, suggesting they have unique functional roles in the plant (Wang et al., 2009). AtPFN3 has an additional 36 amino acid residues at its N-terminus compared to the other vegetative isoforms. When AtPFN3 is overexpressed in plants, the plant exhibits a dwarf phenotype, presumably due to actin rearrangements (Fan et al., 2013). By using various knockout transfer DNA (T-DNA) insertion mutants and RNAi lines, the roles of the three vegetative profilins was recently further studied (Müssar et al., 2015). Single T-DNA insertion mutants for AtPFN2 and AtPFN4, *prf1-4* and *prf2-1*, showed defects in leaf and inflorescence development. AtPRF1 AtPRF2 AtPRF3 RNAi plants showed a dramatic dwarf phenotype and defects in lateral root growth. The phenotypes suggest that when profilin concentrations are too low, there is not enough actin-profilin complexes to promote cell elongation and this can lead to smaller plant size.

Root-knot nematodes are secreting effectors that may alter plant signaling and responses. The Gleason lab is interested in understanding these plant responses to RKN infection. In particular, signaling molecules like jasmonic acid have recently been proposed to play important roles in the nematode-plant interaction (Gutjahr and Paszkowski, 2009). Unfortunately, the most of the data was collected from non-model species, and different groups studying the role of JA in the plant-RKN interaction offer conflicting results. Here in this thesis, we are using *Arabidopsis thaliana* the model plant to reveal how JA is involved in plant-RKN interaction.

1.6 The jasmonic acid biosynthesis pathway

Jasmonic acid is a plant hormone that is important in defense against pathogens, particularly necrotrophic pathogens and herbivorous insects; it is also involved in plant growth development (Glazebrook, 2005; Mengiste, 2012).

In general, jasmonic acid biosynthesis pathway starts with the polyunsaturated α -linolenic acid (18:3), which is provided from ω -3 fatty acid desaturases acting on linoleic acid (18:2). Jasmonic acid may also be synthesized from hexadecatrienoic acid (16:3) (Weber, 2002). Next, the 16:3 and 18:3 fatty acids are oxygenated by either 9-lipoxygenases (LOX1 and LOX5) or 13-lipoxygenases (LOX2, LOX3, LOX4 and LOX6). The 13-LOX makes 13-hydroperoxy-octadecatrienoic acid (13-HPOT), which is a substrate for allene oxide synthase (AOS). The 9-LOX makes 9-hydroperoxy-octadecatrienoic acid, which modulates defence and lateral root formation (Vellosillo et al., 2007). The 13-HPOT undergoes additional enzymatic steps in the plastids/chloroplasts. Allene oxide synthase converts 13-HPOT to cyclase allene oxide, which is converted to *cis*-(+)-12-oxo-phytodienoic acid (*cis*-OPDA) or *dinor*-12-oxo-phytodienoic acid (*dn*-OPDA) by allene oxide cyclase (Stenzel et al., 2003). The OPDAs are then transported into peroxisome. *cis*-OPDA is converted to cyclo-pentanones by the peroxisomal enzyme OPR3. The resulting compounds, 3-oxo-2(2'*Z*)-pentenyl)-cyclopentane-1-octanoic acid (OPC8) and OPC6 respectively, are then subjected to β -oxidation by acyl-CoA oxidase (ACX) enzymes, leading to jasmonic acid (Stintzi and Browse, 2000). Jasmonic acid moves to the plant cytoplasm where it can be converted to many compounds, including (+)-7-iso-jasmonoyl-L-isoleucine (JA-Ile), which can bind to the JA-receptor COI1 in *Arabidopsis*.

Due to the intensive studies in JA biosynthesis genes and their corresponding mutants in Arabidopsis, we know that many of the knockout mutants in JA biosynthesis pathway exhibit a male sterile phenotype as well as increased susceptibility to necrotrophic pathogen and herbivorous insects (Laudert and Weiler, 1998; Verhage et al., 2011). For example, in Arabidopsis there are three ω -3 fatty acid desaturases, FAD3, FA7, and FAD8. The triple knockout fatty acid desaturase (*fad378*) mutant fails to produce JA because it lacks the substrate for JA biosynthesis (McConn and Browse, 1996), and this mutant is very susceptible to the fungal root pathogen *Pythium mastophorum* (Vijayan et al., 1998). In the case of the lipoxygenase enzymes, mutant studies have shown that LOX2 is responsible for JA production in leaf whereas LOX6 is a major player in JA production in Arabidopsis roots (Bannenberget al., 2009; Bell et al., 1995; Grebner et al., 2013). Arabidopsis double mutant *lox3 lox4* is male sterile (Caldelari et al., 2011). However, metabolic profiling showed that LOX3 and LOX4 are only partially involved in the JA production (Grebner et al., 2013). Downstream of the LOXs in the JA biosynthesis pathway is the enzyme allene oxide synthase (AOS). AOS has been considered as the major control point in JA biosynthesis pathway because it is encoded by a single gene in Arabidopsis (Laudert and Weiler, 1998). The Arabidopsis mutant in AOS is deficient in the production of all biologically active jasmonates (Park et al., 2002). As a result, the *aos* plants are more susceptible to necrotrophic and insect pathogens, similar to the mutant *fad378*. The last step of JA biosynthesis that occurs in plastids/chloroplasts involves allene oxide cyclase (AOC). In Arabidopsis there are 4 functional AOCs (AOC1, AOC2, AOC3 and AOC4) and the *aoc* mutants also exhibit a male sterile phenotype (Stenzel et al., 2003).

In the Arabidopsis, there are three genes encoding 12-oxophytodienoate reductases OPR1, OPR2 and OPR3. The OPR activity converts 9S,13S-OPDA to (OPC:8), which can be then converted to JA by further beta-oxidations. Only OPR3 is considered as a relevant enzyme for the JA biosynthesis pathway due to greatly reduced activity of OPR1 and OPR2 on the substrate 9S,13S-OPDA when compared to OPR3 (Schaller et al., 2000). The *opr3* mutant is male sterile (Stintzi and Browse, 2000). However, a recent report suggests that *opr3* is not a null mutant (Chehab et al., 2011). The last steps to produce JA are the beta oxidation steps, which in Arabidopsis, have been shown to be dependent on ACXs especially ACX1 and the enzyme closely related to ACX1 called ACX5. The double mutant *acx1/5* significantly reduces JA production when compared to wild type plant in response to wounding (Schillmiller et al., 2007).

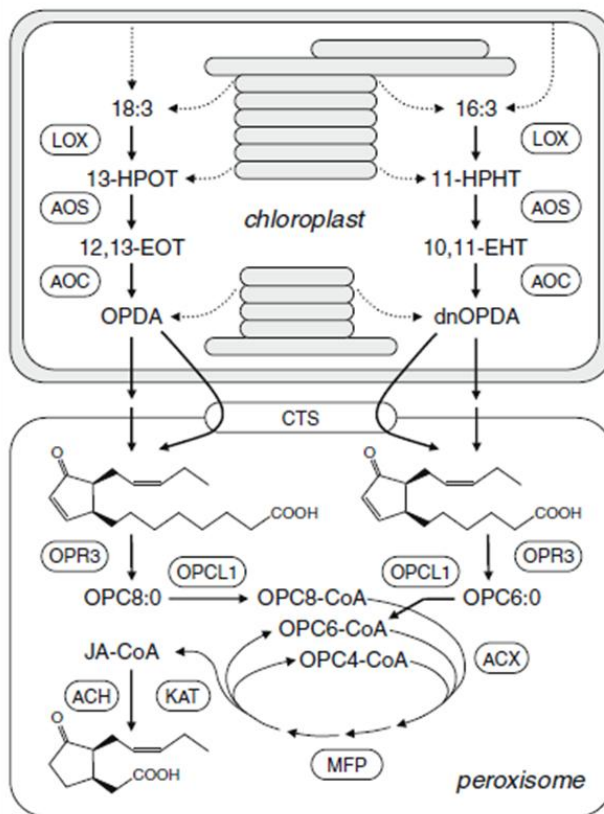


Figure 1.6 The jasmonic acid biosynthesis pathway in plants. The polyunsaturated fatty acids (18:3 and 16:3) are converted by lipoxygenases (9-LOXs and 13-LOXs), allene oxide synthase (AOS) and allene oxide cyclase (AOC) and the end products in chloroplast are 12-oxophytodenoic acid (OPDA) and dinor-OPDA. These products can then be transported from chloroplast/plastid into peroxisome and by the action of OPDA reductase 3 (OPR3) together with 3 beta-oxidation steps, produce jasmonic acid (Schaller and Stintzi, 2009).

1.7 Jasmonic acid signaling pathway

JA can modulate the expression of numerous genes involved in biotic and abiotic stress responses; in addition, JA plays key roles in regulating various plant developmental responses. In *Arabidopsis*, mutant work lead to the identification of the JA receptor called coronatine insensitive 1 (COI1), which can bind to (+)-7-*iso*-JA-I-Ile (JA-Ile), (Guranowski et al., 2007). COI1 encodes an E3 ubiquitin ligase in a Skp/Cullin/F-box complex (SCF^{COI1}), which can target proteins for degradation (Katsir et al., 2008a, 2008b; Thines et al., 2007). When JA levels are low, transcription factors, such as MYC2, are sitting at the target DNA sites. These transcription factors cannot promote gene expression because they are in a complex with negative regulators

called JAZ proteins (Kazan and Manners, 2013). JA-Ile can bind to the receptor SCF^{COI1} and the complex targets JAZ proteins for ubiquitination and subsequent degradation through 26S proteasome pathway. With the JAZ repressors gone, there is a release of suppression of the transcription factor MYC2 and potentially other JA transcriptional regulators (Kazan and Manners, 2013). The activation of the JA responsive genes can be determined by quantifying the induction of known JA dependent marker gene - vegetative storage protein 2 (VSP2) or JA-ET dependent marker gene - plant defensin 1.2 (PDF1.2) (Liu et al., 2005; Penninckx et al., 1998).

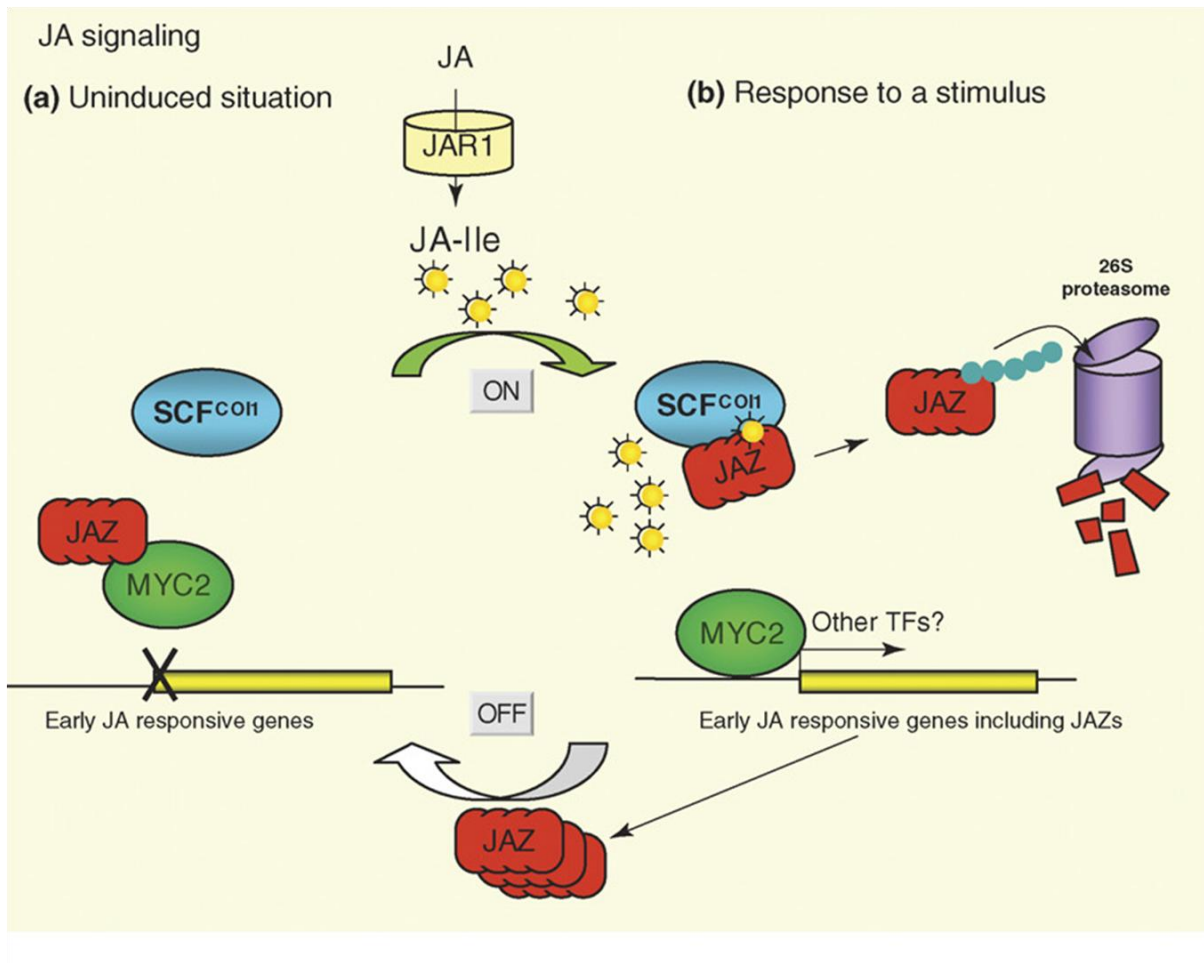


Figure 1.7. The jasmonic acid signaling pathway. In response to certain stresses, jasmonic acid is converted into jasmonic acid isoleucine (JA-Ile) which is the active form of JA. JA-Ile can interact with COI1 protein in SCF^{COI1} complex and change the conformation of COI1 protein. This interaction allows COI1 to interact with the JA repressor, jasmonate ZIM-domain proteins (JAZs), which generally suppress the transcription factors that drive JA responsive genes. The interaction between COI1 and JAZ leads to the degradation of JAZ protein by 26S proteasome and release transcription factors from JAZ suppression (Chico et al., 2008)

1.8 JA-triggered Immunity

Upon pathogen attack and wounding, JA is rapidly synthesized. The accumulation of JA, and the bioactive JA-Ile, leads to significant transcriptional reprogramming. This results in the enhanced expression of defense-related genes, including some pathogenesis-related genes, and the production of a wide array of major secondary metabolites such as alkaloids and terpenoids (De Geyter et al., 2012). JA can also cause morphological changes to the plant that can facilitate plant defense. For example, JA can induce anthocyanin accumulation and trichome initiation (Qi et al., 2011). Although COI1 is a key regulator in JA-mediated gene expression (Devoto et al., 2005), not all JA-responsive genes are COI1-dependent. Also, COI1-independent responses can be mediated by JA-precursors such as OPDA, which does not bind to COI1 (Stotz et al., 2013). This finding has been supported by the transcriptome analysis of OPDA and JA treated plants (Taki et al., 2005). Taki et al could show that OPDA could indeed trigger a distinct set of genes compared JA and some of these genes were COI1-independent (Mueller et al., 2008; Stintzi et al., 2001; Stotz et al., 2013; Taki et al., 2005).

1.9 The manipulation of JA pathway by pathogen effectors

To avoid plant defenses, pathogens have evolved sophisticated strategies in order to become successful. They can secrete a diverse range of molecules to bypass or suppress plant defenses. This exploitation of the plant defense mechanisms seem to be a common strategy among plant pathogens and a good example for the evolution arm race between plant and pathogens. For example, the bacterial pathogen *Pseudomonas syringae* generates toxins to contribute to disease. A well characterized bacterial toxin produced by several strains of *P. syringae*, including *P. syringae* pv *tomato* strain DC3000 (*Pst* DC3000), is called coronatine (COR) (Feys et al., 1994). Studies have shown that COR is a structural mimic of jasmonic isoleucine (JA-Ile) and it even can interact with COI1 with higher affinity than JA-Ile (Katsir et al., 2008b; Zheng et al., 2012). JA-mediated responses often act antagonistically against defense responses mediated by the phytohormone salicylic acid (SA). SA mediated defenses are responsible for plant protection against *P. syringae* infection. Therefore, COR abrogates SA-mediated defenses against this bacterial pathogen (Brooks et al., 2005; Devoto et al., 2005). Interestingly, recent study indicates

other effects from COR treatment, for example, *P. syringae* can invade the plant through the stomata, and COR facilitates this by preventing stomata closure (Geng et al., 2012).

Bacterial pathogens such as *P. syringae* can also secrete virulence proteins into the plant cell via their type three secretion system. At least two effectors from *P. syringae* (HopZ1a and HopX1) are secreted in the plant cell where they target the jasmonate ZIM-domain (JAZ) proteins. Bacterial pathogens are not alone in the manipulation of JA-signaling during plant infection. For example, the fungal pathogen *Fusarium oxysporum* produces bioactive jasmonic acids and exploits COII for disease development (Brodhun et al., 2013; Cole et al., 2014; Thatcher et al., 2009).

1.10 Jasmonic acid in plant defense against RKN

In general, when pathogens infect plants, they try to manipulate the plant defenses to their advantage. There is some evidence that the nematode is trying to suppress defenses during a compatible interaction. For example, transcriptome analysis of micro-dissected gall tissue showed that many defense genes were down-regulated during early giant cell formation (Barcala et al., 2010). In the feeding cells of the cyst nematode *Heterodera glycines*, JA-biosynthesis genes are specifically down-regulated (Ithal et al., 2007). This would suggest that JA promotes defence against the nematodes and the nematodes must actively try to suppress this response. In support of this hypothesis, exogenous MeJA treatment has been shown to induce resistance to RKN in a wide range of plants (tomato, spinach and rice). This suggests the MeJA application can counteract the nematode's suppression of plant defenses (Cooper et al., 2005; Nahar et al., 2011; Soriano et al., 2004). Therefore, it is plausible that activating JA-mediated defense pathways would result in enhanced nematode resistance. To support this hypothesis, Nahar et al showed that MeJA-induced expression of JA biosynthesis and defense genes in rice, including pathogenesis-related genes *OsPRIa* and *OsPRIb*, correlated with the rice resistance to RKN. Overall, it was concluded that JA is key player in plant defense against nematodes.

Unfortunately, understanding the role of JA in the plant nematode interaction has been complicated due to other data which indicates that JA is needed for nematode susceptibility. A

report showed that the JA perception mutant in tomato, *jail*, had significantly reduced *M. incognita* infection (Bhattarai et al., 2008). Furthermore, work in maize showed that a mutant in JA biosynthesis, *Zmlox3*, had increased levels of JA and was more susceptible to RKN (Gao et al., 2007). Lastly, a recent paper provided evidence that the 13-LOX members in Arabidopsis, *LOX3* and *LOX4*, were induced during RKN infection. Interestingly, the Arabidopsis *lox4-1* mutant however had increased levels of JA after RKN infection and showed enhanced RKN susceptibility (Ozalvo et al., 2014). With these results in mind, JA was proposed to be a nematode susceptibility factor rather than a defense molecule.

1.11 The aim of my thesis

Due to the devastating impact from RKNs on various crop plants, it is important to understand the compatible interaction between RKNs and plants.

Therefore, in this thesis I had two main aims:

- 1) The functional characterization of the *M. incognita* effector Mi131. RKN effectors are known to play a role in the compatible RKN-plant interaction. My aim is to find the interaction partner/s of the Mi131 effector in *Arabidopsis thaliana* and to further characterize the function of Mi131 effector based its interaction partner.
- 2) The plant responses to RKN infection during compatible interaction with focus on the phytohormone jasmonic acid. We generally know that phytohormones are important for both plant development and defense. There was conflicting data about the role of JA in the plant-nematode interaction. Therefore, my aim was to improve our understanding in the role of jasmonic acid in the RKN-plant interaction. By using a model plant *Arabidopsis thaliana*, I could utilize well-characterized JA signaling and biosynthesis mutants and try to understand the role of JA and JA-precursors in the plant-nematode interaction.

2. Materials and Methods

2.1 Materials

2.1.1 Devices

Listed below are the all the used devices that were used during the different experiments in this thesis (Table 2.1).

Table 2.1: Equipment used during the experiments of this thesis. Device type, model and producer are listed.

| Device | Model | Source |
|------------------------------------|---|----------------------|
| Analytical Balance | Extend | Sartorius |
| Autoclave | 3870 ELV | Tuttnauer |
| Autoclave | VX95 | Systec |
| Balance | SPO51 | Scaltec |
| Blotting Device (semi-dry) | | University Göttingen |
| Blotting Device (wet) | Criterion Blotter | BioRad |
| Chambers for SDS-PAGE | | University Göttingen |
| Chambers for SDS-PAGE | Mini-PROTEAN [®] tetra cell | BioRad |
| Chambers for Electroporation | | University Göttingen |
| Centrifugation model | Sorvall RC6+ | Thermo Scientific |
| Centrifugation rotor | F13S -14x50CY | Thermo Scientific |
| Chemocam | | Intas |
| Confocal laser scanning microscope | SP5 DM6000 | Leica |
| Cooling centrifuge | Rotina 38R | Hettich |
| Cooling micro centrifuge | Fresco17 | Thermo Scientific |
| Electroporator | Gene Pulser [®] II | BioRad |
| Fluorescence microscope | DM5000 B | Leica |

| | | |
|--------------------------------------|---------------------------|--------------------------|
| Gel documentation device | | MWG Biotech |
| Heating block | TH26 | HLC |
| Heated shaker | MHR11 | HLC |
| Heated stirrer | IKA® RH basic 2 | IKA |
| Incubator | Certomat BS-1 | Sartorius stedim biotech |
| Ice machine | | Ziegra |
| Microcentrifuge | Pico17 | Thermo Scientific |
| Microscope | DM5000B | Leica |
| PCR Cycler | MyCycler | BioRad |
| pH-Meter | pH211 | Hanna Instruments |
| Plant growth chamber | | Percival scientific |
| qRT-PCR cycler | iCycler | BioRad |
| RNA-/DNA/protein-Calculator | NanoDrop 2000 | Thermo Scientific |
| SDS gel documentation camera | | Intras |
| Sonicator | Soniprep 150 | MSE |
| Sterile bench for plant and nematode | Heraguard | Thermo Scientific |
| Sterile bench for bacteria and yeast | SAFE 2020 | Thermo Scientific |
| Water deionization device | arium® pro DI | Sartorius |
| Vacuum pump | Cyclo 1 | Roth |
| Vortex | Vortex Genie 2 | Scientific Industries |
| Ultracentrifugation model | WX Ultra 100 | Thermo Scientific |
| Ultracentrifugation rotor | FIBERLite® F50L 24x1.5 | Thermo Scientific |
| 96 well plate reader | Synergy HT | Biotek |

2.1.2 Consumables

Consumable products are listed in the table below. The product specification and the producer are indicated (Table 2.2).

Table 2.1: Disposable materials used. Product type and producer are presented.

| Product | Producer |
|--|--|
| Blotting paper 3MM | Whatmann |
| Cover slips | Roth |
| Disposable sterile filter | Thermo Scientific |
| Kim-Tech-Science (KimWipes) | Kimberly-Clark |
| Leukopor® | BSNmedical |
| Micotiter plates 96-wells flat bottom | Sarstedt |
| Object plates | Roth |
| Parafilm M | Pechiney Plastic Packaging |
| Plastic one-way material | Biozym, Eppendorf, Greiner, Roth, Sarstedt |
| PVDF membrane Immobilon-P | Milipore |
| Tissue Culture Plate Square 100mmx100mmx20mm | Sarstedt |
| Tissue Culture Plate 6 well | Sarstedt |
| 1.5 ml ultra microtube | Thermo Scientific |

2.1.3 Chemicals

The chemicals used in buffers and media are listed in the table below. The name of the chemical compound and the corresponding manufacturer are indicated (Table 2.3).

Table 2.2: Chemical compounds that were used in the different experiments. Chemical description and producer are presented.

| Chemical | Source |
|---|----------------------------|
| Acid fuchsin | Applicam |
| Acetic acid | Roth |
| 30 % (w/v) Acrylamide: N,N'-methylenebisacrylamide (37.5:1) | Roth |
| Agarose | Biozym |
| Ampicillin (Amp) | AGS |
| Anti-Actin-11 (mAb2345a) | Kerafast |
| Anti-Actin-1 (mAb45a) | Kerafast |
| Anti- α -GFP antibody | Roche |
| Anti-Rabbit Ig biotinylated | Amersham Pharmacia Biotech |
| Anti-HA antibody | Abcam |
| Anti-Mi131 antibody | Eurogentec |
| Anti-Mouse Ig biotinylated | Amersham Pharmacia Biotech |
| APS (Ammonium persulfate) | Biometra |
| BASTA | Raiffeisen Lagerhaus GmbH |
| Bromophenol blue | Roth |
| BSA | Serva/Cytoskeleton |
| Calcium chloride | Roth |
| Cellulase | Sigma |
| Commercial bleach | Dan Klorix |

| | |
|--|-------------------|
| Coronatine | Sigma |
| Daishin Agar | Duchefa Direct |
| Dithiothreitol (DTT) | Roth |
| dNTPs | MBI |
| EDTA | Applichem |
| Ethidiumbromide | Roth |
| Fat-free milk powder | Sucofin ® |
| Fish sperm DNA | Roche Diagnostics |
| Fluoresceine | BioRad |
| Gelrite | Duchefa |
| GFP-Trap® | Chromotek |
| Gentamycine (Gent) | Duchefa |
| Glycerine (86% and 99.5%) | Roth |
| Hydrochloric acid | Roth |
| Hypochloric solution | Sigma Aldrich |
| Kanamycine (Kan) | Sigma |
| Macerozyme | Serva |
| Magnesium chloride | Hilmer Brauer |
| Magnesium Sulfate | Hilmer Brauer |
| Mannitol | Roth |
| β-Mercaptoethanol | Roth |
| Methyl Jasmonate | Sigma Aldrich |
| MES | Roth |
| Murashige and Skoog medium (MS medium) | Duchefa |
| Nonidet P40 (NP40) | Sigma |
| Orange G | Sigma |
| Peptone | BD Biosciences |

| | |
|---|---------------------|
| Phenol | Sigma |
| Pierce® 660 nm Protein assay reagent | Thermo Scientific |
| Potassium chloride | Carl Roth GmbH |
| Protease inhibitor | Boehringer Mannheim |
| Ionic detergent compatibility reagent | Thermo Scientific |
| Isopropanol | Roth |
| Ribonucleic acid from Yeast | AppliChem |
| Rifampicine (Rif) | Duchefa |
| Polypropylene glycol 4000 | Sigma |
| Polypropylene glycol 6000 | Roth |
| Profinity™ IMAC Ni-Chared Resin | Biorad |
| Select Agar | Life Technologies |
| Select yeast extract | Gibco BRL |
| Sodium chloride | Roth |
| Sodium lauryl sulfata (SDS) | Roth |
| Sucrose | Roth |
| SuperSignal™ West Femto Maximum Sensitivity Substrate | Thermo Scientific |
| SYBR Green I | Cambrex |
| TEMED | Roth |
| Tryptone | Oxoid |
| Tween20 | Roth |
| Yeast Nitrogen base extract | Difco Laboratory |

2.1.4 Media

Tables below represent all the media and their compositions used in this thesis are listed.

MS plant media

Table 2.3: Composition Murashige and Skoog plant media. Ingredients and corresponding quantities are presented.

| Ingredient | Amount per 500 ml |
|---------------------------------------|-------------------|
| MS basalt salt mixture incl. Vitamins | 2.2 g |
| Sucrose | 10 g |
| Adjust pH to 5.7 | - |
| H ₂ O | to 500 ml |
| Add Gelrite for solid media | 3.4 g |

KNOPs media (Sijmons et al., 1991)

Table 2.4: Composition KNOPs media. Ingredients and corresponding quantities are presented.

| Ingredient | Amount per 500 ml |
|----------------------------------|-------------------|
| 10xKNOPs salt stock | 50 ml |
| Sucrose | 5 g |
| Adjust pH to 6.4 | - |
| H ₂ O | to 500 ml |
| Add Daishin agar for solid media | 3.4g |

KNOPs 10x salt stock

Table 2.6: Composition of the 10x salt stock for KNOPs. Ingredients and corresponding quantities are presented.

| Ingredient | Amount per 1 l |
|---|----------------|
| MgSO ₄ | 0.488 g |
| Ca(NO ₃) ₂ 4H ₂ O | 2.999 g |
| KH ₂ PO ₄ | 2.041 g |
| KNO ₃ | 1.28 g |
| 72mM FeEDTA | 2.77 ml |
| 2000x micronutrient stock | 5 ml |
| H ₂ O | to 1 l |

2000x micronutrient stock (KNOPs)

Table 2.7: Composition of the 2000x micronutrient stock for KNOPs. Ingredients and corresponding quantities are presented.

| Ingredient | Amount per 1l |
|---|---------------|
| MnSO ₄ | 0.55 g |
| ZnSO ₄ | 0.080973 g |
| CuSO ₄ | 0.029962 g |
| CoCl ₂ 6H ₂ O | 0.011422 g |
| H ₃ BO ₃ | 1.11294 g |
| Na ₂ MoO ₄ H ₂ O | 0.0510 g |
| MgCl ₂ 6H ₂ O | 0.69122 g |
| NaCl | 0.226747 g |
| KCl | 0.33 g |
| H ₂ O | to 1 l |

LB medium

Table 2.8: Composition of LB medium. Ingredients and corresponding quantities are presented.

| Ingredient | Content (end concentration) per 1l |
|------------------|-------------------------------------|
| Tryptone | 10 g |
| Yeast extract | 5 g |
| NaCl | 10 g |
| Adjust pH to 7 | |
| H ₂ O | To 1l |

YEB medium

Table 2.9: Composition of YEB medium. Ingredients and corresponding quantities are presented.

| Ingredient | Content (end concentration) per 1l |
|---------------------------------|---------------------------------------|
| Beef extract | 10 g |
| Yeast extract | 2 g |
| Peptone | 5 g |
| Sucrose | 5 g/L sucrose |
| Adjust pH to 7.0 | |
| H ₂ O | To 1l |
| 1 M MgSO ₄ (sterile) | add 2 ml for 2 mM final concentration |

YPAD (500 ml)

Table 2.10: Composition of YPAD medium. Ingredients and corresponding quantities are presented.

| Ingredient | Amount per 500 ml |
|---|-------------------|
| Difco peptone | 10 g |
| Yeast extract | 5 g |
| adenine | 50 mg |
| Adjusted pH to 5.8 with KOH | |
| H ₂ O | To 450 ml |
| Select agar for solid media | 9 g |
| 40% sucrose added when the media is at RT | 50 ml |

Yeast transformation medium

Table 2.11: Composition of the yeast transformation medium. Ingredients and corresponding quantities are presented.

| Ingredient | Amount per reaction |
|---|---------------------|
| 50 % PEG4000 (filter sterilized) | 240 µl |
| 1M LiAC pH 7.5 (filter sterilized) | 36 µl |
| Single-stranded DNA(denatured by boiling at 100 °C for 10 minutes) from fish sperm (2mg/ml) | 25 µl |
| Plasmid | 250-500 ng |

Semi-solid SC (synthetic complete) drop out medium for Y2H screen (SC –LWH)

Table 2.12: Semi-solid SC media composition. Ingredients and corresponding quantities are presented.

| Ingredient | Amount per 500 ml | Final concentration |
|--|-------------------|---------------------|
| Difco yeast nitrogen base | 3.35 g | |
| CSM -Ade - His -Trp -Leu | 0.305 g | |
| Adenine | 60 mg | |
| H ₂ O | to 450 ml | |
| Autoclave at 121°C for 15 minutes | | |
| 1% gelrite (autoclaved and immediately added to SC drop out media) | 25 ml | 0.05 % |
| 40% sucrose(added when the media temperature is around 55°C) | 50 ml | 2 % |
| 1 M 3-amino-1,2,4-triazole solution (if required) | 2.5 ml | 5 mM |
| Ampicilin stock conc. 100mg/ml (if required) | 500 µl | 100 µg/µl |

Synthetic Complete dropout (SC dropout) medium

Table 2.13: Composition SC dropout media for yeast. Ingredients and corresponding quantities are presented.

| Ingredient | Amount per 500 ml | Final concentration |
|---|-------------------|---------------------|
| Difco yeast nitrogen base (W/O amino acid) | 3.35 g | |
| *General list of amino acid, specific drop out medium can be made by leaving out the amino acid of choice | | |
| Arginine | 25 mg | |
| Aspartic acid | 40 mg | |
| Histidine | 10 mg | |
| Isoleucine | 25 mg | |
| Leucine | 50 mg | |
| Lysine | 25 mg | |
| Methionine | 10 mg | |
| Phenylalanine | 25 mg | |
| Threonine | 50 mg | |
| Tryptophan | 25 mg | |
| Tyrosine | 25 mg | |
| Uracil | 10 mg | |
| Valine | 70 mg | |
| Serine | 10 mg | |
| Adenine | 60 mg | |
| **Alternatively use commercially available amino acid dropout mixtures | | |
| Adjust pH to 5.6 with KOH | | |
| H ₂ O | to 450 ml | |
| Selected agar (for solid media) | 9 g | |
| 40% sucrose (added when the media temperature is around 55°C) | 50 ml | 2% |

| | | |
|--|--------|-----|
| 1 M 3-amino-1,2,4-triazole solution (if required) | 2.5 ml | 5mM |
|--|--------|-----|

2.1.5 Buffers

Below listed in tables are all buffers used in the experiments describes in this thesis.

Immunoprecipitation extraction buffer (50 ml)

Table 2.14: Composition of the immunoprecipitation extraction buffer. Ingredients, amounts and the final concentration of the corresponding ingredient are presented.

| Ingredient | Amount | Final concentration |
|--|-------------|---------------------|
| 1 M Tris-HCl | 2.5 ml | 50 mM |
| 5 M NaCl | 1.5 ml | 150 mM |
| 0.5 M EDTA | 100 μ l | 1 mM |
| 1 M Dithiotheritol (DTT) stock | 250 μ l | 5 mM |
| NP40 | 100 μ l | 0.2 % |
| 100x Protease inhibitor (excluded Protease inhibitor for wash buffer) | 100 μ l | 1x |
| H ₂ O | to 50 ml | |

Acrylamide gel for Western blot

Table 2.15: Acrylamide gel composition used for running gel. Ingredients, amounts and the final concentration of the corresponding ingredient are presented.

| Ingredient | Amount per 20 ml | Final concentration |
|-----------------------|------------------|---------------------|
| Acrylamide | 2.68-13.3 ml | 4-20% |
| 1.5 M Tris-HCl pH 8.8 | 5 ml | 375 mM |
| H ₂ O | 11.9 – 1-28 ml | |
| 10% APS | 200 μ l | 1 % |
| 10% SDS | 200 μ l | 1 % |
| TEMED | 20 μ l | |

Table 2.16: Acrylamide gel composition used for stacking gel. Ingredients, amounts and the final concentration of the corresponding ingredient are presented.

| Ingredient | Amount per 5 ml | Final concentration |
|---------------------|-----------------|---------------------|
| Acrylamide | 670 μ l | 4% |
| 1 M Tris-HCl pH 6.8 | 625 μ l | 0.125 mM |
| H ₂ O | 3.6 ml | |
| 10% APS | 50 μ l | 1 % |
| 10% SDS | 50 μ l | 1 % |
| TEMED | 5 μ l | |

Blocking buffer

Table 2.5: Composition of the blocking buffer for Western blot. Ingredients, amounts and the final concentration of the corresponding ingredient are presented.

| Ingredient | Amount per 20 ml | Final concentration |
|--|------------------|---------------------|
| Skimmed milk powder (Sucofin ®) | 0.4 g | 2 % |
| Added TBST to 20 ml | | |
| First or secondary antibody (if needed) | 4 μ l | 1:5000 |

Transfer buffer (1L)

Table 2.6: Composition of the transfer buffer used for Western blot. Ingredients, amounts and the final concentration of the corresponding ingredient are presented.

| Ingredient | Amount per 1l | Final concentration |
|------------------|---------------|---------------------|
| Tris | 5.82 g | 48 mM |
| Glycin | 2.93 g | 39 mM |
| 20% SDS | 2 ml | 0.04% |
| MeOH | 200 ml | 20% |
| H ₂ O | to 1 liter | |

10X running buffer (1L)

Table 2.7: Composition of concentrated running buffer for SDS-PAGE. Ingredients, amounts and the final concentration of the corresponding ingredient are presented.

| Ingredient | Amount per 1l | Final concentration |
|------------------|---------------|---------------------|
| Tris | 30.24 g | 250 mM |
| Glycin | 142.75 g | 1.9 M |
| 20% SDS | 50 ml | 1 % |
| H ₂ O | to 1 liter | |

10xTBS (1L)

Table 2.8: Composition of concentrated 10xTBS buffer. Ingredients, amounts and the final concentration of the corresponding ingredient are presented.

| Ingredient | Amount per 1l | Final concentration |
|---------------------------|---------------|---------------------|
| Tris | 24.2 g | 200 mM |
| NaCl | 80 g | 1.37 M |
| Adjust pH to 7.6 with HCl | | |
| H ₂ O | to 1 liter | |

1x TBST

Table 2.21: Composition of TBS working solution. Ingredients, amounts and the final concentration of the corresponding ingredient are presented.

| Ingredient | Amount | Final concentration |
|-----------------------------------|--------|---------------------|
| 10X TBS | 100 ml | 1x |
| Tween 20 | 1 ml | 0.1% |
| Added H ₂ O to 1 liter | | |

40% PEG 4000

Table 2.22: Composition of 40% PEG 4000 solution. Ingredients, amounts and the final concentration of the corresponding ingredient are presented.

| Ingredient | Amount per 50 ml |
|----------------------------------|------------------|
| PEG4000 | 20 g |
| 0.75 M Mannitol | 13.3 ml |
| 1M CaCl ₂ | 5 ml |
| H ₂ O | to 50 ml |
| Filter sterile and store at 4 °C | |

Enzyme solution

Table 2.23: Composition of enzyme solution. Ingredients, amounts and the final concentration of the corresponding ingredient are presented.

| Ingredient | Amount per 50 ml |
|----------------------------------|------------------|
| Cellulase | 0.625 g |
| Maceroenzyme | 0.150 g |
| 0.75 M Mannitol | 26.6 ml |
| 0.5 M KCL | 2 ml |
| 0.5 M MES | 2 ml |
| 1M CaCl ₂ | 5 ml |
| H ₂ O | to 50 ml |
| Filter sterile and store at 4 °C | |

W5 buffer

Table 2.24: Composition of W5 buffer. Ingredients, amounts and the final concentration of the corresponding ingredient are presented.

| Ingredient | Amount per 50 ml |
|----------------------------------|------------------|
| 1M NaCl | 7.7 ml |
| 1M CaCl ₂ | 6.25 ml |
| 0.5 M KCl | 0.5 ml |
| 0.5 M MES | 0.2 ml |
| H ₂ O | to 50 ml |
| Filter sterile and store at 4 °C | |

Wi buffer

Table 2.25: Composition of Wi buffer. Ingredients, amounts and the final concentration of the corresponding ingredient are presented.

| Ingredient | Amount per 50 ml |
|----------------------------------|------------------|
| 0.75M Mannitol | 33.3 ml |
| 0.5M KCl | 2 ml |
| 0.5M MES | 0.4 ml |
| H ₂ O | to 50 ml |
| Filter sterile and store at 4 °C | |

MMG buffer

Table 2.26: Composition of MMG buffer. Ingredients, amounts and the final concentration of the corresponding ingredient are presented.

| Ingredient | Amount per 50 ml |
|----------------------------------|------------------|
| 0.75M Mannitol | 26.6 ml |
| 0.5M MgCl ₂ | 1.5 ml |
| 0.5M MES | 0.4 ml |
| H ₂ O | to 50 ml |
| Filter sterile and store at 4 °C | |

Acid fuchsin staining

Table 2.27: Composition of acid fuchsin staining. Ingredients, amounts and the final concentration of the corresponding ingredient are presented.

| Ingredient | Amount per 1l |
|---------------------|---------------|
| Acid fuchsin | 3.5 g |
| Glacial acetic acid | 250 ml |
| H ₂ O | to 1l |

Acidified glycerol

Table 2.28: Composition of acidified glycerol. Ingredients, amounts and the final concentration of the corresponding ingredient are presented.

| Ingredient | Amount |
|------------|-----------|
| Glycerine | 20-30 ml |
| 5N HCl | Few drops |

Lysis buffer

Table 2.29: Composition of lysis buffer. Ingredients, amounts and the final concentration of the corresponding ingredient are presented.

| Ingredient | Amount for 1l |
|--------------------|---------------|
| 1M Tris-HCL pH 8.0 | 100 ml |
| 2M NaCl | 75 ml |
| H ₂ O | to 1l |

His-purification wash buffer

Table 2.30: Composition of His-purification wash buffer. Ingredients, amounts and the final concentration of the corresponding ingredient are presented.

| Ingredient | Amount for 1l |
|-------------------------------------|---------------|
| 1M NaHPO ₄ | 3.4 ml |
| 1M Na ₂ HPO ₄ | 46.6 ml |
| 2M NaCl | 150 ml |
| 1M Imidazole | 5 ml |
| H ₂ O | to 1l |

His-purification elusion buffer

Table 2.31: Composition of His-purification elusionbuffer. Ingredients, amounts and the final concentration of the corresponding ingredient are presented.

| Ingredient | Amount for 500ml |
|-------------------------------------|------------------|
| 1M Na ₂ HPO ₄ | 25 ml |
| 2M NaCl | 75 ml |
| 1M Imidazole | 250 ml |
| H ₂ O | to 500 ml |

DNA extraction buffer

Table 2.32: Composition of His-purification elutionbuffer. Ingredients, amounts and the final concentration of the corresponding ingredient are presented.

| Ingredient | Final concentration |
|-----------------|---------------------|
| Tris-HCl pH 7.5 | 0.2 M |
| NaCl | 1.25 M |
| EDTA | 0.025 M |
| SDS | 0.5% |

2.1.6 Primers

This section presents the primers used for qRT-PCR (Table 2.33) and cloning (Table 2.34). Primers for qRT-PCR were designed using Primer3 (Rozen and Skaletsky, 1998).

Oligonucleotides for qRT-PCR

Table 2.33: Sequence list of used qRT-PCR primers in the direction 5'-3'. Name of the primer and the corresponding sequence are presented.

| Name of nucleotide | Sequence 5' - 3' |
|--------------------|--------------------------------|
| AOS F | TTTGAGGCATGTGTTGTGGT |
| AOS R | CTTACCGGCGCATTGTTTAT |
| FAD3 F | TTTCTGGGCCATCTTTGTTC |
| FAD3 R | CGAGTACTGTGGGGCAATTT |
| FAD7 F | TGAACAGTGTGGTCCGGTCAT |
| FAD7 R | GCATCACGAGAGGCAGTGTA |
| LOX1 F/R | Qiagen quantitect (QT00881174) |
| OPR3 F | AAGCAGTTCACGCTAAGGGA |
| OPR3 R | CCGAGATTGGTTTGTTCGTT |
| MPK3 F/R | Qiagen quantitect (QT00785645) |
| GST6 F/R | Qiagen quantitect (QT00725697) |
| VSP2 F | CAAACCTAAACAATAAACCATACCATAA |
| VSP2 R | GCCAAGAGCAAGAGAAGTGA |

Oligonucleotides for cloning, genotype and control amplifications (excluding Att sites)

Table 2.34: List of primers used for cloning. Name of the primer and the corresponding sequence are presented.

| Name of nucleotide | Sequence 5' - 3' |
|----------------------------------|--|
| Actin 1 F | GGGGACAAGTTTGTACAAAAAAGCAGGCTTCAACATGGCTGATGGT GAAGACATTC |
| Actin 1 R | GGGGACCACTTTGTACAAGAAAGCTGGGTCTCAGAAGCACTTCCTG TGAACA |
| Actin 2 F | GGGGACAAGTTTGTACAAAAAAGCAGGCTTCAACATGGCTGAGGCT GATGATAT |
| Actin 2 R | GGGGACCACTTTGTACAAGAAAGCTGGGTCTTAGAAACATTTTCTG TGAA |
| Actin 7 F | CACCATGGCCGATGGTGAGGATAT |
| Actin 7 R | TTAGAAGCATTTCTGTGAA |
| Actin 8 F | GGGGACAAGTTTGTACAAAAAAGCAGGCTTCAACATGGCCGATGCT GATGACAT |
| Actin 8 R | GGGGACCACTTTGTACAAGAAAGCTGGGTCTTAGAAGCATTTTCTG TGGA |
| COII LP | TGGACCATATAAATTCATGCAGTCAACAAC |
| COII RP | CTGCAGTGTGTAACGATGCTCAAAAGTC |
| LBB1.3 | ATTTTGCCGATTTTCGGAAC |
| LRR6 F | GGGGACAAGTTTGTACAAAAAAGCAGGCTTCAACATGAGAGAAGA CACCTTCTT |
| LRR6 R | GGGGACCACTTTGTACAAGAAAGCTGGGTCTTAGTAATGCACCGGC GTTG |
| Mi131 F | CACCATGTCTTGGCAAGATCTAGTTAACA |
| Mi131 R | TTAATAATTGATGCTTCGAAAGTAA |
| Mi131 R without stop codon | ATAATTGATGCTTCGAAAGTAA |

| | |
|----------|--|
| TRAPP F | CACCATGGCTCCGGTTGGTCCTCG |
| TRAPP R | TTATTCATCATCCTTGTAAG |
| RPA32B F | CACCATGTACGGAGGCGATTTTGA |
| RPA32B R | TCAAGCGTTAGCAGTCGATT |
| GTL1 F | GGGGACAAGTTTGTACAAAAAAGCAGGCTTCAACATGGAGCAAGG AGGAGGTGG |
| GTL1 R | GGGGACCACTTTGTACAAGAAAGCTGGGTCTTACTGAACCATTGTC AAGAA |
| ERD15 F | CACCATGGCGATGGTATCAGGAAG |
| ERD15 R | TCAGCGAGGCTGGTGGATGT |

2.1.7 Organisms

This section lists the organisms used during this thesis. Antibiotic resistance is also mentioned, if applicable (Table 2.35).

Table 2.34: Organisms used during the experiments of this thesis. Name of organism, resistance conditions, and the use of the specific organism are presented.

| Organism | Selection resistance (µg/ml) | Use |
|---|------------------------------|--------------------------------------|
| <i>Agrobacterium tumefaciens</i> – GV3101 | Rif (25), Gent (25) | Stable transformation of Arabidopsis |
| <i>Escherichia coli</i> DH5α | - | Plasmid production |
| <i>Escherichia coli</i> BL21 | - | Protein expression |
| <i>Meloidogyne hapla</i> – VW9 | - | Infection |
| <i>Meloidogyne incognita</i> – “Morelos” | - | Infection, cloning |
| <i>Arabidopsis thaliana</i> -Col-0 | - | Analysis, transformation and etc |
| <i>Solanum lycopersicum</i> – “Green Zebra” | | Nematode multiplication |
| Yeast “AH109” (provided by Joachim Uhrig) | - | Library screen |
| Yeast “Y190” (provided by Joachim Uhrig) | | Yeast-two-library screen |

2.1.8 Plasmids

Below all plasmids are listed that were used either for cloning or directly for experiments. Plasmid name, use, and antibiotic resistance are shown (Table 2.36).

Table 2.36: Plasmids that were used for cloning or experimental procedures. Plasmid name, its use, and the resistance for selection in bacteria and plant are presented.

| Plasmid | Use | Resistance |
|---------------|---|------------|
| pDonr201 | Entry vector | Kan |
| pEnTR | Entry vector | Kan |
| pB2GW7 | Expression vector for Arabidopsis transformation | Spec/Basta |
| pUBC-YFP-dest | Expression vector for Arabidopsis transformation /NB transient expression | Spec |
| pUBQ10GW7 | Expression vector for NB transient expression | Spec |
| pK7WG2 | Expression vector for Arabidopsis transformation | Spec/Kan |
| pB7WGF2 | Expression vector for Arabidopsis transformation /NB transient expression | Spec/Basta |
| pB7WGR2 | Expression vector for NB transient expression | Spec/Basta |
| pASII | Bait vector for yeast-two-hybrid | Amp |
| pGAD-1 | Fish vector for yeast-two-hybrid | Amp |
| pDEST17 | Protein expression vector | Amp |
| pGP172GW | Protein expression vector | Amp |
| pCAMBIA2300 | Expression vector for Arabidopsis transformation /NB transient expression | Kan/Kan |

2.1.9 Kits

The table below presents the kits used during this thesis (Table 2.37).

Table 2.37: List of kits used during this thesis. Kit name and producer are presented.

| Kit name | Producer |
|--|------------------|
| NucleoSpin Gel and PCR Clean Up | Macherey & Nagel |
| NucleoSpin Plasmid | Macherey & Nagel |
| Actin binding protein Biochem kit (Non-muscle actin) Cat. #BK013 | Cytoskeleton |

2.2 Methods

2.2.1 General molecular methods

Phusion DNA polymerase reaction – High fidelity amplifications

Amplification was performed according to the manufacturer's protocol. An example reaction is presented in the table below. An example cycler protocol to amplify a fragment of less than 500bp is presented (Table 2.38-2.39).

Table 2.38: Contents of a standard Phusion DNA Polymerase amplification mix. Components and corresponding quantities are presented.

| Stock component | Volume in 40 μ l reaction |
|-----------------------------|-------------------------------|
| Buffer (HF/GC) 5x | 8 μ l |
| dNTPs 40mM (10 mM each) | 0.8 μ l |
| Forward primer (10 μ M) | 2 μ l |
| Reverse primer (10 μ M) | 2 μ l |
| Template | 1 μ l (~50 ng) |
| Polymerase | 0.2 |
| H ₂ O | 24.6 |

Table 2.39: Standard PCR cycler program to amplify a fragment of 500b. Cycle step, temperature and cycle numbers are presented.

| Cycle step | Temperature and duration | Cycles |
|----------------------------|--------------------------|--------|
| Initial denaturation | 98°C, 30 sec | 1 |
| Denaturation | 98°C, 30 sec | 40 |
| Annealing (can be changed) | 55°C, 30 sec | |
| Extension | 72°C, 30 sec | |
| Final extension | 72°C, 5 min | 1 |

Measurement of DNA and RNA concentrations

The concentration of nucleic acids was determined by measuring their absorption in a NanoDrop 2000 at a wave length of 260 nm (maximum nucleic acid absorption value, due to the π -electron systems of the heterocycles of the nucleotides). Absorption at 280 nm (due to the presence of aromatic rings from amino acids and phenol compounds) was used for references of the purity of the DNA or RNA samples. The optimal ratio of OD_{260}/OD_{280} for RNA is from 1.9-2.0 and for DNA 1.8.

Separation of DNA on agarose gels

The DNA was separated by electrophoresis in horizontal gel chamber filled with 1x TAE buffer. The agarose gel concentration was either 2 % agarose (< 500 kb) or 1.0 % agarose (< 4000 bp), depending on the size of the DNA fragments to be separated. DNA samples were mixed with 1/10 volume of 10x DNA loading buffer, loaded in separate lanes and run at 120 V for 45 min. The gels were stained in ethidium bromide solution (0.1 % w/v) for 15 min, and the detection of the DNA was performed on an UV-transilluminator (260 nm). The signals were documented with a gel-documentation station. For elution of DNA fragments from the gel the visualization was done with larger wavelength UV-light (320 nm) and the DNA fragments in the gel slices were eluted with the NucleoSpin® Gel and PCR Clean-up Kit (Macherey-Nagel).

Gateway cloning

The Gateway® technology is based on the site specific recombination of bacteriophage lambda and thereby provides a fast method to exchange DNA fragments between multiple vectors without the use of conventional cloning strategies (Hartley et al., 2000; Landy, 1989). All cloning steps done with the Gateway® system were performed as described in the Invitrogen manual, Version E, September 22, 2003. Briefly, the Gateway BP II Clonase enzyme kit was used according to the manufacturer's instructions to transfer PCR fragments into the entry vector pDONR207. For introduction into the destination vectors, LR reactions were composed of the entry clone, the destination vector (150 ng/ μ l) and 2 μ l LR Clonase II. After incubation at room temperature for 1 hour, the reaction was used to transform *Escherichia coli* strain DH5 α .

Isolation of high-quality plasmid DNA

High-purity plasmid DNA was isolated for sequencing, cloning and transformation according to the manufacturer instructions of the Macherey-Nagel Mini, Midi and Maxi KitNucleoSpin Kits.

Sequencing of DNA

Sequencing of plasmid DNA was performed at GATC Biotech. A minimum 400 ng plasmid DNA was mixed with 25 pmol required primer and water was added to a final volume of 10 μ L.

Transformation of *Escherichia coli*

The transformation of chemical competent *E. coli* DH5 α cells was done with the heat shock method according to (Hanahan, 1983). An aliquot of competent cells (200 μ L) was thawed for 10 min on ice, 50 ng of plasmid DNA were added and the mixture was incubated for 30 min on ice. The cells were shocked at 42°C for 90 sec, and then placed on ice for 2 min before 500 μ l of LB medium were added. The transformed cells were incubated for 1h at 37°C with 100 rpm shaking. The cells were streaked on plates containing LB medium supplemented with the appropriate antibiotics for transformation selection. Incubation generally took place overnight at 37°C.

Transformation of *Agrobacterium tumefaciens*

Electrocompetent *A. tumefaciens* GV3101 cells were transformed by electroporation method. Thawed cells were mixed with 50 ng of high-quality plasmid DNA, an electric pulse (2.5 kV, 25 μ F, 400 Ω) was applied for 5 s and the cells were immediately incubated with 1 ml YEB medium for 2 h at 28°C. The transformed cells were spread on YEB media containing the appropriate antibiotics and incubated for 2 days at 28°C. Overnight culture was mixed 1:1 ratio with 50% glycerol and stored at -80°C for storage.

Agrobacteria-mediated Arabidopsis transformation

The transformation of Arabidopsis is based on the floral dip method (Clough and Bent, 1998). Briefly, *Arabidopsis thaliana* Col-0 (or otherwise stated) were grown under long day conditions (22°C/ 18°C, 80-100 $\mu\text{mol Photons}/\text{m}^2/\text{s}$, 16h light/8h dark, 60 % humidity) until they started to produce inflorescences. An overnight *A. tumefaciens* culture was grown in 500 mL YEB media with appropriate antibiotics. After centrifugation (4000 rpm in swing bucket centrifuge for 20 min), the pellet was resuspended in 5% sucrose solution + 0.01% Sylvet77 and adjusted the OD₆₀₀ to 0.8. The inflorescences were dipped in *A. tumefaciens* GV3101 solution and the tray was covered with a plastic lid overnight to retain humidity. Plants were allowed to set seed in the long day (22°C/ 18°C, 80-100 $\mu\text{mol Photons}/\text{m}^2/\text{s}$, 16h light/8h dark, 60 % humidity) growth chamber.

Transfection of Arabidopsis ABD2-GFP protoplast

The pCAMBIA2300-ABD2 for Arabidopsis transformation was kindly provided from the Department of Cell Biology, Göttingen. Approximately 10-15 leaves from 4-6 weeks old 35S::ABD2-GFP plant (T2), grown at 22°C/ 18°C, 80-100 $\mu\text{mol Photons}/\text{m}^2/\text{s}$, 12h light/12h dark, 60 % humidity, were collected. The leaf tissue was lysed using a 'Tape-Arabidopsis Sandwich' technique and the peeled leaves were placed into 10 ml of enzyme solution (Table 2.23). The leaves were incubated at room temperature (RT) for 2 hours with constant rotating at 10 rpm on the shaker until the protoplasts were released into the enzyme solution. Then the protoplasts were carefully collected by centrifugation at 750 rpm for 5 minutes and washed the pellet twice with 10 ml W5 buffer. The cells were chilled on ice for 30 minutes prior to the PEG transfection.

For PEG transfection of the protoplasts, the W5 buffer was removed by centrifugation, and the pellet was gently resuspended in 5 ml MMG buffer (or otherwise stated). Protoplasts in MMG buffer (300 μl per reaction) were transferred into a 2 ml Eppendorf tube containing 300 μl of 40% PEG 4000 solution and 7.5-15.0 μg of the plasmid DNA. The solution was gently mixed and incubated at RT for 30 minutes. At the end of the incubation, 800 μl of W5 buffer was added and gently mixed. The supernatant was removed after centrifugation at 750 rpm for 2 minutes

and protoplasts were washed with 800 μ l of Wi buffer. The supernatant was removed and the pellet was resuspended in 300 μ l Wi buffer, mixed gently and incubated at RT for overnight. On the next day, the incubated protoplasts were transferred onto a glass slide for the observation under the confocal laser scanning microscope (x40).

2.2.2 Plant growth conditions

***Arabidopsis thaliana* seed sterilization**

Seeds were surface sterilized by vortexing in 1 ml 70% ethanol for 10 min in a 1.5 ml Eppendorf tube. The seeds were then washed with 100% ethanol and allowed to dry under the laminar airflow.

Growth of plants on substrate

Surface sterilized seeds were sown on steamed soil (Archut, Fruhstorfer Erde, T25, Str1 fein) supplemented with Confidor (50 mg/L) and fertilizer (0,5 ml/L Wuxal) and stratified at 4°C for two days. The plants were grown under short day conditions (22°C/ 18°C, 80-100 $\mu\text{mol Photons/m}^2/\text{s}$, 8h light/16h dark, 60 % humidity), long day conditions (22°C/ 18°C, 80-100 $\mu\text{mol Photons/m}^2/\text{s}$, 16h light/8h dark, 60 % humidity) or 12h/12h-light cycle conditions (22°C/ 18°C, 80-100 $\mu\text{mol Photons/m}^2/\text{s}$, 12h light/12h dark, 60 % humidity).

Plant growth on axenic plates

Surface sterilized seeds were sown on MS plates under the clean bench and sealed with Leukopor®. After stratification of 2 days at 4°C the plants grown under 14h/10h-light cycle conditions (22°C/ 18°C, 80-100 $\mu\text{mol Photons/m}^2/\text{s}$, 14h light/10h dark, 60 % humidity) for 12 to 14 days.

Selection of transgenic plants on axenic plates using BASTA

Surface sterilized seeds were sown on MS plates containing BASTA (5 mg/l) under the clean bench and sealed with Leukopor®. After stratification of 2 days at 4°C the plants grown under 14h/10h-light cycle conditions (22°C/ 18°C, 80-100 $\mu\text{mol Photons/m}^2/\text{s}$, 14h light/10h dark, 60 % humidity) for 7 to 14 days prior to the selection.

2.2.3 Pathogen assays

Nematode egg sterilization

Infected tomato (*Solanum lycopersicum* cultivar green zebra) roots were mixed vigorously for 4 min in a 10% sodium hypochlorite solution and then poured through two sieves (250 and 25 μm sequentially). The eggs were then collected from 25 μm sieve into 50 ml falcon tube and centrifuged at 4000 rpm for 5 min in a swing bucket centrifuge. The eggs were then surface sterilized by placing them in a 10% sodium hypochlorite solution for 5 min with continuous shaking. The eggs were pelleted by centrifugation at 4000 rpm for 5 min. The eggs were then washed three times with sterile H_2O and then re-suspended in 5 ml CT solution (water with 1% SDS and 2% Plant Protection solution). To collect the hatched juveniles, a sterile “Kimwipe filter” was made in which 4 layers of Kimwipes were placed on top of a small beaker containing approximately 30 mL of CT solution. The eggs were gently placed on the Kimwipes and allowed to hatch for 3 days in the dark, at RT. Hatched juveniles (J2) can migrate through the Kimwipes and will settle in the CT solution at the bottom of the beaker.

Nematode infection and penetration assay

Plants grown for 10 days on axenic MS medium were transferred onto square Petri dishes containing KNOPs media. Plants were infected with 100 sterile root-knot juveniles and incubated in phytochamber #2 (long day conditions (22°C/ 18°C, 80-100 $\mu\text{mol Photons}/\text{m}^2/\text{s}$, 14h light/10h dark, 60 % humidity). Galls were visually counted under the stereomicroscope. To estimate penetration of nematodes, infected roots were stained with acid fuchsin 4 days post inoculation.

Acid Fuchsin staining (Byrd et al., 1983)

Plants to be stained were placed into 50% commercial bleach solution for 2 min, rinsed with H_2O and then placed into a boiling, 1/30 diluted, acid fuchsin staining solution (35 mg Acid fuchsin / 100 mL). Plants were incubated in the boiling solution for at least 1 min. The stained plants were shortly rinsed in H_2O and observed under a microscope.

2.2.4 RNA extraction and gene expression analysis

RNA extraction

TRIZOL method (Chomczynski 1993) was used to extract RNA from plant tissue. Phenol/chloroform (dichloromethane) extraction dissolves RNA in the aqueous phase while other compounds like chlorophyll or proteins are in the hydrophobic chloroform phase. RNase activity is inhibited by two thiocyanate compounds in the extraction buffer. Deep frozen fine powder (~200 mg) of ground plant tissue (2 mL reaction tube) was dissolved in 1.3 mL extraction buffer (380 mL/L phenol saturated with 0.1 M citrate buffer pH 4.3, 0.8 M guanidinthiocyanate, 0.4 M ammoniumthiocyanate, 33.4 mL 3 M Na-acetate pH 5.2, 5 % glycerol) and shaken for 15 min at RT. Chloroform (260 µL) was added to each sample and after an additional shaking step of 15 min at RT, the samples were centrifuged for 30 – 40 min at 12.000 rpm and 4°C. The clear supernatant (~900 µL) was transferred into a new 1.5 mL reaction tubes and 325 µL of high salt buffer (1.2 M NaCl, 0.8 M Na-citrate) and 325 µL of isopropanol was added to each tube. The tubes were inverted and incubated for 10 min at RT. After centrifugation for 20 min at 12.000 rpm, 4°C the supernatant was discarded, the pellets were washed two times with 70 % ethanol. The pellets were allowed to air dry at RT. The pellets were dissolved in 20-60 µL water (ultra-pure).

cDNA synthesis

RNA samples were treated with DNase (DNase I, RNase free; 1U/µl, 1000U). The 10µl samples contained 500 ng total RNA, 1 µl of DNase buffer (Buffer DNase I + MgCl₂; 10X reaction buffer) and 1 µl of DNase I. The reaction mixture was then incubated at 37°C for 30 min followed by the addition of 1 µl of 25mM EDTA. The mixture was then incubated at 65°C for 10 min.

cDNA synthesis was performed by adding 0.2 µl of 100 µM oligo dT primers and 1 µl of 200 µM random monomer to the reaction solution. The mixture was then incubated at 70°C for 10 min. 4 µl RT buffer (5X reaction buffer for reverse transcriptase), 2 µl of 10 mM dNTPs, 0.3 µl Reverse Transcriptase (RevertAid H Minus Reverse Transcriptase; 200 U/µl, 10000 U) and 1.5

μl H_2O were added and the solution was incubated at 42°C for 70 min and finally at 70°C for 10 min.

Quantitative real time polymerase chain reaction (qRT-PCR)

For quantification of cDNA qRT-PCR was performed and fluorescence intensity was measured with the iCycler from BioRad. Reaction mix and cycler protocol are presented in table 2.40 and table 2.41. Calculations were performed using the $\Delta\Delta\text{Ct}$ method (Livak and Schmittgen, 2001).

Table 2.40: Standard reaction mix for qRT-PCR using BIOTAQ DNA Polymerase. Stock components as well as the volume for a final 25 μl reaction are presented.

| Stock component | Volume in a 25 μl reaction |
|--|---------------------------------------|
| 10X NH_4 reaction buffer | 2.5 μl |
| MgCl_2 50 mM | 1 μl |
| dNTPs 40 mM (10 mM each) | 0.25 μl |
| F and R primers (each 4 mM) | 2.5 μl |
| Sybr Green (1/1000) | 0.25 μl |
| Fluorescein (1 mM) | 0.25 μl |
| BIOTAQ DNA Polymerase (2500 U) | 0.05 μl |
| cDNA template ($\sim 0.05\mu\text{g}$) | 1 μl |

Table 2.41: Program of qRT-PCR cycler using BIOTAQ DNA Polymerase. Cycle steps, temperature and cycle numbers are presented.

| Cycle step and repeats | Temperature and duration | Cycles |
|--------------------------|-----------------------------|--------|
| Initial denaturation | 95°C ,90 sec | 1 |
| Denaturation | 95°C, 20 sec | 39 |
| Annealing | 55°C, 20 sec | |
| Extension | 72°C, 40 sec | |
| Final extension | 72°C, 4 min | 1 |
| Generation of melt curve | 95°C, 1 min | 1 |
| | 55°C, 1min | 1 |
| | 55°C, 10 sec (+0.5°C/cycle) | 81 |

2.2.5 Subcellular localization of fluorescence tagged proteins

Fluorescence tagged proteins expressed in Arabidopsis/protoplasts were analyzed using confocal laser scanning microscope Leica SP5-DM6000 (Leica GmbH). Protoplasts or leaf discs from fully expanded leaves of four week old plants were used for analysis. Appropriate filter set was used to distinguish between the different fluorophores and auto-fluorescence. Z-stack pictures were taken to obtain a better view of the subcellular localization of the tagged proteins. Pictures were acquired and analyzed using Leica's LAS - AF and LAS - AF lite.

Table 2.42: Excitation and detection values in nm for YFP, GFP and RFP for fluorescence microscopy. The excitation and detection wavelengths of YFP, GFP and RFP are presented.

| Fluorophore/signal | Excitation in nm | Detection in nm |
|--------------------|------------------|-----------------|
| YFP | 514 | 525-600 |
| GFP | 488 | 500-540 |
| RFP | 561 | 580-620 |

2.2.6 Protein analysis using Western blot

Co-immunoprecipitation

Frozen leaf tissue from Arabidopsis was ground to powder. The leaf powder was extracted by adding Co-IP extraction buffer in ratio 2:1 (buffer: powder). Samples were centrifuged using FiberLite® F13-14x50cy fixed angle rotor at 10,000 rpm at for 15 minutes and clear supernatants were transferred into 2ml Eppendorf tubes containing GFP-trap magnetic beads. Immunoprecipitation was performed by incubating the beads together with the samples for 2 hours at 4 °C on a rotation wheel. The magnetic beads were separated from the supernatant by using magnetic rack and the supernatant was removed. The purified beads were washed 3 more times with co-immunoprecipitation washing buffer before adding 45ml of 1x Laemmli buffer containing 5% β-mercaptoethanol. Beads were boiled at 95 °C for 8 minutes with 300 rpm shaking. The samples can be loaded directly onto SDS-PAGE gels or stored at -20 C.

SDS-polyacrylamide gel electrophoresis (SDS-PAGE)

In this study, separating gels used ranging from 4 to 20 % and were overlaid with 4% stacking gels. In short, the preferred separating gels were poured between 1.5mm glass slides and then overlaid with Isopropanol. When the separating gels were completely solidified, isopropanol was removed and a 4% stacking gel was poured on top. Combs suitable for 1.5 mm spaced glass were inserted and the gel was left at room temperature until completely polymerized. Polymerized SDS-PAGE gels can be either used directly or wrapped with wet towel papers in a box and stored at 4 C°. SDS-PAGE-gels were placed in Mini Protean tetra cell (BioRad) chambers and loaded with 1xSDS-running buffer according to the manufacturer's protocol. The combs were removed and samples were loaded. Gels were run at 100 to 160 Volts for approximately 1-2 hours or until the Ladder reach the bottom of the gel.

Western blot analysis

The samples from finished SDS-PAGE gel were blotted onto activated polyvinylidene fluoride membrane covered by 3 layers of Whatmann paper wetted with 1x transfer buffer in semi blot chamber (homemade, University of Göttingen). The transfers of the protein were carried out for 90 minutes at $1\text{mA}/\text{cm}^2$. After proteins were successfully transferred, the membranes were washed briefly in 1x transfer buffer and blocked in 2% nonfat milk powder in TBS-T for at least 30 minutes. After blocking, the first primary antibody (α -GFP) was applied and incubated at room temperature for 120 minutes at room temperature or $4\text{ }^\circ\text{C}$ overnight. After the first antibody incubation, the membranes were washed to remove unattached antibody with 1xTBS-T for 10 minutes at room temperature 3 times. The secondary antibodies were added and incubated for 120 minutes at room temperature. After the incubation, the secondary antibodies were removed by washing with 1xTBST for 5 minutes for 5 times. The membranes were developed by using Super Signal™ West Femto Maximum Sensitivity Substrate and chemiluminescence was visualized using the Intrac ChemoCam camera.

2.2.7 Protein interaction assays using yeast

Yeast transformation

Overnight culture of yeast strain AH109 in YPAD was sub-cultured into new YPAD media and incubated at $28\text{ }^\circ\text{C}$ until the OD_{600} was between 0.6 - 1.2. Yeast cells were collected and wash with sterile H_2O by centrifugation at 4000 rpm for 5 minutes at room temperature in 50 ml falcon tube. The cells were resuspended in 1 ml of water and transferred into a sterile Eppendorf tube before briefly centrifuging at 13,000 rpm to pellet the cells. Cells were resuspended in $550\text{ }\mu\text{l}$ of 100 mM LiAc pH 7.5 and were distributed into 11 x $50\mu\text{l}$ sterile tubes. Supernatant was removed by brief centrifugation followed by adding a transformation mix containing $240\mu\text{l}$ of 50% PEG 4000, $36\text{ }\mu\text{l}$ of 1M LiAc pH 7,5, $25\text{ }\mu\text{l}$ single stranded DNA and 250-500 ng of plasmid. The mixture was vortexed vigorously to resuspend the cells. Next, the mixture was incubated at $30\text{ }^\circ\text{C}$ for 25 minutes with occasional shaking. Transformation was performed by heat shock. The yeast was incubated at $42\text{ }^\circ\text{C}$ for 25 minutes. Subsequently, cells were centrifuged at 4000 rpm for 10 seconds and supernatant was removed. Yeast cells were resuspended in $200\text{ }\mu\text{l}$ of sterile

water. Aliquots were spread onto suitable selective drop out media. Plates were allowed to air dry and incubated at 30 °C for 3 days or until the colonies developed.

For double transformation to confirm interactions, the full length coding sequence of potential interaction candidates were amplified from either Arabidopsis root/leaf/flower cDNA and cloned into the plasmid (pGAD1) vector system using Gateway technology to be used as prey. Mi131 was cloned into pASII. The prey and Mi131 (bait) plasmids were co-transformed into yeast

Yeast library screening

To screen for potential interaction partners, yeast libraries containing cDNA fragments from Arabidopsis thaliana root and cell line were provided by Joachim Uhrig.

cDNA libraries containing prey plasmids (pGAD1), were quickly thawed in a water bath at 42 °C and resuspended in YPAD for 1 hour at 30 °C 200 rpm or until the $OD_{600} = 1.2$. The AH109 containing bait plasmid (pASII-effector candidate) was cultured overnight at 30 °C at 200 rpm in SC-W. 1.85×10^8 yeast cells (Y187) of each library were 1.85×10^8 yeast cells (AH109) containing the bait construct. Cells were pelleted by centrifugation and resuspended in 10 ml of YPAD containing 20% PEG6000 and transferred into a 100 ml Erlenmeyer flask. The mixture was incubated overnight with 80 rpm at 30°C. The next day, mixture was pelleted by centrifugation at 4000rpm for 4 minutes in 50 ml tubes and resuspended in 500ml SC –LWH containing 0.05% Gelrite, 5mM 3`-AT and ampicillin. Mating efficiency was determined by spreading 10µl of mixture onto SC –LW plates. Colonies for mating efficiency were observed after 2 days of incubation and after 10-14 days of incubation for interaction. Colonies developing in the interaction media were picked for plasmid isolation and for subsequent sequencing of the plasmid insert.

Mi131 Protein expression

The *E. coli* strain BL21 was transformed with either pDEST17-Mi131 (6xHis-Mi131) or pGP172GW-Mi131 (Strep-Mi131). BL21 was cultured in 3 ml of LB + 100 µg/µl of Ampicillin (Amp) overnight. The overnight culture was transferred into 30 ml of LB-Amp and grew until $OD_{600} = 0.5$. The protein expression was induced by adding 1 mM Isopropyl β-D-1-thiogalactopyranoside (IPTG) and incubating cells transformed with pDEST17-Mi131 construct at 37°C with 200 rpm shaking for 2 hours. Cells transformed with pGP172GW-Mi131 were incubated at 28 °C with 200 rpm shaking overnight. Cells were harvested by centrifugation at 4000 rpm for 10 minutes and the supernatant was discarded. Cells were resuspended in the lysis buffer and lysed by sonication at 60% power input for 5 minutes on ice. Lysates were aliquoted and approximately 10 µg of lysate proteins were loaded onto SDS-PAGE for protein expression analysis by Coomassie staining.

His-Mi131 purification

Columns were prepared by adding 200 µl of Profinity IMAC resin into a Micro Bio-spin column. The spin columns were centrifuged at 1000g for 15 sec and washed with 250 µl deionized water. Columns were equilibrated by twice adding 250 µl of His purification wash buffer and centrifuging at 1000 x g for 15 sec. 200 µl of the bacterial lysate was added onto equilibrated columns and gently mixed by pipette. Lysates were incubated with resin for at least 5 minutes before a centrifugation step to remove the unbound fraction. The excess unbound proteins were removed by washing the column 3 more times with 250 µl of wash buffer. The bound protein was eluted with 100 µl of His purification elution buffer. The elution step can be repeated for 4 addition times to increase protein concentration. In addition, 100 µl of lysate buffer with 0.05% triton X100 and 2.5% glycerol was added to 100 µl eluted protein fractions in order to prevent the precipitation when stored at -80 °C.

2.2.8 *In vitro* actin sedimentation assay (Cytoskeleton #BK013 protocol)

Prior to the assay, the lysates, BSA, α -actinin and purified His-Mi131 were prepared by ultracentrifugation at 150,000 x g for 60 min at 4 °C and the supernatants were transferred into new Eppendorf tubes.

The G actin sequestration and F actin binding assays were performed following the manufacturer's protocol (Cytoskeleton #BK013 protocol). In brief, a G actin solution was prepared by diluting 1 mg/ml of non-muscle actin with 225 μ l of general actin buffer. The G actin solution was mixed by pipetting up and down several times and incubated on ice for 60 min prior to the assay. After the incubation, 40 μ l of G actin solution was added into each tube with either 10 μ l of test proteins or 10 μ l of actin buffer. The mixture was mixed several time by pipetting up and down and incubated at RT for 30 mins. After the incubation, 2.5 μ l of 10x polymerization buffer was added into each tube, mixed and incubated at RT for 30 min. To separate F actin from G actin, the mixtures were centrifuged at 150,000 x g for 90 min at 24 °C. The supernatant was carefully removed and 5x reducing Laemmli buffer was added to each sample. The samples were centrifuged and the pellets were resuspended in 30 μ l of Milli-Q water and incubated on ice for 10 min. Then 30 μ l of 2 x Laemmli buffer was added to each sample. Samples were run on homemade 4-20 % SDS-gel. The actin and test proteins were visualized by Coomassie staining and photo was documented by intras SDS-gel camera.

For F actin binding assay, F actin solution was pre-prepared by adding 25 μ l of Actin polymerization buffer to the G actin solution. The mixture was incubated at RT for 60 min. To each tube, 40 μ l of F actin solution was added either together with the test protein or with buffer. The mixtures were incubated for 30 min at RT. To separate F actin from G actin, the mixtures were centrifuged at 150,000 x g for 90 min at 24 °C. The supernatant was carefully removed and 5 x educing Laemmli buffer was added to each supernatant sample. The samples were centrifuged and the pellets were resuspended in 30 μ l of Milli-Q water and incubated on ice for 10 min. Then 30 μ l of 2 x Laemmli buffer was added to each sample. Samples were run on homemade 4-20 % SDS-gel. The actin and test proteins were visualized by Coomassie staining and photo was documented by intras SDS-gel camera.

2.2.9 Plant phytohormone measurement by HPLC/MS

Eight day old Col-0 seedlings were transferred from MS media to MS media with or without 50 μ M MeJA. The samples were collected after 48 hours of treatment and approximately 200 mg of root samples (from approximately 500 seedlings) from 3 biological replicates were sent for phytohormone measurement in the Department of Biochemistry, Göttingen. The measurement was performed according to Schatzki et al., 2013.

3. Results

3.1 Functional characterization of *M. incognita* effector Mi131

3.1.1 Searching for an Mi131 interaction partner in plants by performing a yeast two hybrid screen

We hypothesize that Mi131 is secreted by the nematode into plant cells where it is interacting with plant target(s) and helping the nematode establish a successful infection. To find the plant target of Mi131, a yeast two hybrid (Y2H) screen was performed using two plant-specific libraries (Van Criekinge and Beyaert, 1999).

For the yeast-two-hybrid screen, the yeast strain AH109 was transformed with pAS2-Mi131. To first rule out Mi131-autoactivation of the reporters, the yeast containing pAS2-Mi131 were grown on both non-selective media (synthetic complete media (SC) without Trp (SC-W)) and on selective media (SC without Trp and His (SC-WH) supplemented with 5 mM 3-amino-1,2,4-triazole (3-AT)). Yeast containing pAS2-Mi131 could grow on the non-selective media, indicating that yeast transformation was successful. However, the growth was inhibited on the selective media, indicating that the bait alone could not auto-activate the reporters (Figure S1.1).

Next, Mi131 was used as bait in a Y2H screen of Arabidopsis root and cell line libraries. In total, 28 independent colonies could grow on the SC-LWH + 5 mM 3-AT + Amp selection media. The cDNA inserts of these clones were amplified and sequenced. The insert sequences were subjected to a BLASTn search of the non-redundant database, and this analysis showed that the 28 clones represent eight independent genes in total (Table 3.1).

| Colonies | Library | Accession number | Gene name |
|----------|-----------|------------------|--|
| 6 | Root | At2g41430 | ERD15 |
| 5 | Cell line | At5g09810 | Actin 7 |
| 2 | Cell line | At3g22800 | LRR protein famliy |
| 1 | Root | At1g33240 | GTL1 |
| 1 | Cell line | At5g13430 | Ubiquitinol cytochrome C reductase iron-sulfer subunit |
| 1 | Cell line | At1g59359 | Ribosomal S5 protein family |
| 1 | Root | At5g54750 | TRAPP |
| 1 | Root | At3g02920 | RPA32B |

Table 3.1. Putative plant interaction partners of Mi131 from Y2H screen of a cDNA library derived from Arabidopsis cell line and root tissues. cDNA inserts from the positive clones were amplified by PCR and sequenced. The table shows the potential candidates from yeast screen in terms of colonies (number of clones representing the same gene; library cell line or root); accession number and gene name according to TAIR. Black indicates the candidates in which full length CDS could be amplified for further analysis. Red indicates genes for which amplification of the full length CDS from the library was unsuccessful. Cyan indicates possible false positive candidates that are often found as non-specific interactors and which were not further studied.

The interaction between Mi131 and the plant partners was confirmed by yeast co-transformation analysis. Unfortunately, the full length *GTL1* and *LRR* protein family genes could not be amplified and were not included in the co-transformation experiments. In addition, Ubiquitinol cytochrome C reductase iron-sulfer subunit and Ribosomal S5 protein family have been commonly found as false positives in yeast two hybrid screening (Joachim Uhrig, personal communication) and, therefore, these genes were not included in the co-transformation experiments. As a result, the full length coding sequence of the four remaining interaction partners (*ERD15*, *ACT7*, *TRAPP*, and *RPA32B*) were introduced into the activation domain vector (pGAD1) and co-transformed into yeast cells containing pAS2-Mi131. As a negative control, pAS2-Mi131 was transformed into yeast cells with a pGAD1-GFP construct. As a positive control, yeast cells were co-transformed with constructs for SNF1 and SNF4, which have been previously shown to interact in yeast (Celenza et al., 1989). All the yeast cells co-expressing bait and prey proteins, including the GFP-control prey, could grow on the control non-selective plates (SC-LW) (Figure 3.1.1 Right), indicating successful co-transformation.

However, on the selection plate, only yeast co-transformed with the positive controls SNF1/SNF4 and yeast expressing Mi131 in combination with Arabidopsis Actin 7 (AtACT7) could grow (Figure 3.1.1 Left). This result confirms that AtACT7 is an interaction partner of Mi131 in yeast.

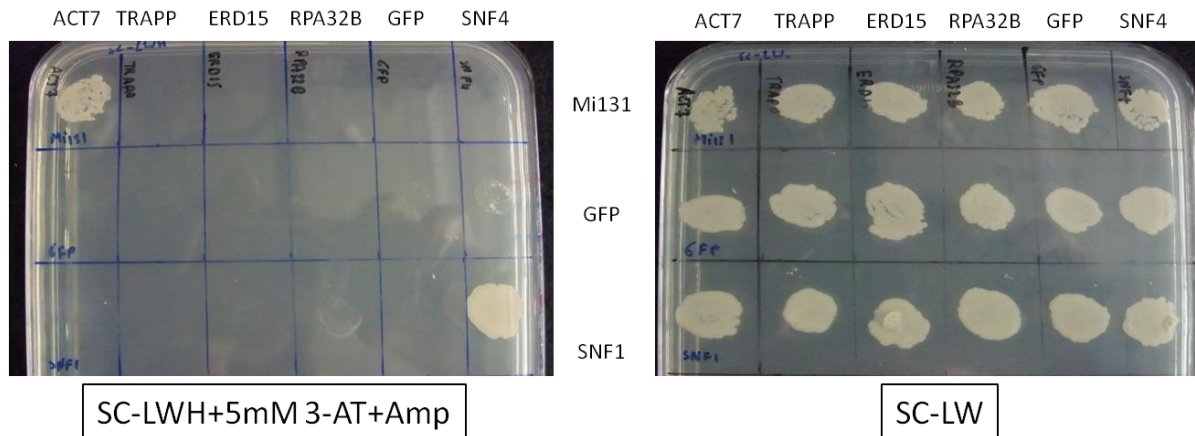


Figure 3.1.1. Mi131 interacts with Arabidopsis Actin 7, as confirmed by yeast co-transformation. Mi131 was used as bait and the full length coding region from the interaction candidates (Table 3.1, black) used as prey. A. On the selective media, only yeast expressing Mi131 and full length AtACT7 can grow. SNF1/SNF4 is a co-transformation positive control and can also grow on selective media. B. Yeast growth on non-selective media confirms the success of the yeast co-transformation.

3.1.2 Further investigation of Mi131 interacting with Arabidopsis actins.

Actin 7 is one of eight actins found in Arabidopsis. The Arabidopsis actin family can be separated into 2 classes, vegetative and reproductive (Kandasamy et al., 2007). Arabidopsis actins 2, 7 and 8 belong to the vegetative class of actins. Meanwhile, the actins 1, 3, 4, 11, and 12 comprise the reproductive class of actin. We have shown that a specific vegetative actin, AtACT7, is a Mi131 interaction partner in a yeast screen. However, reproductive and vegetative actins differ by only 4–7 % at the amino acid level (Kandasamy et al., 2007). Due to the high sequence similarity between AtACT7 and the other plant actins, it may be possible for Mi131 to interact with other plant actins. To test this hypothesis, yeast was double-transformed with Mi131 in a combination with different vegetative isoforms of actin (AtACT2, 7 and 8) and one representative reproductive actin isoform AtACT1. We found that the double-transformed yeast expressing Mi131-AtACT2 and Mi131-AtACT8 could not grow on the selection media,

suggesting no interaction between Mi131 and these vegetative actins in yeast. However, yeast co-transformed with AtACT1 and Mi131 could grow on the selective media, indicating that there was a physical interaction between these two proteins. We also re-confirmed the interaction between AtACT7 and Mi131 in yeast. Lastly, we wanted to determine the specificity of the interaction of AtACT7 with Mi131. To test this, an *M. incognita* effector candidate called Mi-PEPCTI (peptidyl prolyl cis-trans isomerase) was co-transformed with AtACT7. Yeast expressing a combination of Mi-PEPCTI-AtACT7 exhibited no growth on the selection media, indicating that AtACT7 cannot interact with this nematode effector candidate. Overall, the yeast data indicates that Mi131 can interact with AtACT1 and AtACT7, and that AtACT7 can specifically interact with the nematode protein Mi131 and not another nematode effector candidate (Figure 3.1.2).

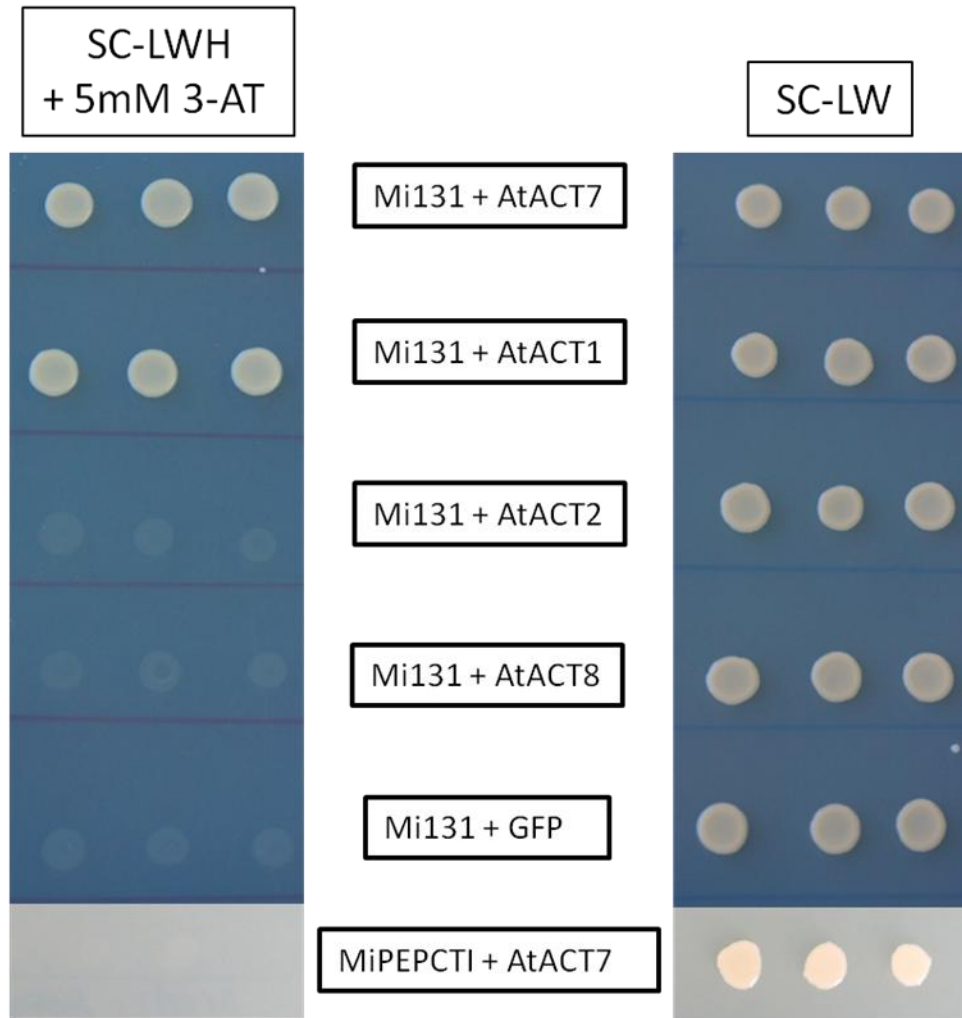
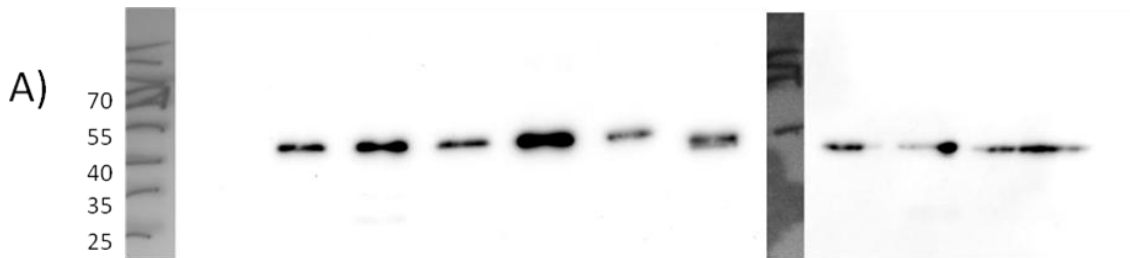


Figure 3.1.2. Mi131 can only interact with Arabidopsis Actin1 and Actin7 in yeast. In a co-transformation experiment, full-length Arabidopsis actin (AtACT 1, 2, 8, 7) or GFP coding sequences were used as prey and Mi131 or the *M. incognita* effector candidate PEPCTI were used as bait. A positive interaction was only seen between Mi131 and AtActin1 and AtActin7. At least 3 independent transformants of each combination were tested twice with similar results. Growth on SC-LWH + 5 mM 3-AT indicates an interaction between the effector and actin (Left) and growth on SC-LW + 5mM 3-AT indicates a successful transformation (Right).

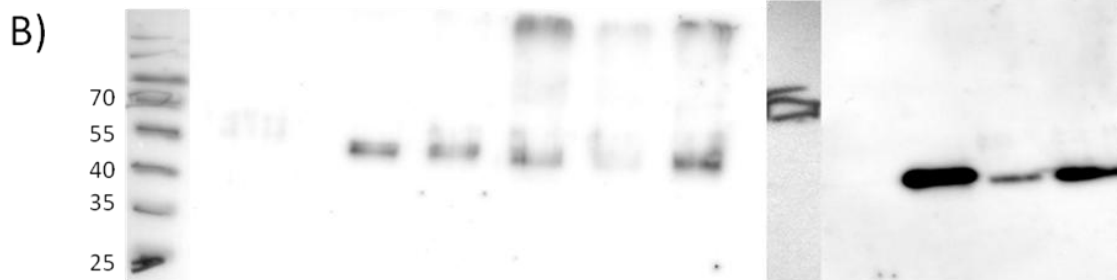
The previous experiments showed that Mi131 can only interact with AtACT7 and AtACT1 in yeast cells, and not AtACT2 and AtACT8. It should be noted that yeast expressing AtACT2 and AtACT8 appeared to grow much slower than yeast transformed with AtACT1 or AtACT7, suggesting that the expression of these actins in yeast may be detrimental to the cells. Therefore, the coimmunoprecipitation (co-IP) assays were performed to determine if Mi131 can interact with specific actins in plants. The interaction between Mi131 and the plant actins was determined by *in planta* co-IP assays of transiently expressed proteins in *Nicotiana benthamiana*.

Mi131 was fused to either C-terminal YFP or N-terminal GFP; both constructs were used in these experiments in case that a specific terminal fusion affected protein stability. A *pUBQ10::Mi131-YFP* construct or *35S::GFP-Mi131* was co-expressed with *pUBQ10::6xHA-AtACT1, 2, 7 or 8* in *N. benthamiana* leaves. Samples were collected at 3 days post infiltration and from the protein extracts, Mi131 was selectively immunoprecipitated with GFP-trap beads, and both the N- and C- terminal fusion proteins were stable. Western blot analysis with anti-HA antibodies showed that all Arabidopsis actins tested co-immunoprecipitated with Mi131 (Figure 3.1.3). This leads to the conclusion that while Mi131 could interact with only AtACT1 and AtACT7 in yeast, it can interact with AtACT1, 2, 7 and 8 in plants.

| | | | | | | | | | | | |
|-----------|---|---|---|---|---|---|---|---|---|---|---|
| Mi131-YFP | - | + | + | + | + | - | + | - | - | - | - |
| GFP-Mi131 | - | - | - | - | - | + | - | + | + | + | + |
| HA-AtACT7 | - | - | + | - | - | - | - | - | + | - | - |
| HA-AtACT2 | - | - | - | + | - | - | - | - | - | + | - |
| HA-AtACT8 | - | - | - | - | + | - | - | - | - | - | + |
| HA-AtACT1 | - | - | - | - | - | + | + | - | - | - | - |



IB : Anti-GFP antibody

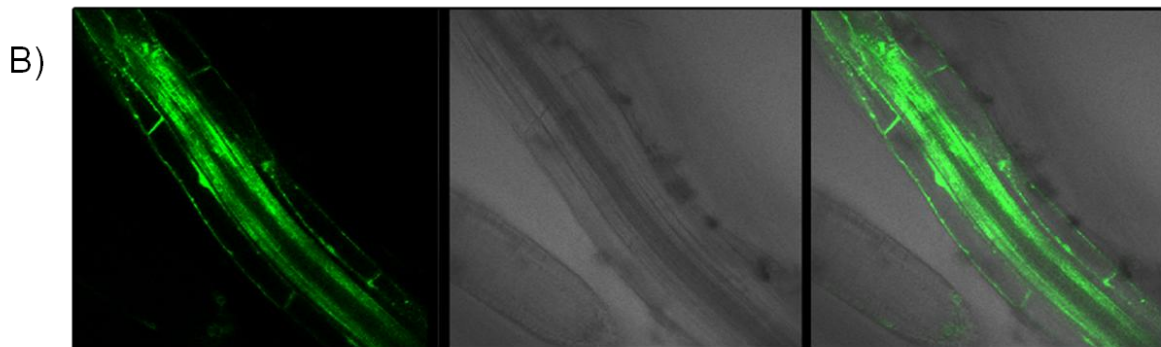
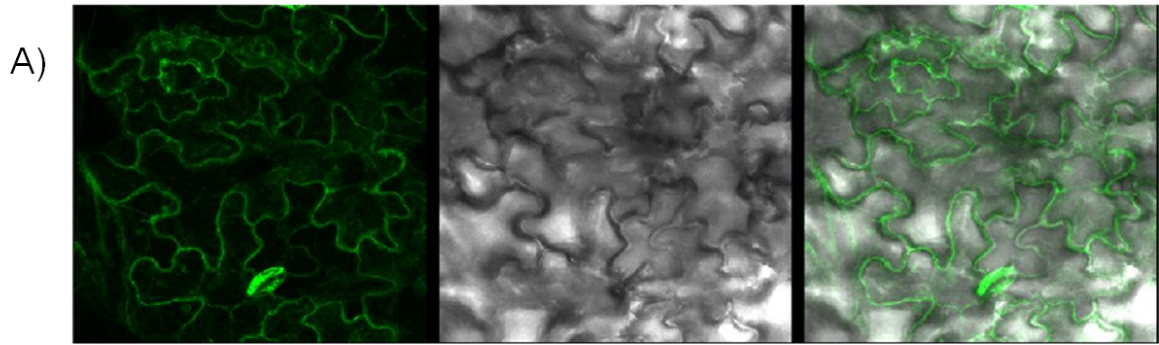


IB : Anti-HA antibody

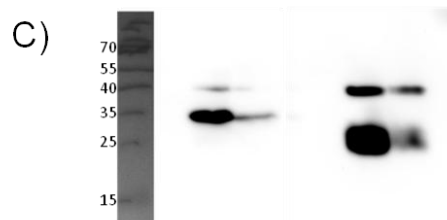
Figure 3.1.3. Immunoprecipitation shows interaction between Mi131 with four Arabidopsis actins: AtACT 1, 2, 7, and 8. Mi131 with a C-terminal YFP or N-terminal GFP fusion was transiently expressed in *Nicotiana benthamiana* leaves together with HA-tagged AtACT1, 2, 7 or 8. Samples were harvested at 3 dpi for protein extraction. The immunoprecipitation was performed by using GFP-trap[®] beads. Proteins were separated on 12% SDS-PAGE followed by Western blot analysis. A) Detection of GFP/YFP Mi131 with anti-GFP antibody. B) Detection of HA-AtACT1, 2, 7 and 8 with anti-HA antibody. Predicted size of GFP-Mi131 and Mi131-YFP are 42 kDa and HA-AtACTs are 50 kDa.

3.1.3 Endogenous AtACT7 coimmunoprecipitates with GFP-Mi131

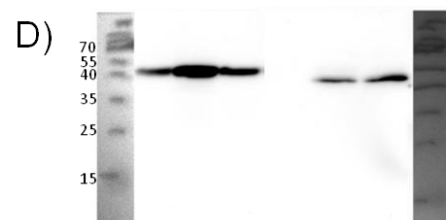
To further reveal the function of Mi131, Arabidopsis plants were transformed with a 35S::GFP-Mi131 construct. Leaf and root samples from three independent T2 lines were collected for protein extraction. To confirm the presence of Mi131 in the transgenic plants, GFP-Mi131 was immunoprecipitated from leaf and root protein extracts using GFP-trap[®] beads and detected via Western blot analysis using an anti-GFP-antibody (Figure 3.1.4 C). When GFP-Mi131 was immunoprecipitated with Anti-GFP beads, AtACT7 was co-immunoprecipitated with GFP-Mi131 (Figure 3.1.4 D). This result confirms the interaction of Mi131 with endogenous AtACT7. The transgenic plants were then analyzed by confocal microscopy to determine the sub-cellular localization of Mi131 in plants. In general, the GFP-Mi131 protein had a cytoplasmic localization in both leaf and root cells (Figure 3.1.4 A and B).



| | | | | | | | | | |
|------------------------|---|---|---|---|---|---|---|---|---|
| Col+0 extract | + | - | - | + | - | - | + | - | - |
| GFP-Mi131 leaf extract | - | + | - | - | + | - | - | + | - |
| GFP-Mi131 root extract | - | - | + | - | - | + | - | - | + |



IB: Anti-GFP antibody



IB: mAb2345a antibody

Figure 3.1.4. Visualization of GFP-Mi131 in *Arabidopsis thaliana* leaf and root cells indicates that Mi131 has a cytoplasmic distribution and can co-immunoprecipitate with endogenous AtACT7. A) Using confocal microscopy, GFP-Mi131 in the leaves show a cytoplasmic distribution within cells B) A fluorescent signal from a root of a GFP-Mi131 seedling appears to be cytoplasmically localized. C) Detection of GFP-Mi131 with Anti-GFP antibody. D) Detection of Arabidopsis AtACT7 with mAb2345a antibody. Predicted size for GFP-Mi131 is 42 kDa and AtACT7 is 42 kDa.

3.1.4 Mi131 sequesters G actin *in vitro*

Because Mi131 has a predicted profilin domain and can interact with Arabidopsis actins in plants, it likely to have an effect on actin organization. To clarify the effects of Mi131 on actin in more detail, actin sedimentation assays were performed. First, purified, tagged Mi131 protein was isolated from bacterial cells. Briefly, the constructs pDEST17-Mi131 (His-Mi131) and pGP172GW-Mi131 (Strep-Mi131) were expressed in *E. coli* BL21 cells (Figure 3.1.5 A and B). After cell lysis, recombinant His-tagged Mi131 was purified using a Ni-NTA purification system. The cell lysates and the purified His-tagged Mi131 were separated by a 4-20 % SDS-PAGE and the soluble protein can be visualized by Coomassie staining. Strep- and His-tagged Mi131 could be detected in the lysate supernatant fraction. In addition, purified His-Mi131 protein (17 μ M) was generated for further experimental use (Figure 3.1.5 A-Elution).

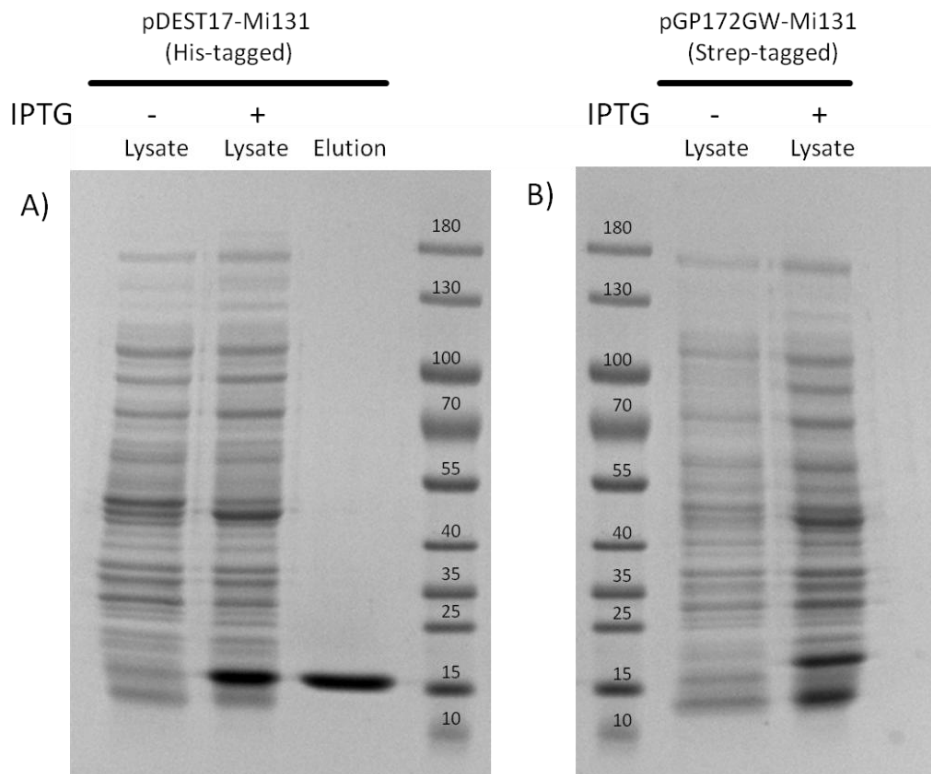


Figure 3.1.5. Both His- and Strep- tagged Mi131 protein can be expressed in *E. coli* BL21. Lysates from supernatant fraction of *E.coli* containing constructs for A) His- or B) Strep- tagged Mi131 were collected from sonicated cells after a two hour incubation at 37 °C or 16 hours incubation at 20°C with or without 1mM IPTG. After a purification step, lysates and elution were separated in 4-20% SDS-PAGE and stained with Coomassie blue to quantify Mi131 protein. A) His-tagged Mi131 B) Strep-tagged Mi131. Predicted sizes for both His- and Strep-Mi131 are 15 kDa.

This purified, recombinant Mi131 protein and lysate containing soluble recombinant Mi131 protein were then used in an *in vitro* sedimentation assay (Fan et al., 2013; Kang et al., 2014). In short, test proteins are incubated with G actin prior to polymerization. A polymerization of the F actin is induced and the solution is centrifuged. The centrifugation separates F and G actin by differential sedimentation, and F actin accumulates in the pellet and G actin in supernatant fraction. Proteins that disrupt the actin polymerization or that can sever F actin will decrease the total amount of F actin in the pellet, and as a result, more G actin will be present in the supernatant after centrifugation.

In the first assay, Bovine Serum Albumin (BSA), buffer and uninduced lysate was incubated with G actin for 30 minutes before actin polymerization. The separation was performed by ultracentrifugation and fractions were separated by SDS-PAGE and stained with Coomassie Blue to visualize the proteins on the gel. When buffer, BSA or uninduced *E. coli* lysate were added to the G actin before polymerization, there was significantly more actin in the pellet fraction compared to the supernatant, indicating that most of the G actin had polymerized into F actin. Neither the buffer, BSA or uninduced lysate could interfere with actin polymerization. On the other hand, when G actin was incubated prior to actin polymerization with either induced lysate (Both Strep- and His-tagged) or 17 μM of purified recombinant Mi131 (Figure 3.1.6 A and Figure S1.2), a larger amount of the actin can be observed in the supernatant. This result indicates that if Mi131 is added to the G actin prior to polymerization, the ratio of G/F actins shifts, and there is relatively less filamentous actin. When the concentration of Mi131 was decreased to 1.7 μM , there was relatively more F actin compared to the G actin fraction after the differential sedimentation, indicating that the ability of Mi131 to affect actin polymerization is dose-dependent (Figure 3.1.6 B).

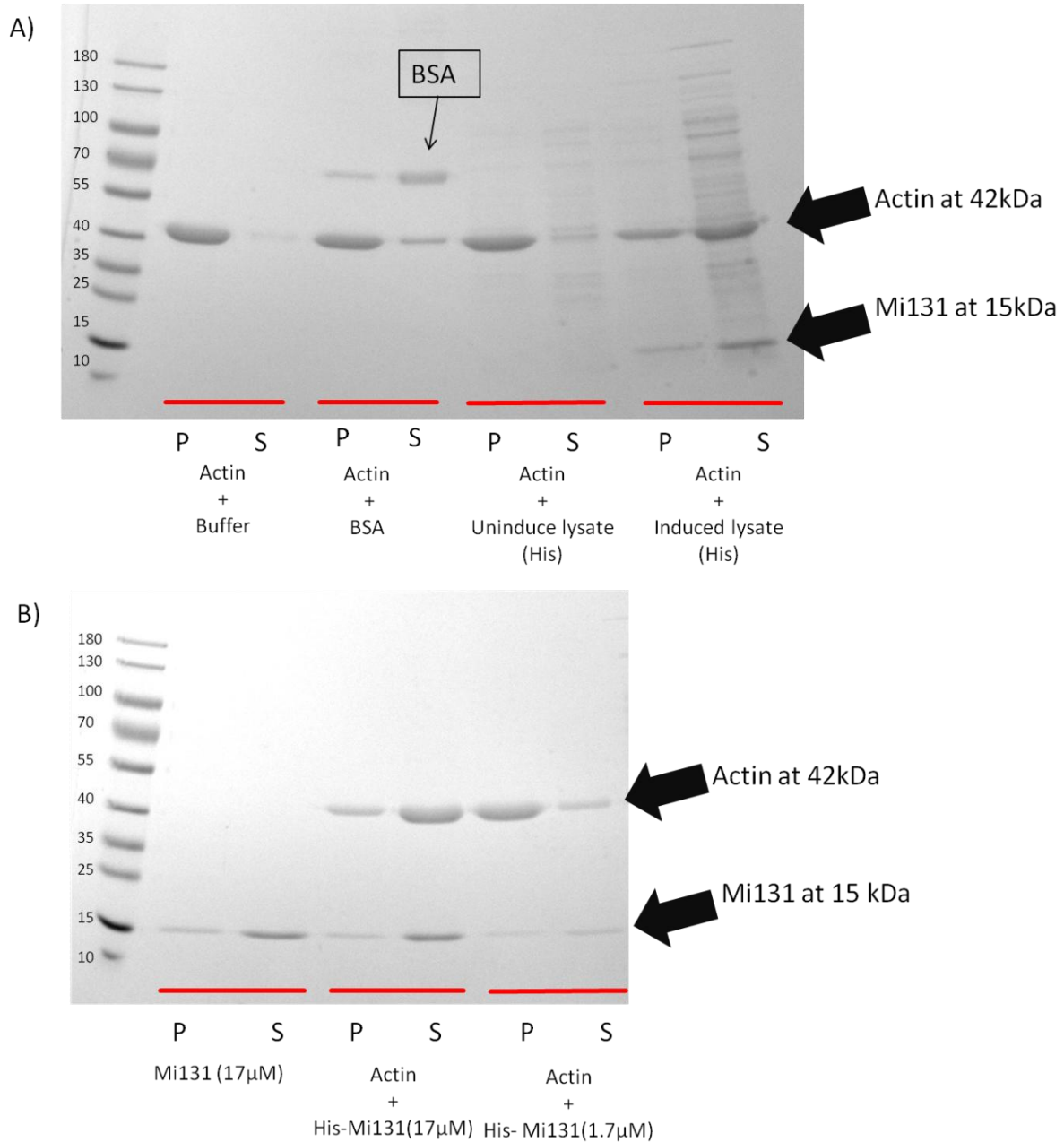


Figure 3.1.6. Mi131 inhibits *in vitro* actin polymerization in a concentration dependent manner. Non-muscle actin (22µM) was incubated with buffer, BSA, lysate control, lysate containing His-Mi131 and 17 µM purified His-Mi131 for 30 minutes before adding polymerization buffer to induce actin polymerization. After a 30 minutes polymerization time, the G and F actin were separated by ultracentrifugation. Samples from the pellet (P) and supernatant (S) fractions were run on 4-20% SDS-PAGE and stained with Coomassie blue to visualize the actin, lysate protein and His-Mi131. A) Actin polymerization after with buffer control, BSA and lysates. B) Actin polymerization after incubated with purified Mi131. Actin in the pellet represents F/polymerized actin and in the supernatant represents G/monomer actin. Predicted size for His-Mi131 is 15 kDa and non-muscle actin is 42 kDa. This assay was repeated twice with similar results.

The initial *in vitro* sedimentation assay clearly showed that after incubation with Mi131, the ratio of G/F actin was shifted. Although we predicted that Mi131 forms a complex with G actin and thereby preventing its polymerization into F actin, it may be possible that Mi131 can directly sever the F actin filament. This scenario would also result in more actin in the soluble fraction. To test this possibility, pre-polymerized F actin was incubated with buffer or purified 17 μ M His-Mi131 for 90 or 150 minutes (including the ultracentrifugation time) and the fractions were separated by SDS-PAGE and visualized by Coomassie blue staining. The F actin was stable at all time points when co-incubated with only buffer. However, when the F actin was co-incubated with His-Mi131, the amount of G actin present in the supernatant increased gradually over time, but a majority of the actin was detected in the supernatant fraction (Figure 3.1.7 and Figure S1.4). Because recombinant His-Mi131 is mostly found in the supernatant fraction, it likely does not stably bind to F actin. Thus, we cannot fully rule out the possibility that Mi131 is directly affecting actin filaments from this data. However, since Mi131 does not seem to bind to F actin, we predict that it is binding to G actin and prevents the G actin from efficiently polymerizing into actin filaments.

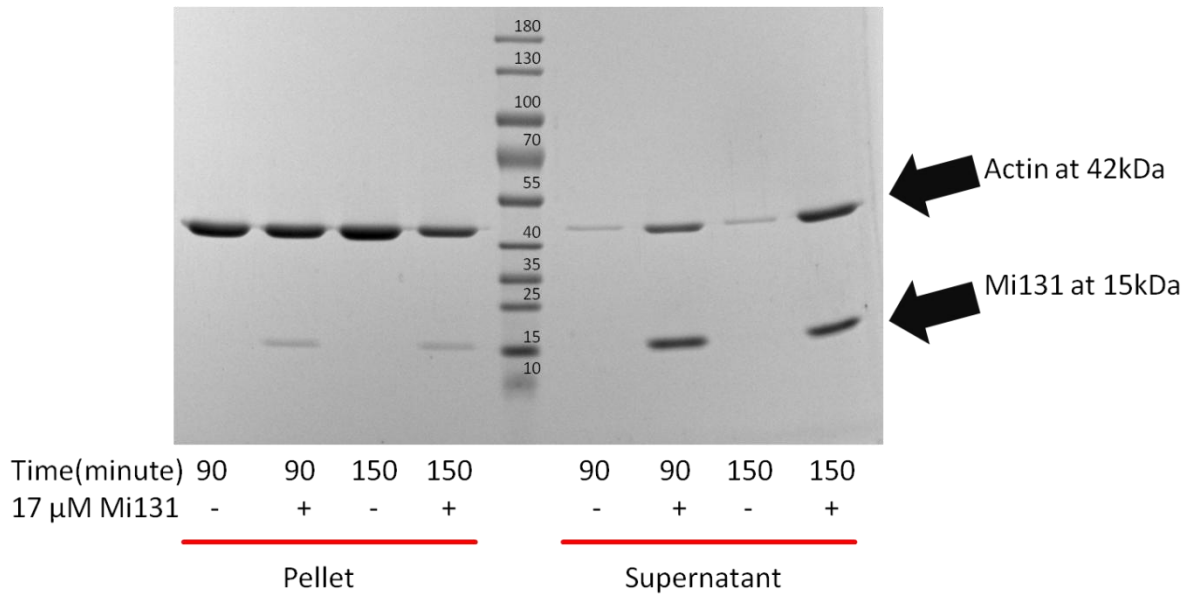


Figure 3.1.7. F actin depolymerizes in a presence of purified Mi131 protein. Non-muscle actin (22μM) was polymerized into F actin, and subsequently co-incubated with buffer or purified His-Mi131 for either 90 or 150 minutes. Samples from the pellet (P) and supernatant (S) fractions for each sample were run on 4-20 % SDS-PAGE and stained with Coomassie blue to visualize the actin and Mi131. Actin in the pellet represents F/polymerized actin and in the supernatant represents G/monomer actin. Predicted size for His-Mi131 is 15 kDa and non-muscle actin is 42 kDa. This assay was repeated twice with similar results.

3.1.5 Mi131 can suppress the AtACT1 overexpression phenotype

It was previously shown that when reproductive AtACT1 was ectopically expressed in plants, approximately 20% of the transgenic plants were dwarves and exhibited an abnormal leaf phenotype (Kandasamy et al., 2007). Interestingly, co-expression of the corresponding reproductive profilin (AtPRF4) but not vegetative profilin (AtPRF1) could suppress/rescue the dwarf phenotype. Kandasamy et al. proposed that the misexpression of a reproductive actin caused abnormal actin structures, leading to the dwarf plants. AtACT1 can specifically interact with AtPRF4, and when both AtACT1 and AtPRF4 are constitutively expressed, the concentration of free AtACT1 is reduced to less toxic levels.

We have shown through immunoprecipitation and Y2H assays that Mi131 can interact with AtACT1. Therefore, we predicted that Mi131 may also be able to suppress the AtACT1 misexpression phenotype. Arabidopsis Col-0 (wt) and two homozygous T3 lines of 35S::Mi131 (B and I) were transformed with 35S::AtACT1. The 35S::Mi131 lines B and I had been

previously characterized and show no obvious growth defects. Seedlings (T1) from each background were first grown on plant media containing kanamycin to select for transformants containing the 35S::AtACT1 construct and then were transferred to soil at 10 days post germination. The AtACT1 protein was quantified by Western blot analysis to ensure the present of AtACT1 in all plant backgrounds (Figure 3.1.8 B). When seedlings started to produce inflorescences, the rosette size and the leaf morphology were graded into three categories: 1) severe abnormal leaf curling/small rosette, 2) intermediate rosette size and 3) wild-type-like rosette size. An example of the severe dwarf phenotype and abnormal leaf morphology in a Col-0 plant misexpressing AtACT1 can be seen in Figure 3.1.8 A and Figure S1.5. When AtACT1 was ectopically expressed in Col-0, approximately 30 % of the T1 population was dwarf. Interestingly, when both transgenic Mi131 lines were transformed with 35::AtACT1, none of the T1 plants exhibited severe leaf morphology or a dwarf phenotype (Figure 3.1.8 C). From this data, it can be concluded that the AtACT1-induced dwarf phenotype was suppressed when Mi131 was co-expressed with AtACT1.

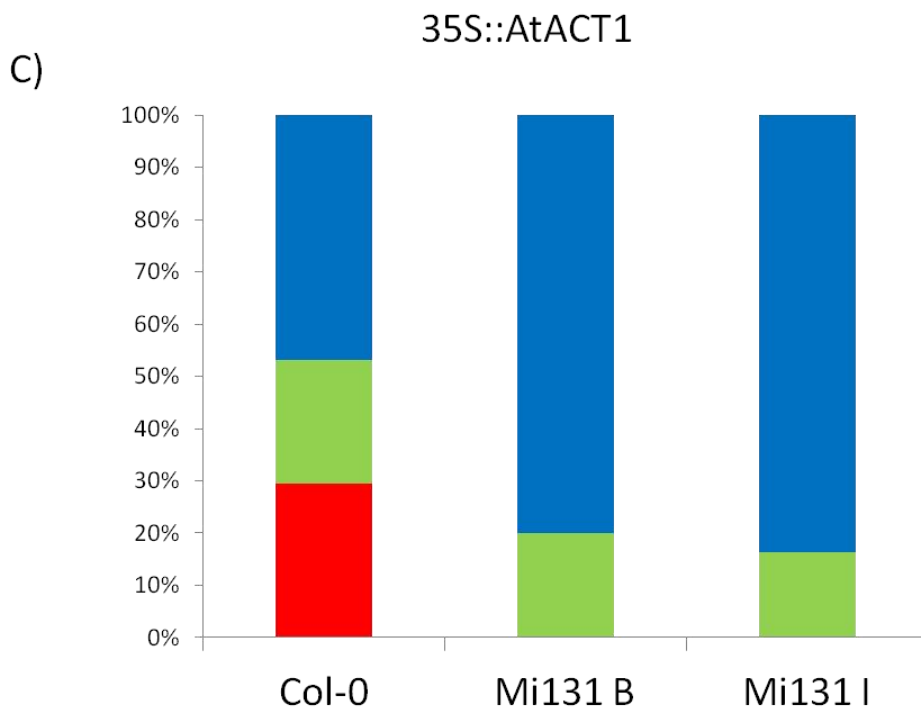
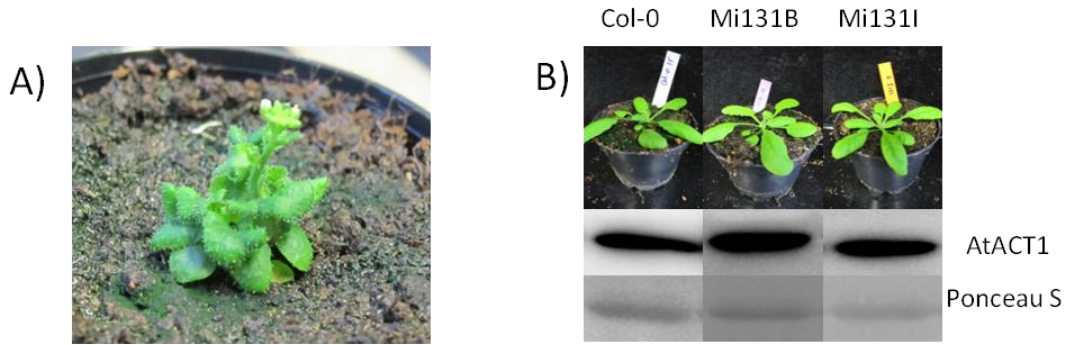


Figure 3.1.8. Overexpression of AtACT1 can lead to dwarf plants, but this phenotype can be rescued in the presence of 35S::Mi131. A) Abnormal plant phenotype from 5 week old, T1 Col-0 plant containing 35S::AtACT1. B) Col-0 and two homozygous T3 lines of 35S::Mi131 were transformed with 35S::AtACT1. Photograph shows representative T1 plants. ACT1 protein in these plants can be detected by Western blot analysis using the mAb45a antibody. C) Growth phenotype of individual T1 plants determined 5 weeks after germination and normalized into percentage of total plants (N=109, 110 and 80 respectively). Red indicates obvious abnormal leaf morphology. Green indicates intermediate leaf morphology or size of the rosette. Blue indicates normal, wildtype- size plants.

3.1.6 Mi131 can disrupt actin filaments *in vivo*

To illustrate the disruption of F actin by Mi131 in plant cells, Arabidopsis protoplasts constitutively expressing ABD2-GFP under a cauliflower mosaic virus 35S promoter were used in this experiment. ABD2-GFP is a truncated fimbrin 1 which contains actin binding domain 2 (Sheahan et al., 2004b; Wang et al., 2004). This ABD2-GFP specifically binds and label actin filaments and therefore the actin structure can be observed using the confocal laser scanning microscope. Protoplasts from 5-6 weeks old ABD2-GFP (T2) leaves show a strong labelling of the actin cytoskeleton (Sheahan et al., 2004b). ABD2-GFP protoplasts were transfected with RFP-Mi131 or RFP-PEPCTI, another nematode effector candidate used as a negative control (Figure 3.1.9 B). RFP-PEPCTI transfected ABD2-GFP protoplasts showed normal actin filament structure, similar to the untransformed ABD2-GFP protoplasts (Figure 3.1.9 A). In contrast, protoplasts expressing RFP-Mi131 showed disrupted actin filaments and reduced the visible levels of ABD2-GFP (Figure 3.1.9 C and D). From this outcome, it can be concluded that Mi131 can affect the organization of the actin filaments in the cells.

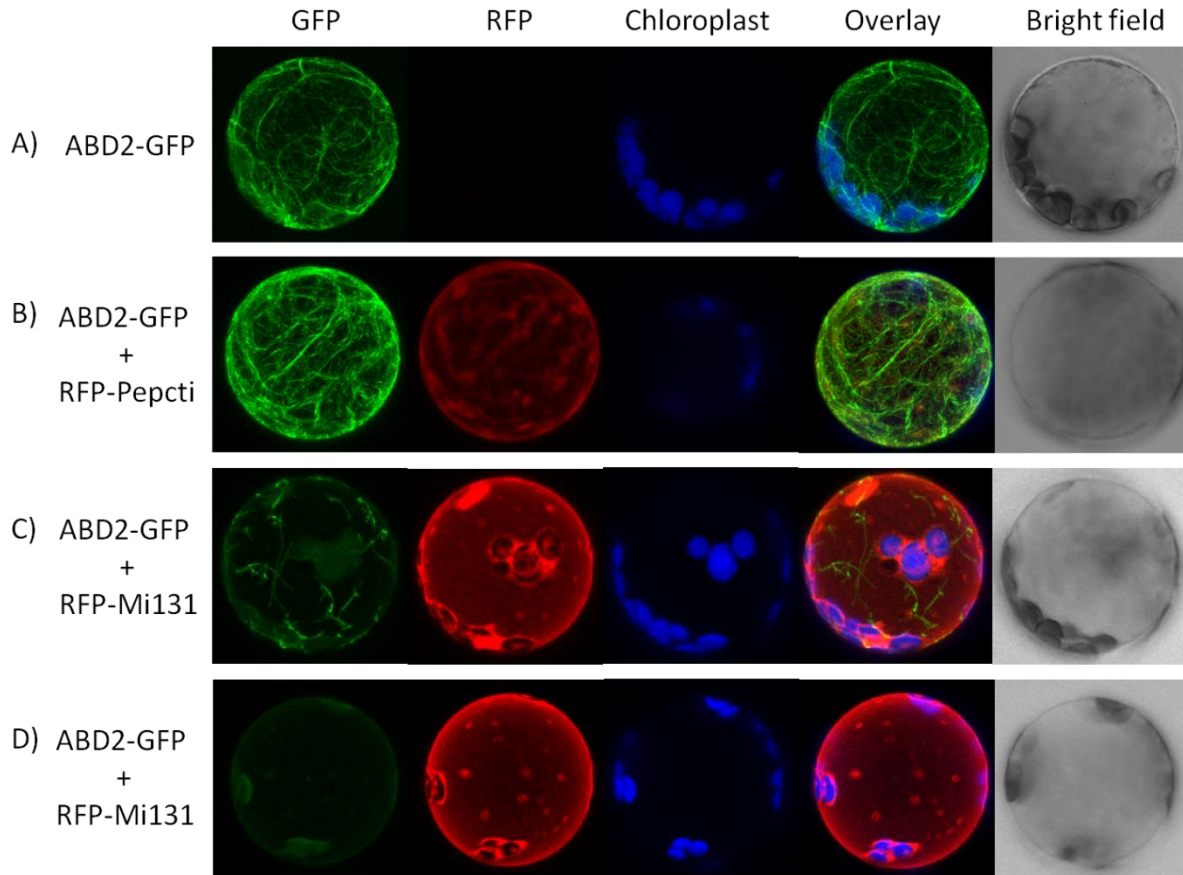


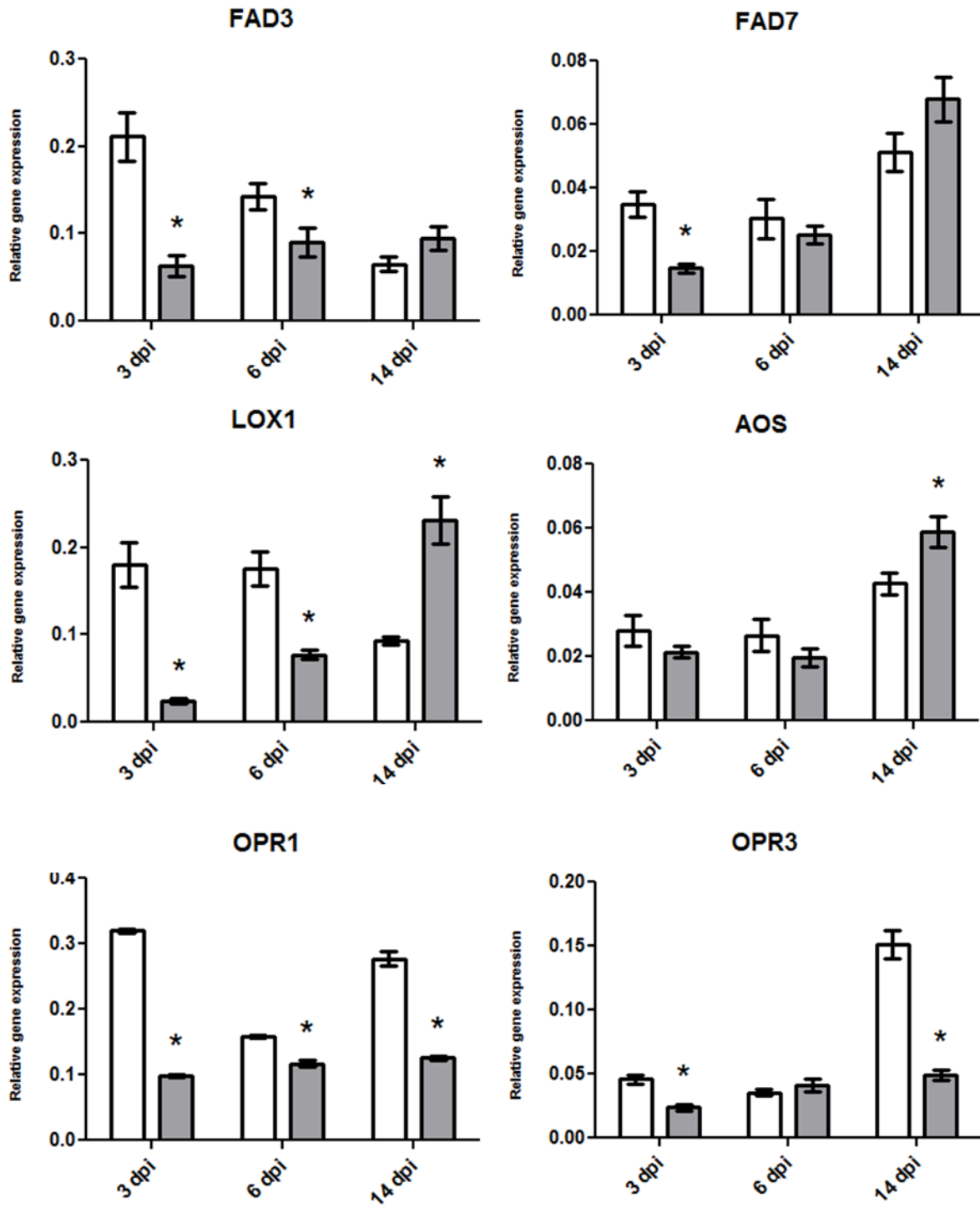
Figure 3.1.9. Mi131 disrupts the actin cytoskeleton *in vivo*. Protoplasts were extracted from ABD2-GFP leaves and transfected with RFP-PEPCTI (negative control) or RFP-Mi131. The disruption of actin cytoskeleton was monitored by laser scanning confocal microscopy (40x magnifications). GFP/RFP/chloroplast fluorescence signals are shown in green/red/blue respectively. Bright field pictures are showed in 1 representative layer. Actin filaments were either partially or fully disrupted when transfected protoplast with RFP-Mi131 but not in untransfected or cells expressing RFP-PEPCTI. These experiments were performed at least two times with similar result and at least 30 of ABD2-GFP protoplasts from each combination were observed with similar outcome.

3.2 Role of Jasmonic acid in plant protection against RKN

3.2.1 The regulation of JA related gene expression in gall-enriched tissue

To investigate the role of JA in plant nematode interaction, transcript abundance for several JA and general defense responsive genes was measured in infected root tissue. Since these JA related genes were normally upregulated during MeJA treatment and wounding, we hypothesized that if jasmonic acid is causing an inhospitable environment for the nematode, RKN might try to suppress the expression of JA biosynthesis genes. If the nematode was using JA as a susceptibility factor, the nematode may be inducing gene expression

Gall-enriched tissue from *M. hapla* infection was collected at 3, 6 and 14 post inoculation. As a control, uninfected root tissue was also collected. Quantitative real-time reverse transcriptase PCR (qRT-PCR) was performed to measure the expression of the following genes involved in JA biosynthesis: fatty acid desaturase gene *FAD3* and *FAD7*, allene oxide synthase (*AOS*), lipoxygenase 1 (*LOX1*), OPDA reductase 1 and 3 (*OPR1* and *OPR3*). In addition to JA biosynthesis gene regulation, the general defense related genes map kinase 3 (*MPK3*) and glutathione-S-transferase 6 (*GST6*) were chosen (Figure 3.2.1). At 3 dpi, only *AOS* expression was the same in the uninfected and gall-enriched tissue. All other genes were down regulated in the gall enriched tissue compared to the uninfected tissue. At 6 days post infection, *FAD3*, *LOX1*, *OPR1* and *MPK3* were down regulated in gall enriched tissue but not *FAD7*, *AOS*, *OPR3* and *GST6*. At the last time point (14dpi), *AOS* and *LOX1* expression were upregulated whereas *OPR1*, *OPR3*, *GST6* and *MPK3* were down regulated. Also at 14dpi, *FAD3* and *FAD7* transcript levels were the same in the gall enriched tissues as in the untreated samples. The down-regulation expression at 3dpi of the majority of the tested genes could be an indication that the nematode is trying to suppress JA-biosynthesis and subsequent defence signaling during the early stages of infection.



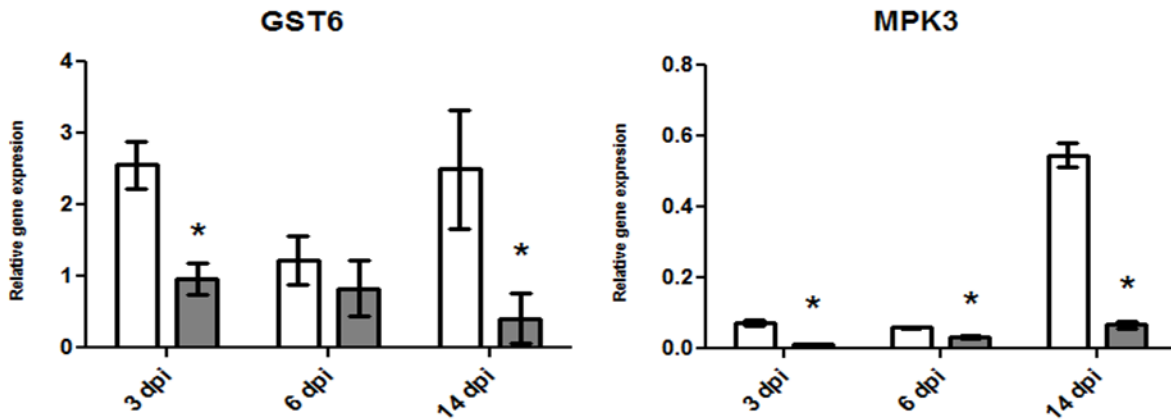


Figure 3.2.1. The regulation of jasmonic acid related genes and defense related genes in the gall-enriched tissue. Col-0 was infected with *M. hapla* J2, and gall enriched root tissue was collected 3, 6 and 14 days post inoculation. As a control, mock root samples were collected from plants inoculated with water. Gene expression was quantified by qRT-PCR. Bars represent relative gene expression to reference gene *UBQ5*. White and gray bars represent mock root and gall enriched tissue sample respectively. The graphs represent results from 2 biological replicates. The error bar represent stand error of mean (n=2). Asterisk indicates a significant different between mock root and infected sample tissue at each time point by using student t-test (p<0.05).

3.2.2 Nematode susceptibility is COI1 independent

Next, the JA perception mutant (*coil-t*), the JA biosynthesis mutant (*aos*) and Col-0 wild-type were used in nematode bioassays. Ten-day-old seedlings of Col-0, *aos*, and *coil-t* were transferred onto KNOPS media and inoculated with *M. hapla* juveniles. The numbers of galls per plant were counted at 14 dpi as a measure of nematode susceptibility. It is necessary to note that *coil-t* homozygous plants are male sterile, and therefore, it is not possible to maintain a *coil-t* homozygous seed batch. Therefore homozygous seedlings, which are insensitive to MeJA, were pre-selected by growing the segregating line on MS media supplemented with 50 μ M MeJA. After 10 days on the MeJA-containing media, only healthy, MeJA-insensitive *coil-t* plants were chosen for the infection experiments and transferred to KNOPS media without MeJA. Galling on the *coil-t* plants that were pre-selected with MeJA was significantly reduced in comparison to Col-0 (Figure 3.2.2). This data corroborates what had been shown in the tomato *jail* mutant, and suggests that COI1 protein is required for RKN susceptibility. Unexpectedly, we found that *aos* mutant was more susceptible to RKN infection than the wild-type.

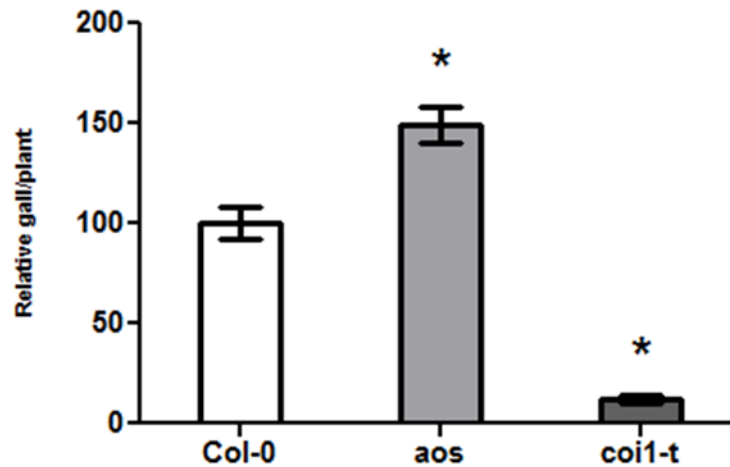


Figure 3.2.2. Mutants in jasmonic acid biosynthesis (*aos*) and perception (*coi1-t*, JA-pre-treated) show altered susceptibility to *Meloidogyne hapla*. Ten-day-old Col-0, *aos*, and *coi1-t* seedlings grown on MS were transferred to Petri dishes containing KNOPs media. Homozygous *coi1-t* was selected on 50 μ M MeJA MS plates prior to transfer to KNOPs media. Each plant was inoculated with 100 *M. hapla* J2 and the number of galls per plant was counted at 14 dpi. Bars represent mean of gall per plant normalized to the internal Col-0 contro. Results are combined from 3 independent experiments. Error bar represents standard error of mean (n= 149, 150 and 148 respectively). Asterisk indicates a significant different between mock and treatment group by using student t-test ($p < 0.05$).

The *coi1-t* seedlings used in the previous experiments were preselected with MeJA, and MeJA pre-treatment may induce plant responses that are independent of COI1 (Devoto et al., 2005; Stotz et al., 2011). As a result, MeJA selection may have led to the reduced galling observed in the *coi1-t* plants. To avoid MeJA pre-selection, the infection was performed on a *coi1-t* seed batch segregating for *coi1* (*coi1/coi1*, *COI1/coi1* and *COI1/COI1*). For individual plants in the experiment, the number of galls was counted. Next, the genotype of each plant was determined by PCR. The PCR analysis was done at the end of the infection experiment to avoid wound inducible responses which might influence nematode behavior and development (Snyder et al., 2006). Overall, *coi1/coi1* plants have similar number of galls/plant as *COI1/COI1* and *COI1/coi1* plant as shows in Figure 3.2.3. This infection data suggests that nematodes do not require COI1 for susceptibility.

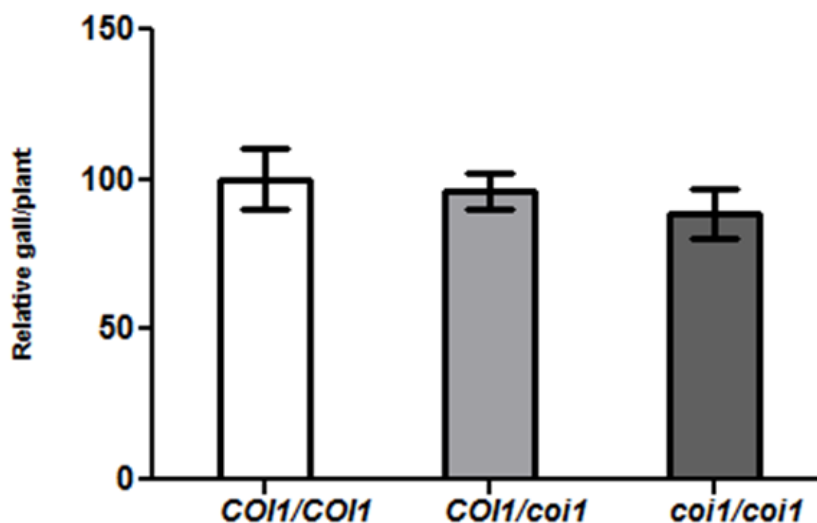


Figure 3.2.3. *coi1-t* plants that are not pre-selected with MeJA are as susceptible as the Col-0 control. Ten-day-old seedlings on KNOPs media were inoculated with 100 *M. hapla* J2 per plant. The severity of the infection was determined by counting galls at 14 dpi. Because a segregating pool of *coi1-t* seeds was used in the experiments, after infections, the genotype of each plant was determined by PCR (*COI1/COI1*, *COI1/coi1* and *coi1/coi1*). Bars represent mean of gall per plant normalized to internal *COI1/COI1* control, and results are combined from 6 independent experiments. Error bars represent the standard error of mean (n= 181, 356 and 132 respectively). No significant differences in galling could be seen between the wildtype (*COI1/COI1*) and the other genotypes (*COI1/coi1* and *coi1/coi1*) using a student t-test (p<0.05).

3.3.3 Exogenous application of MeJA can reduce galling in Arabidopsis

Exogenous application of MeJA has been shown to protect plants from RKN infection in several diverse plants, such as tomato, spinach and rice (Cooper et al., 2005; Nahar et al., 2011; Soriano et al., 2004). However, at the time of the experiments, the effect of exogenous MeJA treatment against RKN in Arabidopsis had not been fully investigated. To determine if an exogenous application of JA could induce resistance to nematode in Col-0 (wild-type) plants, eight day old Col-0 seedlings were transferred to MS plate supplemented with 50 μ M MeJA, 1 μ M coronatine (COR) or EtOH/water control. Root and leaf samples were collected 48 hours post-treatment to determine whether the MeJA and COR treatments could induce JA-marker gene expression in roots and leaves. qRT-PCR was performed to quantify the expression of JA marker gene *VSP2*. As expected, *VSP2* was induced in both leaf and root samples after MeJA treatment and COR treatment (Figure 3.2.4).

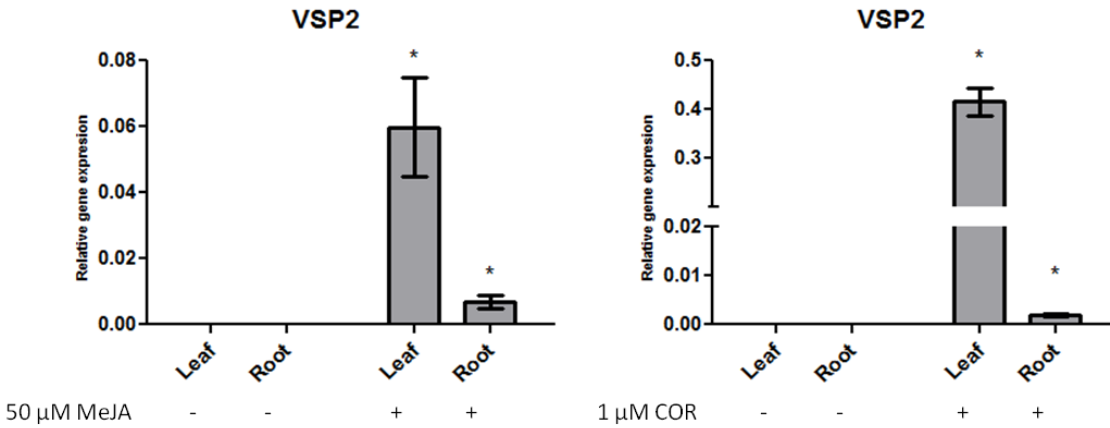


Figure 3.2.4. MeJA and COR treatment induce *VSP2* gene expression in *Arabidopsis* roots and leaves. Eight-day-old Col-0 were grown on MS media. They were then transferred onto either MS media (Mock) or MS supplemented with 50 μ M MeJA or 1 μ M COR for 48 hours. Leaves and roots were collected separately for RNA extraction. qRT-PCR was performed to measure the expression of *VSP2* relative to the reference gene *UBQ5*. Bars represent the average relative gene expression from 4 independent experiments. Error bar indicates the standard error of mean (n=4). Asterisk indicates a significant difference between mock and treatment group by a student t-test ($p < 0.05$).

For the nematode bioassays, eight day old Col-0 seedlings were placed on media with or without 50 μ M MeJA (A) or 1 μ M COR for 48 hours. After this treatment, the seedlings were transferred to KNOPS media for nematode inoculation. MeJA treated Col-0 had galling reduced by 70% whereas coronatine treatment reduced galling up to 40% (Figure 3.2.5). Thus, MeJA pre-treatment significantly reduced the number of galls confirming that, as in other plant species, exogenous application of the MeJA can induce resistance to RKN. The data also shows COR acts similar to MeJA in this assay; pre-treatment with COR also induced nematode resistance.

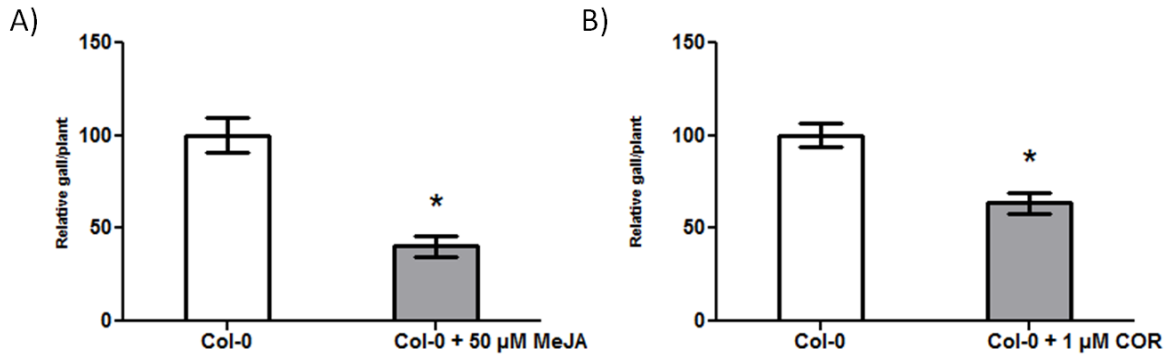


Figure 3.2.5. Gallings is reduced in *Arabidopsis* after MeJA and coronatine treatment. Eight-day-old Col-0 seedlings were transferred to MS only (Mock) or MS containing 50 μM MeJA (A) or 1 μM COR (B). After 48 hours of treatment, seedlings were transferred to KNOPs media and inoculated with 100 *M. hapla* J2 per plant. The severity of the infection was determined by counting the number of galls at 14 dpi. The bars represent number of galls per plant normalized to mock-treated plants from 5 and 3 independent experiments, respectively. Error bar represents the standard error of mean (A) n=150 and 155, B) n= 85 and 111). Asterisk indicates a significant different between mock and treatment group by using student t-test ($p < 0.05$)

3.3.4 MeJA does not interfere with nematode penetration

The MeJA-induced resistance in Col-0 may be due to 1) the MeJA treated plants have altered in their attractiveness to nematodes or are inhibited in nematode penetration and 2) the MeJA treatment induces defense responses that make it inhospitable for the sedentary nematode to establish a feeding site and induce galling. Many studies have been previously described that RKN attraction to plants can be affected by plant phytohormones. For example, ethylene modulates attractiveness to nematodes through the ethylene signaling pathway (Fudali et al., 2012). In maize, the *ZmLOX3* mutant has higher JA production in the root and is more attractive to RKN (Gao et al., 2007). However, in the rice JA biosynthesis mutant *hebiba*, which cannot produce JA, the attraction and penetration of nematodes in the root was not affected (Nahar et al., 2011). To determine whether MeJA treatment of Col-0 has an influence on nematode attraction or penetration, Col-0 seedlings were water (mock) or MeJA-treated for 48 hours prior to infection with RKN juveniles. At 4 dpi, the roots were stained with acid fuchsin to visualize the nematodes that had successfully penetrated the roots. At this time point, only J2 juveniles were observed in the root, indicating that at 4 dpi, the nematodes were still migrating or had only just begun the initiation of the feeding sites. There was no significant difference in the number of

J2 in the root of mock or MeJA treated plants (Figure 3.2.6). This indicates that MeJA does not likely affect the attraction or penetration of the nematodes in the root, but suggests that MeJA may be affecting later stages of the nematode development, such as the establishment or maintenance of the feeding site.

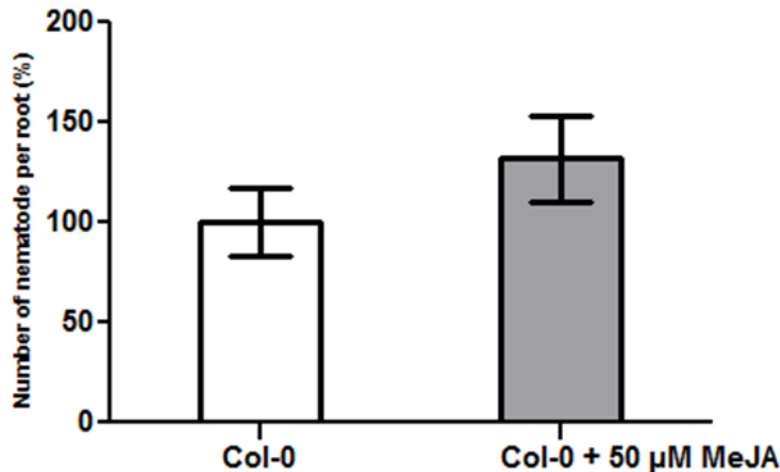


Figure 3.2.6. *M. hapla* penetration rate is not compromised in plants pre-treated with MeJA. Eight-day-old Col-0 seedlings grown on MS media were transferred to MS (Mock) or MS supplemented with 50 μ M MeJA. After 48 hours of treatment, seedlings were transferred to KNOPs media and inoculated with 100 *M. hapla* J2 per plant. At 4 days post infection, the seedlings were stained with acid fuchsin to visualize and count the root knot nematodes within the roots. Bars represent the number of nematodes relative to the mock control (set to 100) from 3 independent experiments. The error bar indicates the standard error of mean (n=54 and 55 respectively). No significant difference could be seen between mock and treatment group by using a student t-test ($p < 0.05$)

3.3.5 MeJA treatment increases OPDA and JA content in Arabidopsis.

We have observed that MeJA-induced resistance is dependent on jasmonic acid but independent of COI1. Recent reports have found that OPDA, 12-oxophytodienoic acid, is a well known intermediate oxylipin which can induce defense responses to certain pathogens in a COI1-independent manner (Park et al., 2013; Taki et al., 2005). Therefore, we predicted that exogenous MeJA-treatment of Arabidopsis could increase in levels of JA and other oxylipins, including OPDA, and that OPDA-mediated signaling may be responsible for the induced defence response that is independent of COI1.

Although it has been previously shown in *Arabidopsis* that MeJA can induce the expression of JA biosynthesis genes (Devoto et al., 2005), the effect of exogenous MeJA treatment on *Arabidopsis* hormone profile has not been fully investigated. Therefore, a metabolic profile of MeJA-treated plants was carried out in the department of Plant Biochemistry, Göttingen. For this experiment, I collected roots of eight day old seedlings that had been transferred onto MS plates, with or without MeJA, for 48 hours. Using these materials, a measurement of OPDA, dinor-OPDA, JA and JA-Ile was done by HPLC-MS/MS (Schatzki et al., 2013). The data reveal that after 48 hours MeJA treatment, OPDA, dinor-OPDA, JA and JA-Ile accumulated significantly in the MeJA treated roots (Figure 3.2.7). These results confirmed that MeJA treatment induces an accumulation of JA as well as JA-precursors.

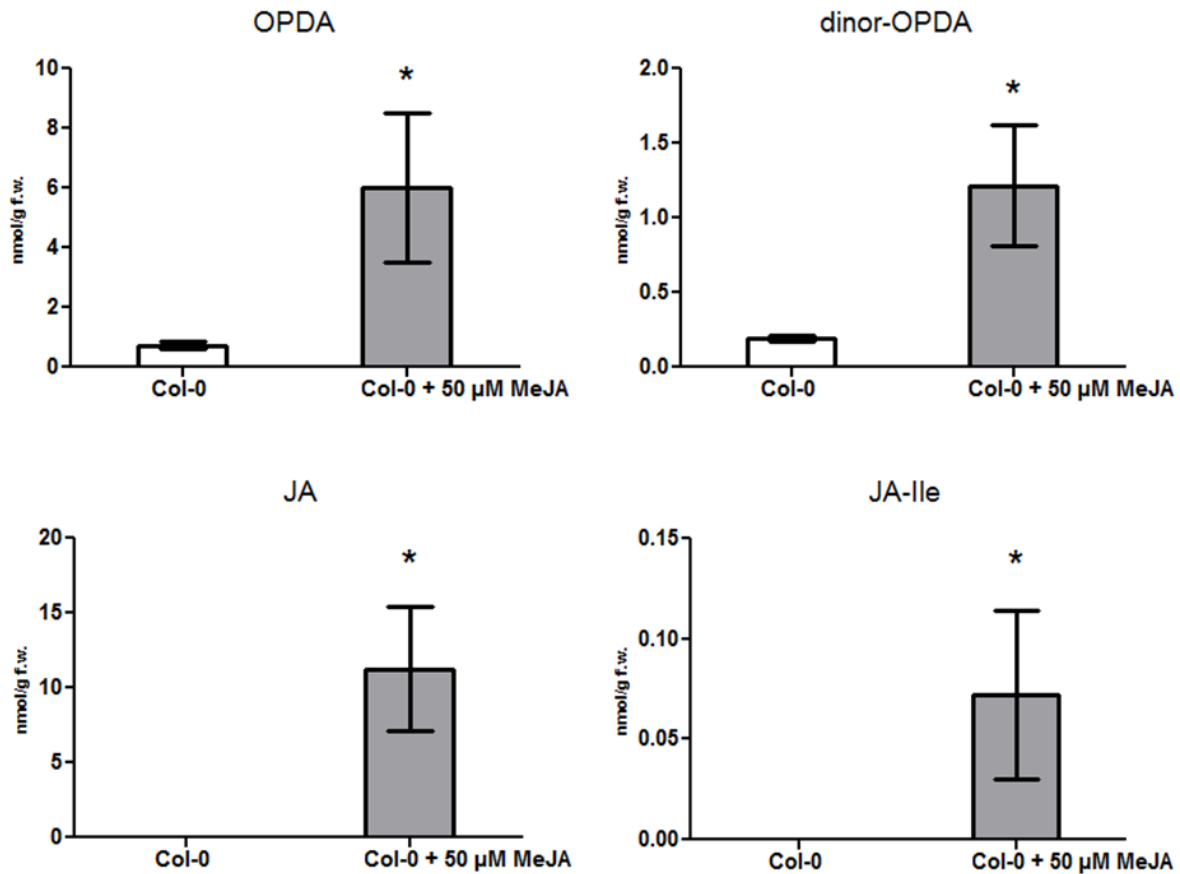


Figure 3.2.7. Measurement of OPDA, dinor-OPDA, JA and JA-Ile after MeJA treatment in Col-0 root. Eight day old seedlings were transferred onto MS media with or without 50 μ M MeJA. After 48 hours of treatment, approximately 200 mg of root materials were collected and rapidly frozen in liquid nitrogen for measurements. Bars represent average nmol/gram fresh weight of different hormones measured in by HPLC-MS/MS. Error bar indicates standard error of mean (n=3). Asterisk indicates a significant different between the mock and MeJA treated roots at each time point by using the student t-test ($p < 0.05$).

3.3.6 MeJA treated *aos* seedlings are susceptible to RKN

I have shown that *aos* but not *coil-t* seedlings are more susceptible to nematodes than Col-0 (Figure 3.2.2). The next question was to determine if the MeJA induced resistance is dependent on AOS. The MeJA treated *aos* seedlings were just as susceptible as the mock-treated *aos* seedlings (Figure 3.2.8). Therefore, MeJA-induced resistance is AOS-dependent, COI1 independent.

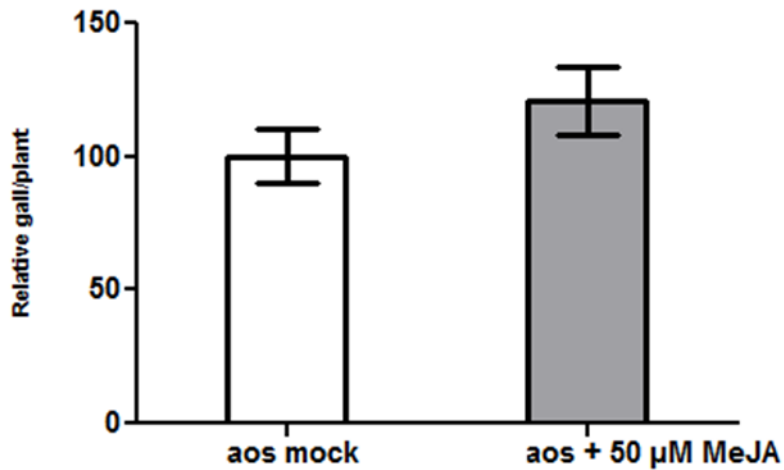


Figure 3.2.8. MeJA-treatment of *aos* plants fails to induce nematode resistance. Eight-day-old *aos* seedlings grow on MS plate were transferred to MS media (Mock) or MS supplemented with 50 μ M MeJA. After 48 hours of treatment, the seedlings were transferred to KNOPs media and inoculated with 100 *M. hapla* J2 per plant. The severity of the infection was determined by gall count at 14 dpi. Bars represent the number of galls per plant relative to the mock (set to 100) and results are combined from 3 independent experiments. The error bar indicates the standard error of mean (n=110 and 110 respectively). No significant different could be seen between the mock and treatment group by using student t-test ($p < 0.05$)

4. Discussion

4.1 The role of Mi131 as RKN effector

4.1.1 Mi131 interacts with Arabidopsis actins

We were interested in understanding the role of effector Mi131 during RKN plant interaction. To search for proteins that physically interacted with Mi131, we performed a Y2H screen. From this screen, we found that AtACT7 showed a positive interaction with Mi131. This interaction was verified *in planta* when Mi131-YFP co-immunoprecipitated with HA-AtACT7 after these two proteins were transiently expressed together in *Nicotiana benthamiana* leaves. In transgenic Arabidopsis expressing GFP-Mi131, AtACT7 could be also co-immunoprecipitated with Mi131 (Figure 3.1.4). Altogether, we conclude that Mi131 can interact with endogenous AtACT7.

Since we know that Mi131 can interact with AtACT7, the next question was to determine if this interaction was specific to only AtACT7. In Arabidopsis, there are 8 actins which can be divided into 2 classes by their expression patterns: reproductive and vegetative (Kandasamy et al., 2007). AtACT7 belongs to vegetative class of Arabidopsis actin along with AtACT2 and 8. Meanwhile AtACT1, 3, 4, 11 and 12 are reproductive actins. These two classes of actin diverged from a common ancestral gene at least 200 million years ago and they do not differ very much at the amino acid level (93-96% identity) (Kandasamy et al., 2007). We were curious if Mi131 was specific in its interaction with AtACT7 or if it could also interact with other actins. To answer this question, we transformed yeast Mi131 together with the full-length AtACT1, 2 or 8. From these co-transformation experiments, we found that only AtACT1 showed an interaction with Mi131 yeast cells but not AtACT2 or 8. This is not really unexpected due to the similarity of AtACT7 to AtACT1 (95.8%) is higher than to AtACT2 (92.6%) and AtACT8 (92.9%). In addition, AtACT1 can partially complement *act7-4* root phenotypes, suggesting that they can substitute for each other (Kandasamy et al., 2007).

Unfortunately, these yeast co-transformation results might be misleading because expression of Arabidopsis actins in yeast can alter its growth and maybe leading to false-negatives in the experiments (Kandasamy et al., 2007). In fact, it has been shown that expression of reproductive AtACT12 and vegetative AtACT8 in yeast alter yeast morphology and change the yeast cytoskeleton architecture. We also saw similar growth defects when we transformed our yeast

with either AtACT2 or AtACT8. Therefore, we postulated that if AtACT8 can integrate into yeast filament, it is likely that this phenomenon would also occur in AtACT2 due to their high homology (99.7%). In addition, because of their integration to the yeast actin filaments, it has been suggested that AtACT2 and AtACT8 cannot interact with yeast accessory proteins, therefore, it might be possible that these actins cannot be properly transported into the nucleus to activate the reporter genes (Kandasamy et al., 2009; Stüven et al., 2003). This scenario also leads to no growth on the selective media.

Surprisingly, AtACT7 is a vegetative actin belongs to the same actin class as AtACT2 and AtACT8, but expression of AtACT7 in yeast did not affect yeast growth. AtACT7 may be unique; it is the only actin in Arabidopsis which can be induced by stimuli such as wounding and hormone treatments (McDowell et al., 1996). Furthermore, the *act7* mutants exhibit the short twisting root phenotype which does not occur in *act2* or *act8* single mutants or the *act2/8* double mutant (Gilliland et al., 2002, 2003; Kandasamy et al., 2012). The most important feature of AtACT7 is that this actin makes-up approximately 60% of the total actin in the root and roughly 17% in the shoot (Kandasamy et al., 2009). The finding that AtACT7 comprises more of the root actin correlates to the report showing that *act7* plants have severe root phenotypes but no obvious above ground phenotype. AtACT7 is also interesting because it has been previously shown to be a target of the *P. syringae* effector HopW1 (Jelenska et al., 2014; Kang et al., 2014). Overall, expression of AtACT7 in yeast may not lead to any developmental defects because it appears to be functionally distinct from the vegetative actins AtACT2 and AtACT8.

To bypass potential problems of expression actins in yeast, we further investigated the potential interaction between Mi131 and other Arabidopsis actins through co-immunoprecipitation experiments and showed that Mi131 could interact with AtACT1, 2 and 8 in plants (Figure 3.1.3). Therefore, we concluded that Mi131 can interact with all tested Arabidopsis actins.

4.1.2 Mi131 can rescue 35S::ACT1 dwarf phenotype

Misexpression of AtACT1 caused an abnormal dwarf plant phenotype in approximately 20% of the transformant population but this abnormal phenotype can be specifically rescued by coexpressing a reproductive Arabidopsis profilin 4 (AtPFN4) (Kandasamy et al., 2007). It is believed that AtPFN4 is titrating out the high AtACT1 levels, bringing them down to a concentration that are less detrimental to plant growth. Since we have shown that Mi131 can interact with AtACT1, we suspected that if Mi131 is co-expressed with 35S::AtACT1, Mi131 should be able to suppress the dwarf phenotype caused by AtACT1 misexpression. As expected, approximately 30% of the 35S::AtACT1 (T1) in the Col-0 background showed a severe dwarf phenotype, which is quite similar to what had been observed by Kandasamy (Figure 3.1.8 C and Figure S1.5). Interestingly, when 35S::AtACT1 was co-expressed in transgenic plants expressing 35S::Mi131, no severe abnormal/small rosette phenotype was observed in all T1 plants. From this result, we concluded that the rescue/suppression of abnormal phenotype in Mi131 lines is likely due to the titration of AtACT1.

Kandasamy could show that the concentration of AtACT1 had a direct correlation to the plant phenotype. The dwarf plants had significantly more AtACT1 content than normal sized transgenic plants (Kandasamy et al., 2007). We did not find a concentration dependent effect of AtACT1 on plant phenotypes. One reason for this discrepancy is that Kandasamy et al., performed the quantification experiments in the *act2-1* mutant background and these plants have a 40% reduction of total actin compared to Col-0. As a result, these plants are likely to be more sensitive to changes in AtACT1 concentrations.

It should be noted that the two transgenic 35S::Mi131 lines used in the AtACT1 complementation experiments (Mi131 lines B and D) had relatively low levels of Mi131 protein and exhibit a normal growth and developmental phenotypes. Interestingly, it was difficult to obtain transformants with high concentrations of Mi131. After a screen of many transgenic plants, we found that plants with high Mi131 protein content, such as the GFP-Mi131 lines, were dwarf (Figure S1.6). The dwarf GFP-Mi131 phenotype resembles plants which overexpress Arabidopsis PFN3 (Fan et al., 2013). This suggests that at low concentrations of Mi131, any visible effects of Mi131 may be buffered by plant cytoskeleton systems, but at higher Mi131 concentrations, this buffering system is overwhelmed, resulting in a mutant dwarf phenotype.

4.1.3 Mi131 sequesters non-muscle actin *in vitro*

Since Mi131 could bind to actin in Arabidopsis, we wanted to see the possible effects of Mi131 on actin filaments. I assayed the effects of recombinant Mi131 on F actin polymerization using *in vitro* sedimentation assays. These assays allowed me to see if Mi131 could interfere with actin polymerization.

The formation of actin filament starts with a lag phase which corresponds to a nucleation period where actin monomers start to form dimers and oligomers, which is more stable form of actin. This nucleation period is followed by a growth phase in which actin monomers are assembled at the exposed ends of the oligomer actin, causing the actin to elongate from both ends. The steady state or equilibrium phase is reached when the assembly rate of the monomers to plus end is equal to the disassembly rate at the minus end of the filament or vice versa. The depolymerization of the F actin is commonly due to the hydrolysis that occurs on the actin-ATP, leading to actin-ADP. Which is a unstable and prone to dropping off the filament end (generally refers minus end) (Korn et al., 1987; Ranjith et al., 2010).

This polymerization rate can be determined by using an equation (adapted from Bruce Alberts et al., 2007; Doolittle et al., 2013)

$$\text{Actin polymerization rate} = K_{\text{on}}G - K_{\text{off}}$$

K_{on} = Polymerization rate constant

G = the free subunit of actin (G actin-ATP)

K_{off} = Depolymerization rate constant

Meaning that if

$K_{\text{on}}G > K_{\text{off}}$ this causes the filament to elongate

$K_{\text{on}}G = K_{\text{off}}$ when it reaches the equilibrium phase

$K_{\text{on}}G < K_{\text{off}}$ the filament will start to shrink or shorten

In our first experiment, we found that when G actin was co-incubated with buffer or BSA prior to polymerization, there was no effect on the efficiency of F actin formation. However, when the

G actin was co-incubated with purified recombinant Mi131 or bacterial lysate containing recombinant Mi131, there was significantly more G actin than F actin at the end on of the experiment, which indicates that Mi131 interfered with the polymerization process (Figure 3.1.6 A and B). However, it may also be possible that Mi131 is actively severing the actin filaments.

To determine if Mi131 has F actin severing activity, we next polymerized actin prior to the co-incubation with purified His-Mi131. We found that amount of F actin in the pellet fraction was gradually reduced in the presence of Mi131, and this corresponded to an increase in the amount of G actin in the supernatant fraction. In addition, the reduction of F actin in the presence of Mi131 was time dependent (Figure 3.1.7 and Figure S1.4). Thus, it was not clear if Mi131 can sever the F actin or interfere with the F actin polymerization process. However, we hypothesize that the latter is correct for two reasons: 1) our experiments show that Mi131 cannot bind to F actin, it can only bind to G actin. This is indicated by the fact that there was very little purified Mi131 detected with F actin in the pellet fractions (Figure 3.1.7 and Figure S1.3). 2). Mi131 contains a profilin domain, and these domains typically bind G actin and do not have enzymatic activity. Therefore, to explain the reduction in polymerized F actin in the presence of Mi131, we suspect that Mi131 sequesters G actin and this reduces the amount of G actin in the system. As a result, the actin polymerization rate in the present of Mi131 can be rewritten

$$\text{Polymerization rate} = K_{\text{on}}[G_{\text{free}}] - K_{\text{off}}.$$

When $G_{\text{free}} = G \text{ actin-ATP (total)} - G \text{ actin-ATP (in complex with Mi131)}$.

In the presence of Mi131 (17 μM), Mi131-bound G actin is as abundant as the free G actin-ATP, this causes $K_{\text{on}}[G_{\text{free}}]$ value to be close to 0. This leads to the depolymerization of F actin filament ($K_{\text{on}}[G_{\text{free}}] < K_{\text{off}}$) at a constant rate until it reaches a new equilibrium phase when $K_{\text{on}}[G_{\text{free}}] = K_{\text{off}}$. This phenomenon resulted in gradually increases amount of G actin and decrease amount of F actin over time as illustrated in Figure 4.1.1.

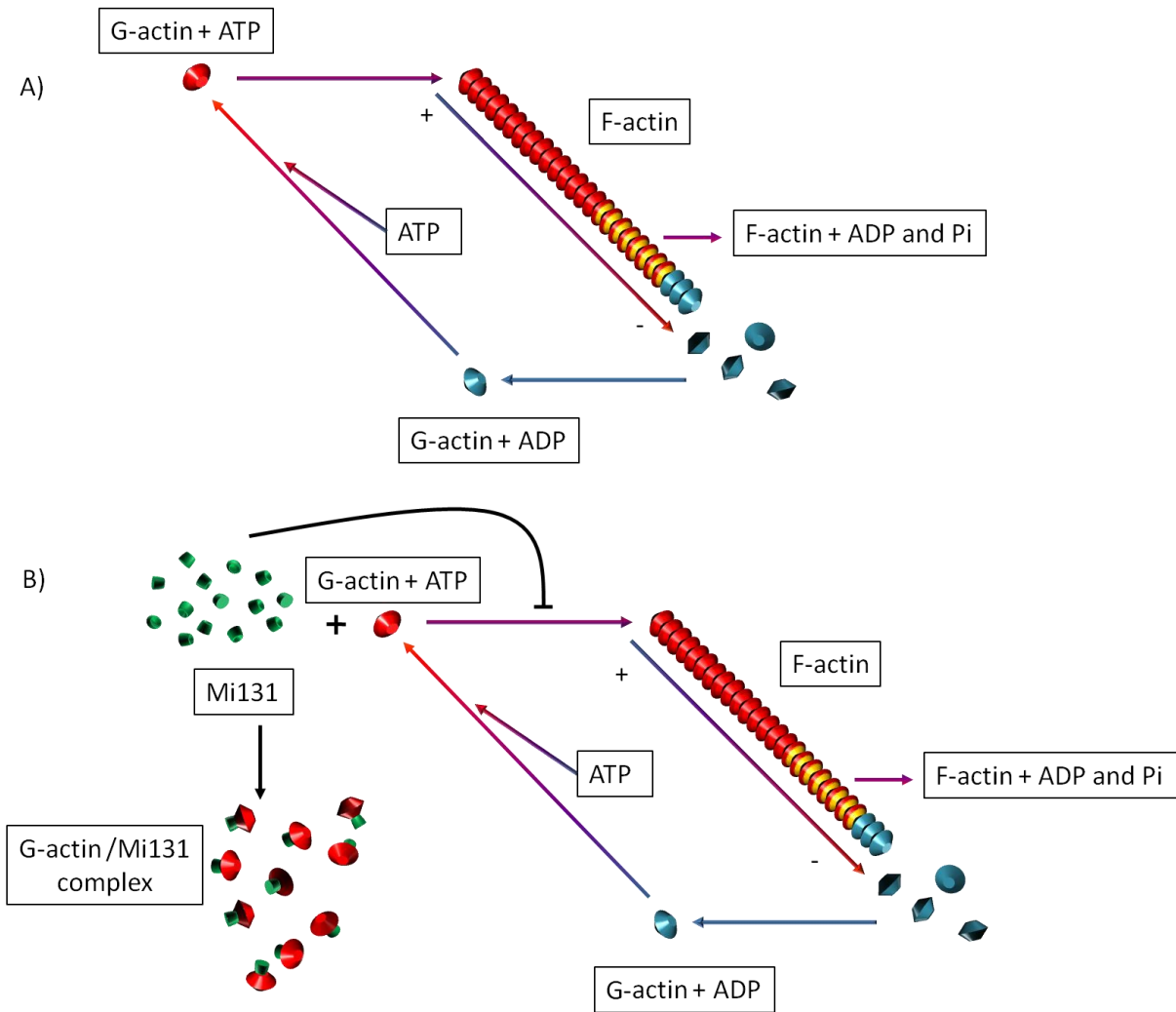


Figure 4.1.1. Simplified model for *in vitro* actin polymerization assay.

A) Normal turnover of the actin.

B) Mi131 disturbs the actin turnover which leads to a shrinkage of the actin filament in a time and concentration dependent manner.

Further evidence for a Mi131-specific effect on actin filaments comes from our work in live plant cells. We used protoplasts containing ABD2-GFP. This fluorescent protein decorates the actin filaments and they can be monitored under the confocal laser scanning microscope for changes in the F actin organization. Protoplasts expressing ABD2-GFP showed a fine structure of actin filaments in the cells (Figure 3.1.9 A). The ABD2-GFP protoplasts transfected with Mi131 showed only fragmented or completely disrupted actin filaments (Figure 3.1.9 C and D).

Altogether, we conclude that expressing Mi131 in the cells leads to a diffuse, fragmented actin filaments in the plant cells.

4.1.4 Why would RKNs secrete profilin into plant cells?

The idea that the nematode may be secreting a profilin into the plant cell to manipulate the feeding site formation is intriguing. A secreted nematode profilin would suggest that the nematodes are trying to manipulate the plant actin cytoskeleton. One reason for this may be because the actin cytoskeleton is linked to plant defence, and a second, but not mutually exclusive, reason is the nematode is rearranging the plant cytoskeleton to establish its feeding cells.

Interestingly, the idea that the nematode is secreting effectors to manipulate the plant cell for giant cell formation had been proposed several years ago (De Almeida Engler et al., 2004). Cell biology studies looking at the actin and microtubules in the giant cells showed the cytoplasmic actin is diffuse and fragmented whereas the actin in the cell cortex appears as thick cables (De Almeida Engler et al., 2004). Interestingly, the expression of *AtACT2* and *AtACT7* was seen up-regulated in the feeding cells, suggesting that there is more globular actin in the giant cells (de Almeida Engler and Gheysen, 2012). Moreover, the actin binding protein *ADF2* (actin depolymerization factor 2) was upregulated upon infection of Arabidopsis roots. *ADF*/cofilins sever actin filaments and also increase the rate at which actin monomers fall off the pointed end of the actin filaments (Maciver and Hussey 2002). A knockdown of *ADF2* resulted in an accumulation of actin bundles, presumably due to defects in actin turnover, and when the *ADF2* knockdown plants were infected with root-knot nematodes, gall expansion was inhibited, suggesting that actin stabilization negatively affects the feeding site expansion and gall development (Clément et al., 2009). This result provides evidence that the nematode needs to disrupt and re-organize cytoplasmic actin filaments to generate feeding cells and complete its lifecycle. This idea is further supported by pharmacological studies that use chemicals to induce actin depolymerization. Treating roots with cytochalasin D, that blocks actin polymerization, lead to arrested gall development (De Almeida Engler et al., 2004).

Altogether the data suggest that the actin cytoskeleton in feeding cells is dependent on actin re-assembly and re-organization. The giant cells undergo a cytokinetic mitosis to become large, multinucleate feeding cells, and the dynamic re-organization of the actin cytoskeleton in the feeding cells may be prerequisite to prevent cytokinesis during giant cell morphogenesis. It may also lead to a less viscous giant cell cytoplasm, which may make nematode feeding through the stylet easier (De Almeida Engler et al., 2004). How the nematode is able to manipulate the giant cell cytoskeleton is unknown, but it is tempting to speculate that effectors are involved. Therefore, we propose that Mi131 is involved in the initiation of the feeding cells by disrupting actin filament and therefore changing/inhibiting the cell division processes in order to manipulate a normal cell into a giant cell (Hoshino et al., 2003; Liu et al., 2011; Livanos et al., 2012; Sheahan et al., 2004a).

We cannot rule out that the nematode is targeting the cytoskeleton in an attempt to block plant defenses that rely on cytoskeletal rearrangements. Cytoskeleton rearrangements have been shown to contribute to plant defence responses against diverse pathogens (oomycetes and fungi). Confocal work using labeled actin filaments has shown that actin filaments are redistributed in plants after attack by non-host oomycetes, and upon oomycete infection of parsley cells, profilin localizes at the site of infection, suggesting that the pathogen-induced actin remodeling requires profilin (Hardham et al., 2008; Takemoto and Hardham, 2004). The rearrangements of the actin filaments may contribute to transport and secretion of defence-related cargo, including pathogenesis related proteins, to the infection sites (Schmidt and Strittmatter, 2007). For example, the penetration resistance protein PEN2, involved in the interaction of Arabidopsis with the non-adapted pathogen, *Colletotrichum truncatum*, is transported to the site of infection by actin (Mano et al., 2002). Actin-dependent deposition of cell wall constituents may also strengthen the cell wall to prevent pathogen penetration (Hardham et al., 2008). To counteract these defenses, pathogens have effectors that will interfere with the plant cytoskeleton. For example, the bacterial effector HopW1 actively targets actin filaments for de-polymerization (Kang et al., 2014). Additional experimental evidence showing pathogens interfering with actin filaments comes from work on a *Verticillium dahliae*, which has been shown to secrete a toxin that causes fragmentation of the actin filaments (Yuan et al., 2006). Thus the cytoskeleton can be the target of pathogen effectors.

4.2 OPDA mediates RKN defense

4.2.1 COI1 is not involved in defense against RKN

My data showed that when MeJA is applied to Arabidopsis, the plants are more resistant to nematodes. One possibility is that the exogenous MeJA that remains on the plant roots may be toxic to RKNs. Although we did not test for MeJA toxicity, it has been previously shown that RKN soaked in a MeJA solution could still infect and proliferate normally in tomato, indicating that MeJA has no direct toxic effects on the RKNs (Cooper et al., 2005). A second possibility is that the MeJA treatment reduced the attractiveness and/or penetration rate of plants. It has been previously reported that changes in phytohormone levels can alter the nematode attractiveness to plant root (Fudali et al, 2012 and Gao et al, 2007). However, our results show that exogenous application of MeJA did not affect the number of nematodes in the root at early stages of infection (Figure 3.2.6). This finding suggests that the reduction of galling after MeJA treatment is not due to changes in root attractiveness/penetration.

Exogenous application of MeJA can induce resistance against RKN infection in many plant species (Cooper et al., 2005; Fujimoto et al., 2011a; Nahar et al., 2011; Soriano et al., 2004). For example, in rice, exogenous MeJA induced resistance to *Meloidogyne graminicola*, and this resistance is dependent on an intact JA biosynthesis pathway (Nahar et al., 2011). They further tested and discovered that an exogenous application of ethylene could induce JA-responsive genes in the roots and make the roots more resistant to nematodes. Gene expression analyses in susceptible soybean show that syncytia have a local down-regulation of jasmonic acid biosynthesis genes and responses (Ithal et al., 2007; Kammerhofer et al., 2015). Overall, these data would suggest that plant parasitic nematodes are trying to actively suppress JA-mediated responses during infection and an exogenous application of MeJA overcomes the nematode suppression and leads to JA-mediated defense.

Interestingly, work in tomato contradicts this model and instead, suggests that JA acts a susceptibility factor for root-knot nematodes. This conclusion is based upon the observation that the *jail* mutant in tomato, which lacks JA-perception and downstream signaling, is more resistant to nematodes compared to the wild-type tomato (Bhattarai et al., 2008). Interestingly, the receptor mutant *coi1* is also more resistant to the fungal pathogen *Verticillium longisporum*,

suggesting that COI1-dependent signaling processes are needed for susceptibility (Ralhan et al., 2012). To further investigate if JA is playing a key role in nematode susceptibility, I utilized various Arabidopsis mutants in JA perception and biosynthesis which had not been previously tested with RKN. Nematode bioassays on MeJA preselected *coil-t* seedlings showed that these mutant seedlings were more resistance to RKN (Figure 3.2.2) similar to the finding in *jail* tomato (Bhattarai et al., 2008; Fujimoto et al., 2011b), However, we suspected that the MeJA pre-selection may have influenced nematode responses in *coil-t*. Therefore, we performed the bioassay on seedlings that were segregating for *coil-t*, and found that homozygous *coil-t* seedlings showed no resistance to RKN (Figure 3.2.3). The nematode resistance observed in *coil-t* in the initial screen with MeJA pre-selection is probably due to the effects of MeJA, which must be COI1-independent. Although this finding contradicts the results from tomato mutant *jail*, it should be noted that these tomato plants had also been pre-selected with MeJA to select for the homozygous plants. Although the pre-selection occurred 7 weeks prior to the RKN inoculation, the effects of MeJA seem to be long lasting. A recent report has found that MeJA treatment could induce nematode resistance for at least 1 week after the foliar application in tomato plants (Fujimoto et al., 2011a), and therefore, it is possible that the pre-treated *jail* tomato plants were primed for nematode resistance.

Surprisingly, during the course of my thesis, Fujimoto et al published two reports showing that *coil-1* seedlings are more resistant to RKN infection (Fujimoto et al 2011 and 2015). Although they did not preselect *coil-1* seedling with MeJA, differences in the experimental conditions and the different species of root-knot nematode used in their experiments (*M. incognita*) may be contributing to the discrepancies in our results.

Although we did not see an effect of COI1 on nematode susceptibility, the biosynthesis mutant *aos* was more susceptible to *M. hapla* infection (Figure 3.2.2). This finding of *aos* susceptibility leads us to hypothesize that JA may be playing a role in plant defense against RKN in a COI1 independent manner.

Since there are many JA biosynthesis mutants available in Arabidopsis, addition nematode bioassays were performed in the Gleason lab to determine if mutants in JA biosynthesis or signaling had altered susceptibility similar to *aos* mutant. Work in the Gleason lab that was carried out concurrently with my thesis showed that the mutant *fad378*, which lacks the 18:3

precursors for JA biosynthesis, was more susceptible to root-knot nematodes similar to *aos* mutant (Figure S2.1 A). This data would fit with our model that JA acts as a defense molecule against nematodes. However, additional work in the lab showed that *opr3* mutant had wild-type-like levels of disease (Figure S2.1 C). The *opr3* prevents the conversion of OPDA to JA and, therefore, accumulates OPDA. This suggests that OPDA is important in the defense against nematodes. However, it is important to note that these mutant show a conditional JA deficiency (Schilmiller et al., 2007; Stintzi and Browse, 2000), suggesting that it may have a “leaky” phenotype. Therefore, I additionally tested the *acx1/5* mutant, which a mutation in the enzymes involved in catalyzing the first step of fatty acid beta-oxidation. The preliminary data of the infected *acx1/5* seedlings also had wild-type levels of disease (Figure S2.1 D). This would suggest that product(s) that are downstream of AOS and upstream of OPR3 in the JA biosynthesis pathway are playing a role in plant resistance to nematodes. Overall, the infection data suggests that the JA biosynthesis step in the plastid but not peroxisome is likely to be important for the nematode defense. This leads to the conclusion that the oxylipins that are produced between the AOS and OPR3 biosynthesis steps have an effect on plant protection against nematodes, but that this plant protection is occurring independently of COI1 function.

The primary JA precursor, 12-oxo-phytodienoic acid [OPDA], lies between AOS and OPR3 in the JA biosynthesis pathway. OPDA can induce a subset of genes that are part of a COI1 independent pathway (Park et al., 2013; Ribot et al., 2008; Taki et al., 2005), and in tomato, OPDA has recently been shown to be important in mediating defense against necrotrophic fungi in a COI1-independent manner (Scalschi et al., 2015). Due to fact that *coil-t* and *opr3* but not *aos* have wild type levels of OPDA (Park et al., 2013), we hypothesized that OPDA, not JA, is key to nematode defense signaling in plants

To test this hypothesis, we measured the susceptibility of a mutant in Peptidyl-prolyl cis-trans isomerase 3 (CYP20-3), the OPDA receptor (Park et al., 2013). The perception of OPDA leads to the formation of the cysteine synthesis complex (CSC), and this increases the production of thiol and glutathione. This changes the cellular redox homeostasis in the cell, which triggers the expression of stress/defense responsive genes. Nematode bioassays were performed on *cyp20-3* seedlings and found that these plants are more the susceptible to nematodes (Figure S2.1 B), similar to *aos* and *fad378*. This finding confirms our hypothesis that OPDA signaling plays a

major role in controlling nematodes. Therefore, it is plausible that plant defenses against nematodes are dependent on OPDA.

4.2.2 MeJA application induces accumulation of JA and OPDA in the root

Because we could induce nematode resistance in *coil-t* plants with an exogenous MeJA treatment, we hypothesized that exogenous MeJA could induce JA biosynthesis, and there would be induction of jasmonates and other reactive electrophilic species, such as OPDA. This positive feedback loop has been previously shown in barley leaves treated with MeJA. In this case, the exogenous MeJA treatment increased the concentration of linolenic acid, the substrate in JA biosynthesis processes as well as other JA related derivatives (Bachmann et al., 2002). In Arabidopsis, the transcriptional upregulation of JA biosynthesis genes after MeJA application suggests that MeJA treatment can stimulate the biosynthesis of JA (Chaturvedi et al., 2008; Devoto et al., 2005; Melan et al., 1993). Therefore, metabolic profiling was performed on seedlings treated with MeJA in order to observe the accumulation of JA and other metabolites in Arabidopsis roots. The results for this analysis showed that MeJA application could increase the amount of OPDA, dinor-OPDA, JA and JA-Ile in the root (Figure 3.2.7).

We next asked if exogenous MeJA could have an effect on nematode resistance in plants in which the JA biosynthesis pathway was altered and not able to produce OPDA. To answer this question *aos* mutant, a early JA biosynthesis mutant, was chosen because it is a null mutant in which the biosynthesis pathway to produce OPDA and JA is disrupted (Grebner et al., 2013; Laudert and Weiler, 1998). There should be no enhanced accumulation of OPDA or JA in the MeJA-treated *aos* plants due to the lack of AOS enzyme. The *aos* seedlings treated with MeJA were just as susceptible as the non-treated *aos* plants (Figure 3.2.8). This result further supports our hypothesis that OPDA accumulation is required for basal defense against RKN.

4.2.3 Suppression of JA biosynthesis genes in gall-enriched tissue

Since RKN has an intimate relationship with plant host, it is plausible that RKNs are actively suppressing plant defense in order to become successful biotrophic pathogens (Abad et al., 2003; Chitwood and Perry, 2009; Hewezi and Baum, 2012). RKNs are likely using proteins secreted from glands and their cuticle to suppress plant defense. For example, it was shown that a fatty acid and retinol binding protein (Mj-FAR1) effector is secreted from the *M. javanica* cuticle and this effector acts in the plant apoplast, perhaps to suppress host lipid based defenses (Iberkleid et al., 2013).

Our data suggests that the plant may be trying to mount a defense against the nematodes by turning on JA-biosynthesis, which in turn, is likely suppressed by nematode secreted proteins, also known as “effectors”. If this were true, JA biosynthesis gene expression might be differently regulated upon the infection with RKNs. Transcriptional analysis via qRT-PCR was performed for various JA biosynthesis genes and general plant defense genes in the gall-enriched tissue (3, 7 and 14 dpi). In this experiment, we used *LOXI* as a control gene which has been previously shown to be induced upon MeJA treatment and suppressed in RKN infection at day 7 and 14 dpi (Jammes et al., 2005; Melan et al., 1993). Our quantification shows the suppression of *LOXI* at 3 and 6 dpi however, *LOXI* expression was induced after 14 dpi in our experimental conditions. This might be due to the variation in root-knot nematode bioassays. Because we did not synchronize our infections, this could result in a mix of nematodes at different life-stages at a set time point after inoculation. Interestingly, we found that many of JA biosynthesis genes were downregulated at the early stages of infection (3 dpi) and this suppression of gene regulation shifted to the expression level that similar to control root or even higher at 14 dpi for *FAD3*, *FAD7* and *AOS*. The expression of *OPR1* and *OPR3*, however, was significantly down-regulated at most time points. This finding reveals the suppression of the expression of various JA biosynthesis genes likely happens during the early stages of infection.

Furthermore, we quantified the expression of *GST6* and *MPK3*. These genes are normally upregulated upon pathogen challenge (Asai et al., 2002; Dubreuil-Maurizi and Poinssot, 2012). However we could show that *MPK3* and *GST6* transcript level were decreased at all time points. A recent report has shown that a nematode molecule called ascaroside could trigger *MPK3*

protein accumulation and *GSTF6* gene expression in Arabidopsis (Manosalva et al., 2015). The purified ascaroside elicits PAMP-triggered immunity (PTI) in plants. However, during nematode infection, there is no induction of typical PTI responses. This suggests that nematode effectors are suppressing PTI. From our quantification of *MPK3* and *GST6*, the suppression of these genes likely supports the hypothesis that RKNs are actively suppressing plant defenses during RKN parasitism (Cabrera et al., 2014; Goverse and Smant, 2014; Jaouannet et al., 2013).

Together with our expression data of JA biosynthesis genes in gall-enriched tissue, it is tempting to speculate that RKN is actively suppressing jasmonic acid biosynthesis and defense related genes expression in order to successfully infect the plant, maintain their feeding site and complete their life cycle.

When we combine all our data 1) the infection data on various JA biosynthesis and signaling mutants. 2) OPDA/JA measurement in the root of Arabidopsis (Col-0) after MeJA treatment and 3) transcriptional analysis of JA biosynthesis genes, we can conclude that plants require OPDA in order to defend themselves against RKN infection (Figure 4.2.1). Moreover, when plants are treated with MeJA, this leads to an increased OPDA content in the root, which results in a more resistant phenotype against RKN infection. To understand how OPDA mediates plant defense against RKNs would be interesting to study in the future.

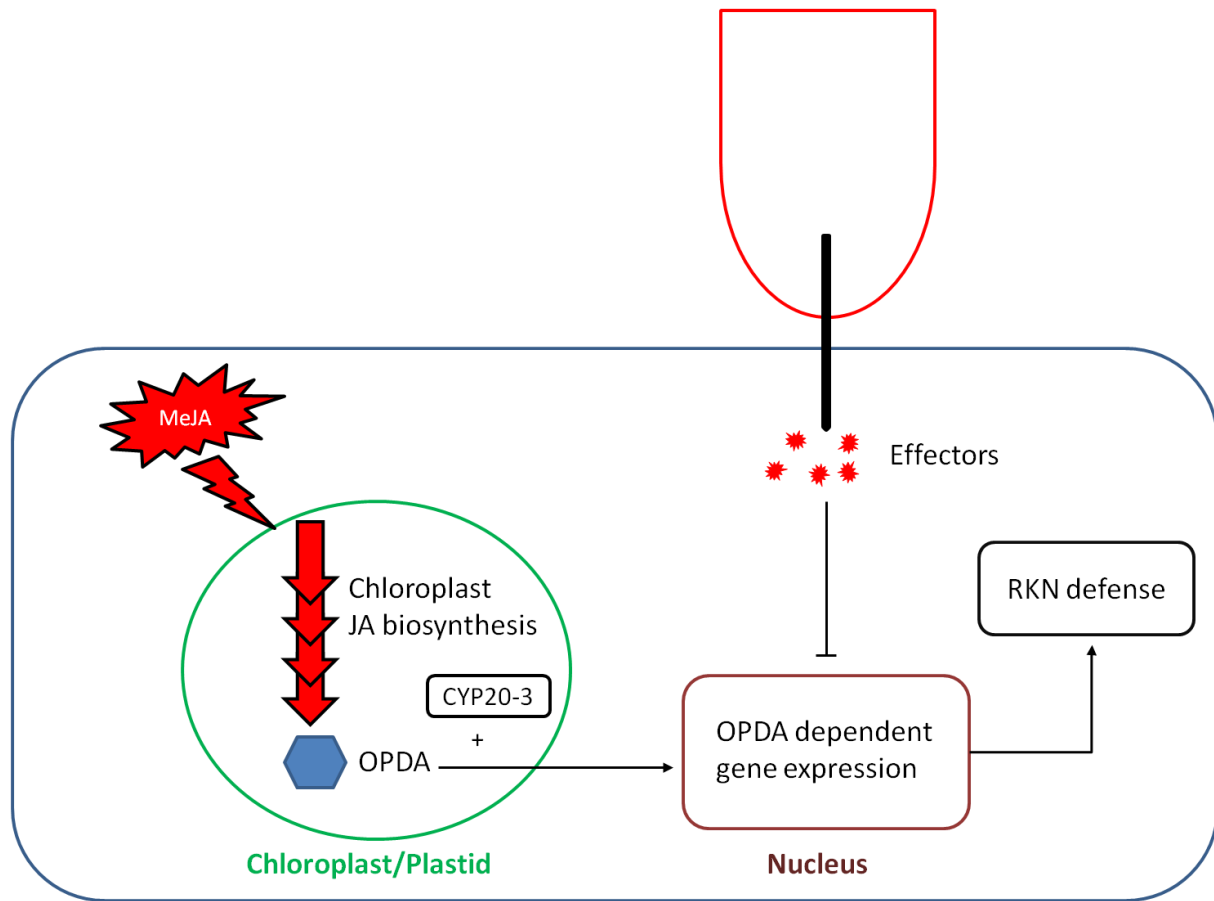


Figure 4.2.1, The model of OPDA mediate RKN defense. RKNs are known to able to secrete the effector proteins through stylet or cuticle. From our experimental data, we found an indication that OPDA signaling can give plant protection against *M. hapla*, however, the mechanism behind plant protection is still elusive.

5. References

- Abad, P., Favery, B., Rosso, M.-N., and Castagnone-Sereno, P. (2003). Root-knot nematode parasitism and host response: molecular basis of a sophisticated interaction. *Mol. Plant Pathol.* 4, 217–224.
- Abad, P., Gouzy, J., Aury, J.-M., Castagnone-Sereno, P., Danchin, E.G.J., Deleury, E., Perfus-Barbeoch, L., Anthouard, V., Artiguenave, F., Blok, V.C., et al. (2008). Genome sequence of the metazoan plant-parasitic nematode *Meloidogyne incognita*. *Nat. Biotechnol.* 26, 909–915.
- Absmanner, B., Stadler, R., and Hammes, U.Z. (2013). Phloem development in nematode-induced feeding sites: the implications of auxin and cytokinin. *Front. Plant Sci.* 4.
- Asai, T., Tena, G., Plotnikova, J., Willmann, M.R., Chiu, W.L., Gomez-Gomez, L., Boller, T., Ausubel, F.M., and Sheen, J. (2002). MAP kinase signalling cascade in Arabidopsis innate immunity. *Nature* 415, 977–983.
- Bachmann, A., Hause, B., Maucher, H., Garbe, E., K.Vörös, Weichert, H., Wasternack, C., and Feussner, I. (2002). Jasmonate-Induced Lipid Peroxidation in Barley Leaves Initiated by Distinct 13-LOX Forms of Chloroplasts. *Biol. Chem.* 383, 1645–1657.
- Bannenberg, G., Martínez, M., Hamberg, M., and Castresana, C. (2009). Diversity of the enzymatic activity in the lipoxygenase gene family of *Arabidopsis thaliana*. *Lipids* 44, 85–95.
- Barcala, M., García, A., Cabrera, J., Casson, S., Lindsey, K., Favery, B., García-Casado, G., Solano, R., Fenoll, C., and Escobar, C. (2010). Early transcriptomic events in microdissected Arabidopsis nematode-induced giant cells. *Plant J.* 61, 698–712.
- Bebber, D.P., Holmes, T., and Gurr, S.J. (2014). The global spread of crop pests and pathogens. *Ecol. Biogeogr.* 23, 1398–1407.
- Bell, E., Creelman, R.A., and Mullet, J.E. (1995). A chloroplast lipoxygenase is required for wound-induced jasmonic acid accumulation in Arabidopsis. *Proc. Natl. Acad. Sci.* 92, 8675–8679.
- Bellafiore, S., Shen, Z., Rosso, M.N., Abad, P., Shih, P., and Briggs, S.P. (2008). Direct identification of the *Meloidogyne incognita* secretome reveals proteins with host cell reprogramming potential. *PLoS Pathog.* 4
- Bhattacharai, K.K., Xie, Q.G., Mantelin, S., Bishnoi, U., Girke, T., Navarre, D.A., and Kaloshian, I. (2008). Tomato Susceptibility to Root-Knot Nematodes Requires an Intact Jasmonic Acid Signaling Pathway. *Mol. Plant. Microbe Interact.* 21, 1205–1214.

- Bird, A.F., and Wallace, H.R. (1965). The Influence of Temperature On *Meloidogyne hapla* and *M. Javanica*. *Nematologica* 11, 581–589.
- Brodhun, F., Cristobal-Sarramian, A., Zabel, S., Newie, J., Hamberg, M., and Feussner, I. (2013). An iron 13S-lipoxygenase with an α -linolenic acid specific hydroperoxidase activity from *Fusarium oxysporum*. *PLoS One* 8, e64919.
- Brooks, D.M., Bender, C.L., and Kunkel, B.N. (2005). The *Pseudomonas syringae* phytotoxin coronatine promotes virulence by overcoming salicylic acid-dependent defences in *Arabidopsis thaliana*. *Mol. Plant Pathol.* 6, 629–639.
- Bruce A., Alexander J., Julian L., Martin R., Keith R., and Peter W. (2007). *Molecular Biology of the Cell* fifth edition. Garland science
- Bubb, M.R., Yarmola, E.G., Gibson, B.G., and Southwick, F.S. (2003). Depolymerization of actin filaments by profilin. Effects of profilin on capping protein function. *J. Biol. Chem.* 278, 24629–24635.
- Byrd, D.W., Kirkpatrick, T., and Barker, K.R. (1983). An Improved Technique for Clearing and Staining Plant Tissues for Detection of Nematodes. *J. Nematol.* 15, 142–143.
- Caldelari, D., Wang, G., Farmer, E.E., and Dong, X. (2011). *Arabidopsis* *lox3 lox4* double mutants are male sterile and defective in global proliferative arrest. *Plant Mol. Biol.* 75, 25–33.
- Carlsson, L., Nyström, L.E., Lindberg, U., Kannan, K.K., Cid-Dresdner, H., Lövgren, S., and Jörnvall, H. (1976). Crystallization of a non-muscle actin. *J. Mol. Biol.* 105, 353–366.
- Castagnone-Sereno, P., Wajnberg, E., Bongiovanni, M., Leroy, F., and Dalmasso, A. (1994). Genetic variation in *Meloidogyne incognita* virulence against the tomato *Mi* resistance gene: evidence from isofemale line selection studies. *Theor. Appl. Genet.* 88, 749–753.
- Castagnone-Sereno, P., Danchin, E.G.J., Perfus-Barbeoch, L., and Abad, P. (2013). Diversity and Evolution of Root-Knot Nematodes, Genus *Meloidogyne*: New Insights from the Genomic Era. *Annu. Rev. Phytopathol.* 51, 203–220.
- Celenza, J.L., Eng, F.J., and Carlson, M. (1989). Molecular analysis of the SNF4 gene of *Saccharomyces cerevisiae*: evidence for physical association of the SNF4 protein with the SNF1 protein kinase. *Mol. Cell. Biol.* 9, 5045–5054.
- Chaturvedi, R., Krothapalli, K., Makandar, R., Nandi, A., Sparks, A.A., Roth, M.R., Welti, R., and Shah, J. (2008). Plastid omega3-fatty acid desaturase-dependent accumulation of a systemic acquired resistance inducing activity in petiole exudates of *Arabidopsis thaliana* is independent of jasmonic acid. *Plant J. Cell Mol. Biol.* 54, 106–117.

- Chehab, E.W., Kim, S., Savchenko, T., Kliebenstein, D., Dehesh, K., and Braam, J. (2011). Intronic T-DNA insertion renders *Arabidopsis opr3* a conditional jasmonic acid-producing mutant. *Plant Physiol.* 156, 770–778.
- Chico, J.M., Chini, A., Fonseca, S., and Solano, R. (2008). JAZ repressors set the rhythm in jasmonate signaling. *Curr. Opin. Plant Biol.* 11, 486–494.
- Chitwood, D.J. (2003). Nematicides. In *Encyclopedia of Agrochemicals*. John Wiley & Sons, Inc.
- Chitwood, D.J., and Perry, R.N. (2009). Reproduction, Physiology and Biochemistry. In *Root-Knot Nematodes*, CAB International, 182–200.
- Clément, M., Ketelaar, T., Rodiuc, N., Banora, M.Y., Smertenko, A., Engler, G., Abad, P., Hussey, P.J., and de Almeida Engler, J. (2009). Actin-Depolymerizing Factor2-Mediated Actin Dynamics Are Essential for Root-Knot Nematode Infection of *Arabidopsis*. *Plant Cell* 21, 2963–2979.
- Clough, S.J., and Bent, A.F. (1998). Floral dip: a simplified method for *Agrobacterium*-mediated transformation of *Arabidopsis thaliana*. *Plant J. Cell Mol. Biol.* 16, 735–743.
- Cole, S.J., Yoon, A.J., Faull, K.F., and Diener, A.C. (2014). Host perception of jasmonates promotes infection by *Fusarium oxysporum* formae speciales that produce isoleucine- and leucine-conjugated jasmonates. *Mol. Plant Pathol.* 15, 589–600.
- Cooper, W.R., Jia, L., and Goggin, L. (2005). Effects of Jasmonate-Induced Defenses on Root-Knot Nematode Infection of Resistant and Susceptible Tomato Cultivars. *J. Chem. Ecol.* 31, 1953–1967.
- Curtis, R.H.C. (2008). Plant-nematode interactions: environmental signals detected by the nematode's chemosensory organs control changes in the surface cuticle and behaviour. *Parasite Paris Fr.* 15, 310–316.
- De Almeida Engler, J., and Gheysen, G. (2012). Nematode-Induced Endoreduplication in Plant Host Cells: Why and How? *Mol. Plant. Microbe Interact.* 26, 17–24.
- De Almeida Engler, J., Van Poucke, K., Karimi, M., De Groodt, R., Gheysen, G., Engler, G., and Gheysen, G. (2004). Dynamic cytoskeleton rearrangements in giant cells and syncytia of nematode-infected roots. *Plant J.* 38, 12–26.
- De Geyter, N., Gholami, A., Goormachtig, S., and Goossens, A. (2012). Transcriptional machineries in jasmonate-elicited plant secondary metabolism. *Trends Plant Sci.* 17, 349–359.
- Devoto, A., Ellis, C., Magusin, A., Chang, H.-S., Chilcott, C., Zhu, T., and Turner, J.G. (2005). Expression profiling reveals COII to be a key regulator of genes involved in wound and methyl

jasmonate-induced secondary metabolism, defence, and hormone interactions. *Plant Mol. Biol.* 58, 497–513.

Doolittle, L.K., Rosen, M.K., and Padrick, S.B. (2013). Measurement and Analysis of in vitro Actin Polymerization. *Methods Mol. Biol. Clifton NJ* 1046, 273–293.

Dubreuil-Maurizi, C., and Poinssot, B. (2012). Role of glutathione in plant signaling under biotic stress. *Plant Signal. Behav.* 7, 210–212.

Fan, T., Zhai, H., Shi, W., Wang, J., Jia, H., Xiang, Y., and An, L. (2013). Overexpression of profilin 3 affects cell elongation and F-actin organization in *Arabidopsis thaliana*. *Plant Cell Rep.* 32, 149–160.

Feys, B., Benedetti, C.E., Penfold, C.N., and Turner, J.G. (1994). *Arabidopsis* Mutants Selected for Resistance to the Phytotoxin Coronatine Are Male Sterile, Insensitive to Methyl Jasmonate, and Resistant to a Bacterial Pathogen. *Plant Cell* 6, 751–759.

Fudali, S.L., Wang, C., and Williamson, V.M. (2012). Ethylene Signaling Pathway Modulates Attractiveness of Host Roots to the Root-Knot Nematode *Meloidogyne hapla*. *Mol. Plant. Microbe Interact.* 26, 75–86.

Fujimoto, T., Tomitaka, Y., Abe, H., Tsuda, S., Futai, K., and Mizukubo, T. (2011a). Expression profile of jasmonic acid-induced genes and the induced resistance against the root-knot nematode (*Meloidogyne incognita*) in tomato plants (*Solanum lycopersicum*) after foliar treatment with methyl jasmonate. *J. Plant Physiol.* 168, 1084–1097.

Fujimoto, T., Tomitaka, Y., Abe, H., Tsuda, S., Futai, K., and Mizukubo, T. (2011b). Jasmonic acid signaling pathway of *Arabidopsis thaliana* is important for root-knot nematode invasion. *Nematol. Res. Jpn. J. Nematol.* 41, 9–17.

Gao, X., Starr, J., Göbel, C., Engelberth, J., Feussner, I., Tumlinson, J., and Kolomiets, M. (2007). Maize 9-Lipoxygenase ZmLOX3 Controls Development, Root-Specific Expression of Defense Genes, and Resistance to Root-Knot Nematodes. *Mol. Plant. Microbe Interact.* 21, 98–109.

Geng, X., Cheng, J., Gangadharan, A., and Mackey, D. (2012). The Coronatine Toxin of *Pseudomonas syringae* Is a Multifunctional Suppressor of *Arabidopsis* Defense. *Plant Cell* 24, 4763–4774.

Gilliland, L.U., Kandasamy, M.K., Pawloski, L.C., and Meagher, R.B. (2002). Both Vegetative and Reproductive Actin Isovariants Complement the Stunted Root Hair Phenotype of the *Arabidopsis act2-1* Mutation. *Plant Physiol.* 130, 2199–2209.

- Gilliland, L.U., Pawloski, L.C., Kandasamy, M.K., and Meagher, R.B. (2003). Arabidopsis actin gene ACT7 plays an essential role in germination and root growth. *Plant J. Cell Mol. Biol.* 33, 319–328.
- Glazebrook, J. (2005). Contrasting mechanisms of defense against biotrophic and necrotrophic pathogens. *Annu. Rev. Phytopathol.* 43, 205–227.
- Grebner, W., Stingl, N.E., Oenel, A., Mueller, M.J., and Berger, S. (2013). Lipoxygenase6-Dependent Oxylinin Synthesis in Roots Is Required for Abiotic and Biotic Stress Resistance of Arabidopsis1. *Plant Physiol.* 161, 2159–2170.
- Guranowski, A., Miersch, O., Staswick, P.E., Suza, W., and Wasternack, C. (2007). Substrate specificity and products of side-reactions catalyzed by jasmonate: amino acid synthetase (JAR1). *FEBS Lett.* 581, 815–820.
- Gutjahr, C., and Paszkowski, U. (2009). Weights in the Balance: Jasmonic Acid and Salicylic Acid Signaling in Root-Biotroph Interactions. *Mol. Plant. Microbe Interact.* 22, 763–772.
- Hanahan, D. (1983). Studies on transformation of Escherichia coli with plasmids. *J. Mol. Biol.* 166, 557–580.
- Hardham, A.R., Takemoto, D., and White, R.G. (2008). Rapid and dynamic subcellular reorganization following mechanical stimulation of Arabidopsis epidermal cells mimics responses to fungal and oomycete attack. *BMC Plant Biol.* 8, 63.
- Hartley, J.L., Temple, G.F., and Brasch, M.A. (2000). DNA cloning using in vitro site-specific recombination. *Genome Res.* 10, 1788–1795.
- Henty-Ridilla, J.L., Shimono, M., Li, J., Chang, J.H., Day, B., and Staiger, C.J. (2013). The Plant Actin Cytoskeleton Responds to Signals from Microbe-Associated Molecular Patterns. *PLoS Pathog* 9
- Hewezi, T., and Baum, T.J. (2012). Manipulation of Plant Cells by Cyst and Root-Knot Nematode Effectors. *Mol. Plant. Microbe Interact.* 26, 9–16.
- Hoshino, H., Yoneda, A., Kumagai, F., and Hasezawa, S. (2003). Roles of actin-depleted zone and preprophase band in determining the division site of higher-plant cells, a tobacco BY-2 cell line expressing GFP-tubulin. *Protoplasma* 222, 157–165.
- Hussey, P.J. (2004). *The Plant Cytoskeleton in Cell Differentiation and Development*. CRC Press.
- Hussey, P.J., Ketelaar, T., and Deeks, M.J. (2006). Control of the actin cytoskeleton in plant cell growth. *Annu. Rev. Plant Biol.* 57, 109–125.

- Iberkleid, I., Vieira, P., de Almeida Engler, J., Firester, K., Spiegel, Y., and Horowitz, S.B. (2013). Fatty acid-and retinol-binding protein, Mj-FAR-1 induces tomato host susceptibility to root-knot nematodes. *PloS One* 8
- Ithal, N., Recknor, J., Nettleton, D., Maier, T., Baum, T.J., and Mitchum, M.G. (2007). Developmental Transcript Profiling of Cyst Nematode Feeding Cells in Soybean Roots. *Mol. Plant. Microbe Interact.* 20, 510–525.
- Jammes, F., Lecomte, P., de Almeida-Engler, J., Bitton, F., Martin-Magniette, M.-L., Renou, J.P., Abad, P., and Favery, B. (2005). Genome-wide expression profiling of the host response to root-knot nematode infection in Arabidopsis. *Plant J.* 44, 447–458.
- Janssen, G.J.W., Scholten, O.E., Norel, A. van, and Hoogendoorn, C. J. (1998). Selection of virulence in *Meloidogyne chitwoodi* to resistance in the wild potato *Solanum fendleri*. *Eur. J. Plant Pathol.* 104, 645–651.
- Jelenska, J., Kang, Y., and Greenberg, J.T. (2014). Plant pathogenic bacteria target the actin microfilament network involved in the trafficking of disease defense components. *Bioarchitecture* 4, 149–153.
- Jockusch, B.M., Murk, K., and Rothkegel, M. (2007). The profile of profilins. *Rev. Physiol. Biochem. Pharmacol.* 159, 131–149.
- Jones, M.G.K., and Goto, D.B. (2011). Root-knot Nematodes and Giant Cells. In *Genomics and Molecular Genetics of Plant-Nematode Interactions*. Springer Netherlands, pp. 83–100.
- Jones, M.G.K., and Gunning, B.E.S. (1976). Transfer cells and nematode induced giant cells in *Helianthemum*. *Protoplasma* 87, 273–279.
- Jones, J.T., Haegeman, A., Danchin, E.G.J., Gaur, H.S., Helder, J., Jones, M.G.K., Kikuchi, T., Manzanilla-López, R., Palomares-Rius, J.E., Wesemael, W.M.L., et al. (2013). Top 10 plant-parasitic nematodes in molecular plant pathology. *Mol. Plant Pathol.* 14, 946–961.
- Kammerhofer, N., Egger, B., Dobrev, P., Vankova, R., Hofmann, J., Schausberger, P., and Wiczorek, K. (2015). Systemic above- and belowground cross talk: hormone-based responses triggered by *Heterodera schachtii* and shoot herbivores in *Arabidopsis thaliana*. *J. Exp. Bot.* 10.1093/jxb/erv398
- Kandasamy, M.K., Burgos-Rivera, B., McKinney, E.C., Ruzicka, D.R., and Meagher, R.B. (2007). Class-Specific Interaction of Profilin and ADF Isovariants with Actin in the Regulation of Plant Development. *Plant Cell* 19, 3111–3126.
- Kandasamy, M.K., McKinney, E.C., and Meagher, R.B. (2009). A Single Vegetative Actin Isovariant Overexpressed under the Control of Multiple Regulatory Sequences Is Sufficient for Normal Arabidopsis Development. *Plant Cell* 21, 701–718.

- Kandasamy, M.K., McKinney, E.C., Roy, E., and Meagher, R.B. (2012). Plant Vegetative and Animal Cytoplasmic Actins Share Functional Competence for Spatial Development with Protists. *Plant Cell* 24, 2041–2057.
- Kang, Y., Jelenska, J., Cecchini, N.M., Li, Y., Lee, M.W., Kovar, D.R., and Greenberg, J.T. (2014). HopW1 from *Pseudomonas syringae* disrupts the actin cytoskeleton to promote virulence in *Arabidopsis*. *PLoS Pathog.* 10, e1004232.
- Katsir, L., Chung, H.S., Koo, A.J., and Howe, G.A. (2008a). Jasmonate signaling: a conserved mechanism of hormone sensing. *Curr. Opin. Plant Biol.* 11, 428–435.
- Katsir, L., Schilmiller, A.L., Staswick, P.E., He, S.Y., and Howe, G.A. (2008b). COI1 is a critical component of a receptor for jasmonate and the bacterial virulence factor coronatine. *Proc. Natl. Acad. Sci.* 105, 7100–7105.
- Kazan, K., and Manners, J.M. (2013). MYC2: the master in action. *Mol. Plant* 6, 686–703.
- Korn, E.D., Carlier, M.F., and Pantaloni, D. (1987). Actin polymerization and ATP hydrolysis. *Science* 238, 638–644.
- Kyndt, T., Vieira, P., Gheysen, G., and Almeida-Engler, J. de (2013). Nematode feeding sites: unique organs in plant roots. *Planta* 238, 807–818.
- Landy, A. (1989). Dynamic, structural, and regulatory aspects of lambda site-specific recombination. *Annu. Rev. Biochem.* 58, 913–949.
- Laudert, D., and Weiler, E.W. (1998). Allene oxide synthase: a major control point in *Arabidopsis thaliana* octadecanoid signalling. *Plant J.* 15, 675–684.
- Liu, P., Qi, M., Xue, X., and Ren, H. (2011). Dynamics and functions of the actin cytoskeleton during the plant cell cycle. *Chin. Sci. Bull.* 56, 3504–3510.
- Liu, Y., Ahn, J.E., Datta, S., Salzman, R.A., Moon, J., Huyghues-Despointes, B., Pittendrigh, B., Murdock, L.L., Koiwa, H., and Zhu-Salzman, K. (2005). *Arabidopsis* Vegetative Storage Protein Is an Anti-Insect Acid Phosphatase. *Plant Physiol.* 139, 1545–1556.
- Livak, K.J., and Schmittgen, T.D. (2001). Analysis of relative gene expression data using real-time quantitative PCR and the 2(-Delta Delta C(T)). *Method. Methods San Diego Calif* 25, 402–408.
- Livanos, P., Apostolakos, P., and Galatis, B. (2012). Plant cell division. *Plant Signal. Behav.* 7, 771–778.

- Mano, S., Nakamori, C., Hayashi, M., Kato, A., Kondo, M., and Nishimura, M. (2002). Distribution and Characterization of Peroxisomes in Arabidopsis by Visualization with GFP: Dynamic Morphology and Actin-Dependent Movement. *Plant Cell Physiol.* 43, 331–341.
- Manosalva, P., Manohar, M., von Reuss, S.H., Chen, S., Koch, A., Kaplan, F., Choe, A., Micikas, R.J., Wang, X., Kogel, K.-H., et al. (2015). Conserved nematode signalling molecules elicit plant defenses and pathogen resistance. *Nat. Commun.* 6. 10.1038/ncomms8795
- Mbeunkui, F., Scholl, E.H., Opperman, C.H., Goshe, M.B., and Bird, D.M. (2010). Proteomic and bioinformatic analysis of the root-knot nematode *Meloidogyne hapla*: the basis for plant parasitism. *J. Proteome Res.* 9, 5370–5381.
- McConn, M., and Browse, J. (1996). The Critical Requirement for Linolenic Acid Is Pollen Development, Not Photosynthesis, in an Arabidopsis Mutant. *Plant Cell* 8, 403–416.
- McDowell, J.M., An, Y.Q., Huang, S., McKinney, E.C., and Meagher, R.B. (1996). The arabidopsis ACT7 actin gene is expressed in rapidly developing tissues and responds to several external stimuli. *Plant Physiol.* 111, 699–711.
- Melan, M.A., Dong, X., Endara, M.E., Davis, K.R., Ausubel, F.M., and Peterman, T.K. (1993). An Arabidopsis thaliana lipoxygenase gene can be induced by pathogens, abscisic acid, and methyl jasmonate. *Plant Physiol.* 101, 441–450.
- Mengiste, T. (2012). Plant Immunity to Necrotrophs. *Annu. Rev. Phytopathol.* 50, 267–294.
- Mitkowski, N.A., and Abawi, G.S. (2003). Root-knot nematodes. Plant Health Instructor. [accessed 10/11/2015] <http://www.apsnet.org/>
- Mueller, S., Hilbert, B., Dueckershoff, K., Roitsch, T., Krischke, M., Mueller, M.J., and Berger, S. (2008). General detoxification and stress responses are mediated by oxidized lipids through TGA transcription factors in Arabidopsis. *Plant Cell* 20, 768–785.
- Müssar, K.J., Kandasamy, M.K., McKinney, E.C., and Meagher, R.B. (2015). Arabidopsis plants deficient in constitutive class profilins reveal independent and quantitative genetic effects. *BMC Plant Biol.* 15, 177.
- Nahar, K., Kyndt, T., Vleeschauwer, D.D., Höfte, M., and Gheysen, G. (2011). The Jasmonate Pathway Is a Key Player in Systemically Induced Defense against Root Knot Nematodes in Rice. *Plant Physiol.* 157, 305–316.
- Opperman, C.H., Bird, D.M., Williamson, V.M., Rokhsar, D.S., Burke, M., Cohn, J., Cromer, J., Diener, S., Gajan, J., Graham, S., et al. (2008). Sequence and genetic map of *Meloidogyne hapla*: A compact nematode genome for plant parasitism. *Proc. Natl. Acad. Sci.* 105, 14802–14807.

- Ozalvo, R., Cabrera, J., Escobar, C., Christensen, S.A., Borrego, E.J., Kolomiets, M.V., Castresana, C., Iberkleid, I., and Brown Horowitz, S. (2014). Two closely related members of Arabidopsis 13-lipoxygenases (13-LOXs), LOX3 and LOX4, reveal distinct functions in response to plant-parasitic nematode infection. *Mol. Plant Pathol.* 15, 319–332.
- Park, J.H., Halitschke, R., Kim, H.B., Baldwin, I.T., Feldmann, K.A., and Feyereisen, R. (2002). A knock-out mutation in allene oxide synthase results in male sterility and defective wound signal transduction in Arabidopsis due to a block in jasmonic acid biosynthesis. *Plant J. Cell Mol. Biol.* 31, 1–12.
- Park, S.W., Li, W., Viehhauser, A., He, B., Kim, S., Nilsson, A.K., Andersson, M.X., Kittle, J.D., Ambavaram, M.M.R., Luan, S., et al. (2013). Cyclophilin 20-3 relays a 12-oxo-phytodienoic acid signal during stress responsive regulation of cellular redox homeostasis. *Proc. Natl. Acad. Sci. U. S. A.* 110, 9559–9564.
- Penninckx, I.A.M.A., Thomma, B.P.H.J., Buchala, A., Métraux, J.P., and Broekaert, W.F. (1998). Concomitant Activation of Jasmonate and Ethylene Response Pathways Is Required for Induction of a Plant Defensin Gene in Arabidopsis. *Plant Cell* 10, 2103–2113.
- Perry, R.N., Moens, M., and Starr, J.L. (2009). Root-knot Nematodes. CABI.
- Petrillo, M.D., and Roberts, P.A. (2005). Isofemale Line Analysis of *Meloidogyne incognita* Virulence to Cowpea Resistance Gene *Rk*. *J. Nematol.* 37, 448–456.
- Porta, J.C., and Borgstahl, G.E.O. (2012). Structural Basis for Profilin-Mediated Actin Nucleotide Exchange. *J. Mol. Biol.* 418, 103–116.
- Qi, T., Song, S., Ren, Q., Wu, D., Huang, H., Chen, Y., Fan, M., Peng, W., Ren, C., and Xie, D. (2011). The Jasmonate-ZIM-domain proteins interact with the WD-Repeat/bHLH/MYB complexes to regulate Jasmonate-mediated anthocyanin accumulation and trichome initiation in Arabidopsis thaliana. *Plant Cell* 23, 1795–1814.
- Ralhan, A., Schöttle, S., Thurow, C., Iven, T., Feussner, I., Polle, A., and Gatz, C. (2012). The Vascular Pathogen *Verticillium longisporum* Requires a Jasmonic Acid-Independent COI1 Function in Roots to Elicit Disease Symptoms in Arabidopsis Shoots. *Plant Physiol.* 159, 1192–1203.
- Ranjith, P., Mallick, K., Joanny, J.-F., and Lacoste, D. (2010). Role of ATP-Hydrolysis in the Dynamics of a Single Actin Filament. *Biophys. J.* 98, 1418–1427.
- Ribot, C., Zimmerli, C., Farmer, E.E., Reymond, P., and Poirier, Y. (2008). Induction of the Arabidopsis PHO1;H10 Gene by 12-Oxo-Phytodienoic Acid But Not Jasmonic Acid via a CORONATINE INSENSITIVE1-Dependent Pathway. *Plant Physiol.* 147, 696–706.

- Scalschi, L., Sanmartín, M., Camañes, G., Troncho, P., Sánchez-Serrano, J.J., García-Agustín, P., and Vicedo, B. (2015). Silencing of OPR3 in tomato reveals the role of OPDA in callose deposition during the activation of defense responses against *Botrytis cinerea*. *Plant J. Cell Mol. Biol.* 81, 304–315.
- Schaller, F., Biesgen, C., Müssig, C., Altmann, T., and Weiler, E.W. (2000). 12-Oxophytodienoate reductase 3 (OPR3) is the isoenzyme involved in jasmonate biosynthesis. *Planta* 210, 979–984.
- Schatzki, J., Schoo, B., Ecke, W., Herrfurth, C., Feussner, I., Becker, H.C., and Möllers, C. (2013). Mapping of QTL for seed dormancy in a winter oilseed rape doubled haploid population. *TAG Theor. Appl. Genet. Theor. Angew. Genet.* 126, 2405–2415.
- Schillmiller, A.L., Koo, A.J.K., and Howe, G.A. (2007). Functional diversification of acyl-coenzyme A oxidases in jasmonic acid biosynthesis and action. *Plant Physiol.* 143, 812–824.
- Schmidt, E.F., and Strittmatter, S.M. (2007). The CRMP family of proteins and their role in Sema3A signaling. *Adv. Exp. Med. Biol.* 600, 1–11.
- Sheahan, M.B., Rose, R.J., and McCurdy, D.W. (2004a). Organelle inheritance in plant cell division: the actin cytoskeleton is required for unbiased inheritance of chloroplasts, mitochondria and endoplasmic reticulum in dividing protoplasts. *Plant J.* 37, 379–390.
- Sheahan, M.B., Staiger, C.J., Rose, R.J., and McCurdy, D.W. (2004b). A green fluorescent protein fusion to actin-binding domain 2 of *Arabidopsis* fimbrin highlights new features of a dynamic actin cytoskeleton in live plant cells. *Plant Physiol.* 136, 3968–3978.
- Sijmons, P.C., Grundle, F.M.W., von Mende, N., Burrows, P.R., and Wyss, U. (1991). *Arabidopsis thaliana* as a new model host for plant-parasitic nematodes. *Plant J.* 1, 245–254.
- Snyder, D.W., Opperman, C.H., and Bird, D.M. (2006). A Method for Generating *Meloidogyne incognita* Males. *J. Nematol.* 38, 192–194.
- Soriano, I.R., Asenstorfer, R.E., Schmidt, O., and Riley, I.T. (2004). Inducible Flavone in Oats (*Avena sativa*) Is a Novel Defense Against Plant-Parasitic Nematodes. *Phytopathology* 94, 1207–1214.
- Stenzel, I., Hause, B., Miersch, O., Kurz, T., Maucher, H., Weichert, H., Ziegler, J., Feussner, I., and Wasternack, C. (2003). Jasmonate biosynthesis and the allene oxide cyclase family of *Arabidopsis thaliana*. *Plant Mol. Biol.* 51, 895–911.
- Stintzi, A., and Browse, J. (2000). The *Arabidopsis* male-sterile mutant, *opr3*, lacks the 12-oxophytodienoic acid reductase required for jasmonate synthesis. *Proc. Natl. Acad. Sci.* 97, 10625–10630.

- Stintzi, A., Weber, H., Reymond, P., Browse, J., and Farmer, E.E. (2001). Plant defense in the absence of jasmonic acid: The role of cyclopentenones. *Proc. Natl. Acad. Sci. U. S. A.* 98, 12837–12842.
- Stotz, H.U., Jikumaru, Y., Shimada, Y., Sasaki, E., Stingl, N., Mueller, M.J., and Kamiya, Y. (2011). Jasmonate-Dependent and COI1-Independent Defense Responses Against *Sclerotinia sclerotiorum* in *Arabidopsis thaliana*: Auxin is Part of COI1-Independent Defense Signaling. *Plant Cell Physiol.* 52, 1941–1956.
- Stotz, H.U., Mueller, S., Zoeller, M., Mueller, M.J., and Berger, S. (2013). TGA transcription factors and jasmonate-independent COI1 signalling regulate specific plant responses to reactive oxylipins. *J. Exp. Bot.* 64, 963–975.
- Stüven, T., Hartmann, E., and Görlich, D. (2003). Exportin 6: a novel nuclear export receptor that is specific for profilin.actin complexes. *EMBO J.* 22, 5928–5940.
- Sun, T., Li, S., and Ren, H. (2013). Profilin as a regulator of the membrane-actin cytoskeleton interface in plant cells. *Front. Plant Sci.* 4, 512.
- Takemoto, D., and Hardham, A.R. (2004). The Cytoskeleton as a Regulator and Target of Biotic Interactions in Plants. *Plant Physiol.* 136, 3864–3876.
- Taki, N., Sasaki-Sekimoto, Y., Obayashi, T., Kikuta, A., Kobayashi, K., Ainai, T., Yagi, K., Sakurai, N., Suzuki, H., Masuda, T., et al. (2005). 12-Oxo-Phytodienoic Acid Triggers Expression of a Distinct Set of Genes and Plays a Role in Wound-Induced Gene Expression in *Arabidopsis*. *Plant Physiol.* 139, 1268–1283.
- Teillet, A., Dybal, K., Kerry, B.R., Miller, A.J., Curtis, R.H.C., and Hedden, P. (2013). Transcriptional Changes of the Root-Knot Nematode *Meloidogyne incognita* in Response to *Arabidopsis thaliana* Root Signals. *PLoS ONE* 8, e61259.
- Thatcher, L.F., Manners, J.M., and Kazan, K. (2009). *Fusarium oxysporum* hijacks COI1-mediated jasmonate signaling to promote disease development in *Arabidopsis*. *Plant J.* 58, 927–939.
- Thines, B., Katsir, L., Melotto, M., Niu, Y., Mandaokar, A., Liu, G., Nomura, K., He, S.Y., Howe, G.A., and Browse, J. (2007). JAZ repressor proteins are targets of the SCF(COI1) complex during jasmonate signalling. *Nature* 448, 661–665.
- Trudgill, D.L., and Blok, V.C. (2001). APOMICTIC, POLYPHAGOUS ROOT-KNOT NEMATODES: Exceptionally Successful and Damaging Biotrophic Root Pathogens. *Annu. Rev. Phytopathol.* 39, 53–77.
- Van Criekinge, W., and Beyaert, R. (1999). Yeast Two-Hybrid: State of the Art. *Biol. Proced. Online* 2, 1–38.

- Vellosillo, T., Martínez, M., López, M.A., Vicente, J., Cascón, T., Dolan, L., Hamberg, M., and Castresana, C. (2007). Oxylipins produced by the 9-lipoxygenase pathway in Arabidopsis regulate lateral root development and defense responses through a specific signaling cascade. *Plant Cell* 19, 831–846.
- Verhage, A., Vlaardingbroek, I., Raaymakers, C., Van Dam, N.M., Dicke, M., Van Wees, S.C.M., and Pieterse, C.M.J. (2011). Rewiring of the Jasmonate Signaling Pathway in Arabidopsis during Insect Herbivory. *Front. Plant Sci.* 2, 1-12
- Vijayan, P., Shockey, J., Lévesque, C.A., Cook, R.J., and Browse, J. (1998). A role for jasmonate in pathogen defense of Arabidopsis. *Proc. Natl. Acad. Sci. U. S. A.* 95, 7209–7214.
- Wang, Y.-S., Motes, C.M., Mohamalawari, D.R., and Blancaflor, E.B. (2004). Green fluorescent protein fusions to Arabidopsis fimbrin 1 for spatio-temporal imaging of F-actin dynamics in roots. *Cell Motil. Cytoskeleton* 59, 79–93.
- Weber, H. (2002). Fatty acid-derived signals in plants. *Trends Plant Sci.* 7, 217–224.
- Witke, W. (2004). The role of profilin complexes in cell motility and other cellular processes. *Trends Cell Biol.* 14, 461–469.
- Wolven, A.K., Belmont, L.D., Mahoney, N.M., Almo, S.C., and Drubin, D.G. (2000). *In Vivo* Importance of Actin Nucleotide Exchange Catalyzed by Profilin. *J. Cell Biol.* 150, 895–904.
- Wyss, U., Grundler, F.M.W., and Munch, A. (1992). The Parasitic Behaviour of Second-Stage Juveniles of *Meloidogyne Incognita* in Roots of *Arabidopsis Thaliana*. *Nematologica* 38, 98–111.
- Yarmola, E.G., and Bubb, M.R. (2006). Profilin: emerging concepts and lingering misconceptions. *Trends Biochem. Sci.* 31, 197–205.
- Yuan, H.-Y., Yao, L.-L., Jia, Z.-Q., Li, Y., and Li, Y.-Z. (2006). *Verticillium dahliae* toxin induced alterations of cytoskeletons and nucleoli in *Arabidopsis thaliana* suspension cells. *Protoplasma* 229, 75–82.
- Zheng, X., Spivey, N.W., Zeng, W., Liu, P.-P., Fu, Z.Q., Klessig, D.F., He, S.Y., and Dong, X. (2012). Coronatine promotes *Pseudomonas syringae* virulence in plants by activating a signaling cascade that inhibits salicylic acid accumulation. *Cell Host Microbe* 11, 587–596.

6. Supplementary figures

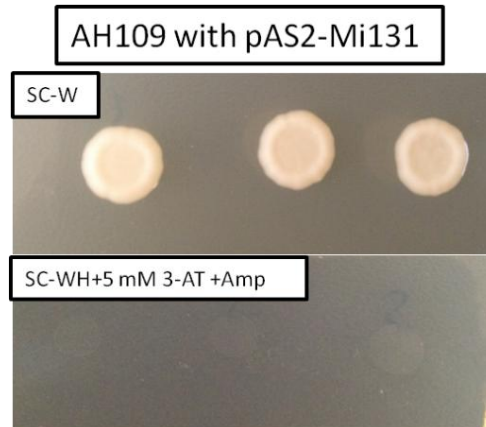


Figure S1.1. Mi131 does not auto-activate the reporter in yeast. Yeast strain AH109 was transformed with bait plasmid (pAS2) containing Mi131. The absence of growth on SC-WH +5mM 3-AT + ampicilin indicates no auto-activation of the reporter gene in this condition. The presence of the plasmid in the yeast was verified by growth on plates lacking selection (SC-W).

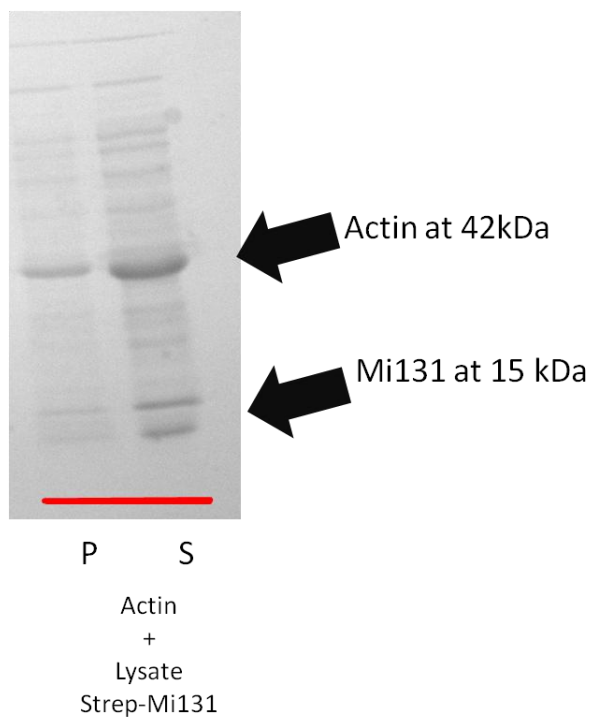


Figure S1.2. Strep-Mi131 inhibits *in vitro* actin polymerization. Non-muscle actin (22 μ M) was incubated with Strep-Mi131 for 30 minutes before adding polymerization buffer to induce actin polymerization. After a 30 minutes polymerization time, the G and F actin were separated by ultracentrifugation. Samples from the pellet (P) and supernatant (S) fractions were run on 4-20% SDS-PAGE and stained with Coomassie blue to visualize the actin and Mi131. Actin in the pellet represents F/polymerized actin and in the supernatant represents G/monomer actin. Predicted size for Strep-Mi131 is 15 kDa and non-muscle actin is 42 kDa. This assay was repeated twice with similar results.

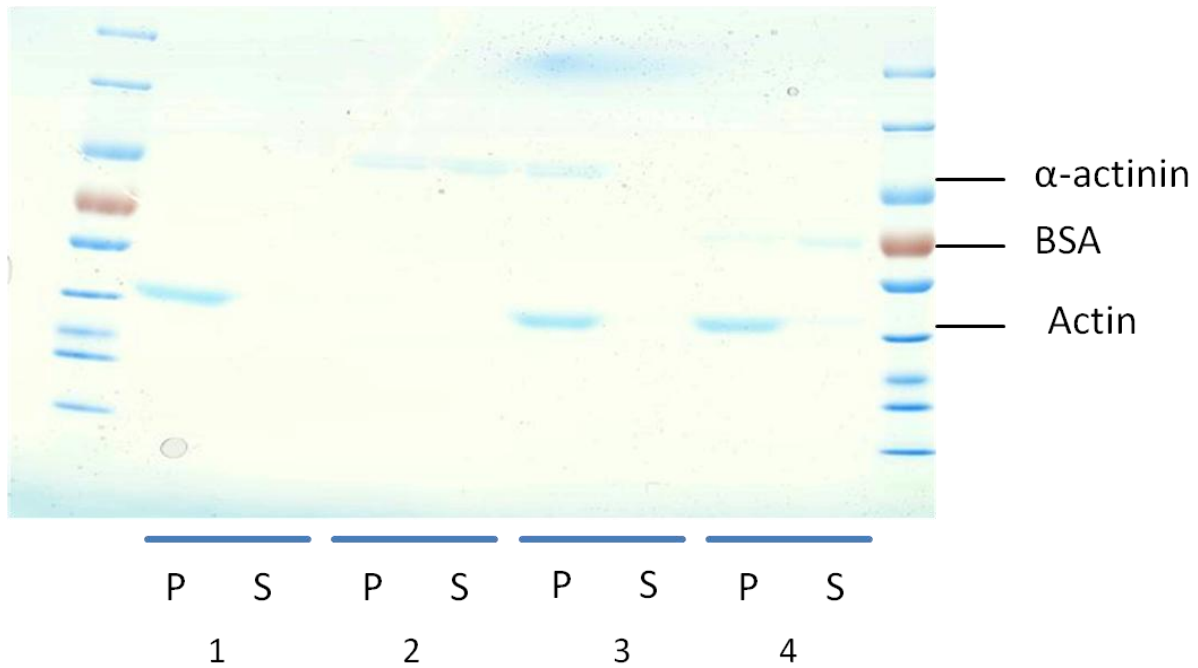


Figure S1.3. The controls for *in vitro* actin sedimentation assay. 1) buffer + G actin, 2) α -actinin, 3) α -actinin + G actin and 4) BSA + G actin prior. After F actin polymerization, G and F actin were separated by ultracentrifugation and the supernatant (S) and pellet (P) fractions were run on 12 % SDS gel; proteins were visualized by Coomassie stain. In this experiment, actin can polymerize in filaments since a majority of actin can be found in the P fraction. Buffer, BSA and the F actin binding α -actinin had no effect on actin polymerization.

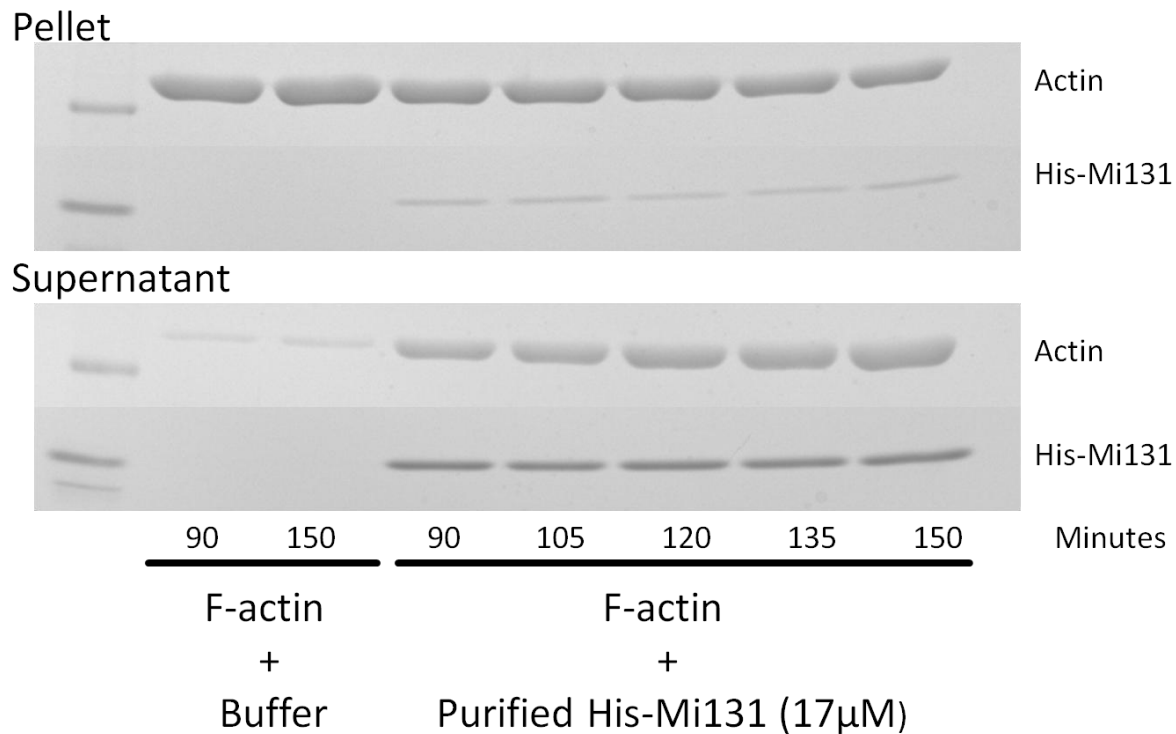


Figure S1.4. F actin depolymerization in a time course experiment. Pre-polymerized F actin was incubated with either buffer or recombinant His-Mi131 for 90 to 150 minutes (include the centrifugation time). The G and F actin were separated by ultracentrifugation. Samples from the pellet (P) and supernatant (S) fractions were run on 4-20% SDS-PAGE and stained with Coomassie blue to visualize the actin and recombinant His-Mi131. Actin in the pellet is F or polymerized actin. Actin in the supernatant is G actin. Predicted size for Strep-Mi131 is 15 kDa and non-muscle actin is 42 kDa. This assay was repeated twice with similar results.

Col-0 with pK7WG2:ACT1



Mi131 B with pK7WG2:ACT1



Figure S1.5. 35S::AtACT1 phenotype. Five weeks old Arabidopsis transformed with 35S::AtACT1 were observed for the dwarf phenotype.

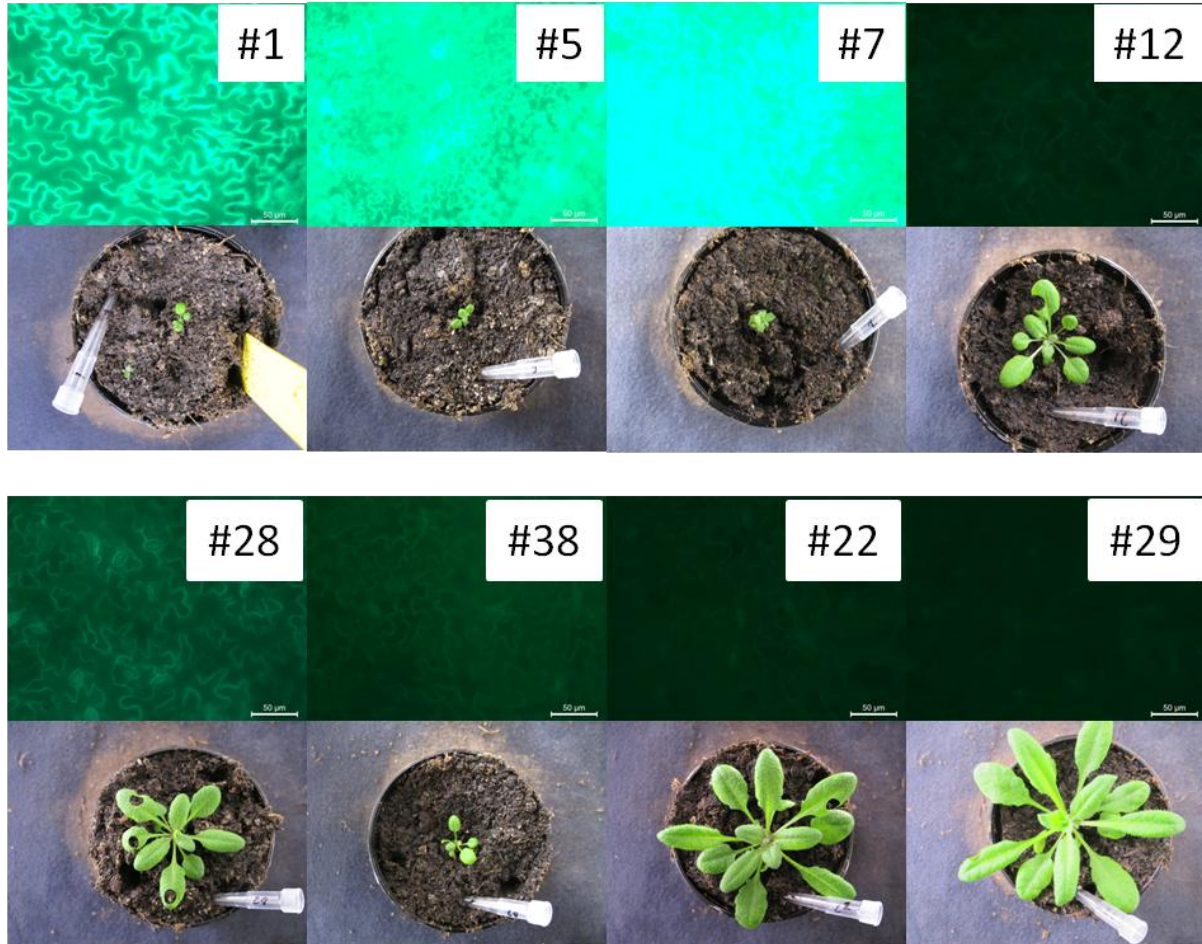


Figure S1.6. 4 weeks old 35S::GFP-Mi131 (T1) after basta selection. Leaf disks were taken from eight T1 plants that were BASTA resistant. The presence of GFP-Mi131 protein was determined using fluorescence microscope.

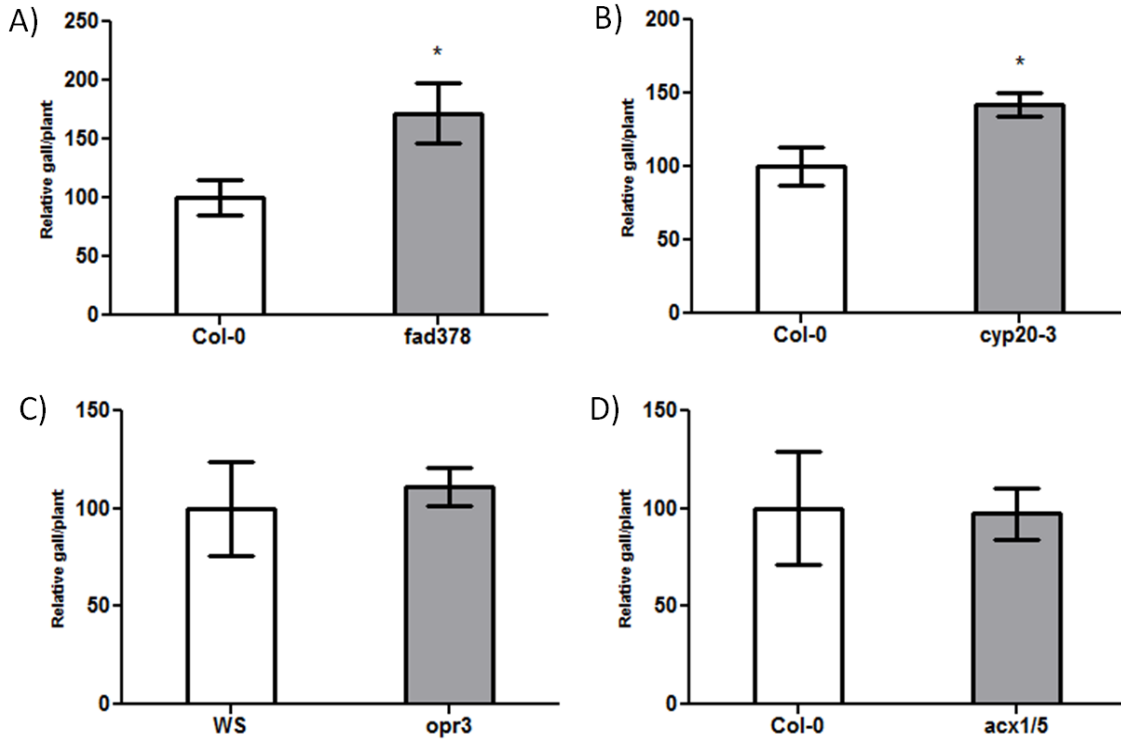


Figure S2.1 The *M. hapla* infection on A) *fad378*, B) *cyp20-3*, C) *opr3* and D) *acx1/5* mutant (Cynthia Gleason and Rania Almohammedsaleh, personal communication). Ten-day-old Col-0 and mutants were grown on MS were transferred to petri dishes containing KNOPs media. Each plant was inoculated with 100 *M. hapla* J2 and the number of galls per plant was counted at 14 dpi. Bars represent mean of gall per plant normalized to internal Col-0 control combined. Error bar represents standard error of mean (n=2). Asterisk indicates a significant different between Col-0 and the mutant by using student t-test (p<0.05)

Acknowledgement

I would like to thank Cynthia Gleason for giving me the opportunity to work on this projects and all the supports during my thesis. Also thanks to Gleason's lab members, Frederik Polzin, Martin Muthreich and Jan Utermark for the nice and motivating atmosphere.

Since many of my works involve working in Gatz and Lipka labs. Therefore, I would like to mention the supports from the members from both groups which are helpful during the time I have questions.

I also want to thank Christiane Gatz and Thomas Teichmann for being in my thesis committee and giving me guidance during my study as well as my examination board namely Prof. Volker Lipka, Prof. Andrea Polle, and Prof. Ivo Feußner.

Surely I cannot have an opportunity to join this project if there is no support from my family.

Curriculum vitae

Personal information

Name : Natthanon Leelarasamee

Date of birth : 01.06.1984

Place of birth : Bangkok, Thailand

Nationality : Thai

Email : seihhung@hotmail.com

Education

May 2012 – present

Doctoral studies

George-August-Universität Göttingen, Germany

Department of Plant Biology (Jun. Prof. Dr. Cynthia Gleason)

George August University School of Science (GAUSS) program

Dissertation title: The functional characterization of a root knot nematode effector Mi131 and an investigation of the role of jasmonic acid during the Arabidopsis-root knot nematode interaction (Department of molecular plant biology, Jun. Prof. Cynthia Gleason)

August 2009 -June 2011

Master of medical science

Main field of study: Infection Biology

Faculty of medicine

Uppsala University, Uppsala, Sweden in corroboration with Swedish University of Agriculture science, Uppsala, Sweden

Thesis title: Improve crop tolerance to stress (Department of Plant Biology and Forest genetics, Prof. Dr. Johan Meijer, SLU)

May 2002 – March 2007 Bachelor of Pharmacy

Faculty of Pharmacy

Silpakorn University, Nakhon pathom, Thailand

Thesis title: Electrospun Polyvinyl Alcohol Polymeric Fibrous System as Carriers for Extracts from Fruit Hull of mangosteen.

May 1990 – March 2002 Elementary and High School

Saint Gabriel's College, Bangkok, Thailand

Working experience

November 2007- July 2009 Production pharmacist

Golden cup pharmaceutical co., ltd., Bangkok, Thailand.